EUROPEAN ORGANIZATION FOR NUCLEAR RESEARCH

CERN/PS/BR 81-28
22 December 1981

MULTITURN INJECTION INTO THE CERN PROTON SYNCHROTRON BOOSTER*)

P.D.V. van der Stok

*) This report is the subject of a thesis for the doctor's degree at the University of Amsterdam, the Netherlands.

ABSTRACT

The Multiturn Injection Process into the Proton Synchrotron Booster (PSB) is discussed. First a short history of the PSB is presented, followed by an introduction to some basic accelerator theory.

Then a model for the description of the multiturn injection process is developed. It is based on the determination of a geometrical pattern in the phase space into which the particles must be injected if they are to be preserved in the accelerator. From these patterns the value of the injection parameters can be calculated such that the number of particles injected into the PSB is maximal. The particle distribution is then introduced to calculate the total injected current and the injection parameters, such that the beam injected into the PSB has some predetermined size.

The theoretical results are compared with measurements of the injection parameters in the PSB. The coupling of the vertical and the horizontal motion of the particles in the PSB allows the injection of more particles. The model is then extended to include the calculation of the injected intensity when a horizontal–vertical coupling term is present.

Finally, the principal effects of the space-charge forces on the multiturn injection process are analysed, and measurements are presented to uphold this analysis.

CONTENTS

CHAPTER I: THE CERN PROTON SYNCHROTRON BOOSTER 1
I.1 INTRODUCTION 1
I.2 A BOOSTER: WHY? 1
I.3 DESCRIPTION OF THE 800 MeV BOOSTER 2
I.4 REASONS FOR CHOOSING AN 800 MeV BOOSTER 4
I.5 THE RELEVANCE OF THIS WORK TO THE PERFORMANCE OF THE PSB 5
I.6 SOME INSTRUMENTATION IN THE PSB 6
I.6.1 Beam-current transformers 6
I.6.2 Pick-Up electrodes in the PSB 6
I.6.3 Scintillation screens 7
I.6.4 The apparatus for the measurement of the emittance of the 50 MeV beam of the Linac 7
I.6.5 The apparatus for the measurement of the energy dispersion of the 50 MeV beam of the Linac 7
I.6.6 BEAMSCOPE 7
I.6.7 The PSB target system 7

CHAPTER II: PHASE-PLANE TRAJECTORIES IN ALTERNATING-GRADIENT PROTON SYNCHROTRONS 9
II.1 BASIC ACCELERATOR THEORY 9
II.1.1 Transverse particle motion 9
II.1.2 Emittance and acceptance 10
II.1.3 Instability regions 12
II.2 INJECTION PROCESSES 14
II.2.1 Monoturn injection 15
II.2.2 Multiturn injection 17

CHAPTER III: MULTITURN INJECTION INTO THE PSB: MODEL CALCULATIONS AND MEASUREMENTS 18
III.1 GENERAL REMARKS 18
III.2 CALCULATION OF THE OPTIMIZED INJECTION PARAMETERS 22
III.3 THEORETICAL PREDICTIONS AND COMPARISON WITH MEASUREMENT 27
III.3.1 Results of the calculations for the model 27
III.3.2 Comparison of the model predictions with experiment 29
III.3.3 Investigation into the DS and optimized n_t values 31
III.3.4 Relative merits of this model 32
III.4 THE INFLUENCE OF SMALL FLUCTUATIONS IN THE INJECTION PARAMETERS ON THE MULTITURN INJECTION PROCESS 33
III.4.1 Injected beam parameters and their fluctuations 33
III.4.2 Fluctuations in the particle energy or in the magnetic field of the PSB 36
III.4.3 Influence of fluctuations in injection parameters on overall efficiency 37

CHAPTER IV: INCREASE OF MULTITURN INJECTION EFFICIENCY BY MEANS OF SKEW QUADRUPOLES 39
IV.1 INTRODUCTION 39
IV.2 COUPLING THEORY 40
IV.3 PRINCIPLES OF MULTITURN INJECTION WITH A HORIZONTAL–VERTICAL COUPLING TERM PRESENT 42
IV.4 EXPERIMENTAL RESULTS 43
IV.5 THEORETICAL CONSIDERATIONS 47

CONTENTS

CHAPTER I: THE CERN PROTON SYNCHROTRON BOOSTER 1
I.1 INTRODUCTION 1
I.2 A BOOSTER: WHY? 1
I.3 DESCRIPTION OF THE 800 MeV BOOSTER 2
I.4 REASONS FOR CHOOSING AN 800 MeV BOOSTER 4
I.5 THE RELEVANCE OF THIS WORK TO THE PERFORMANCE OF THE PSB 5
I.6 SOME INSTRUMENTATION IN THE PSB 6
I.6.1 Beam-current transformers 6
I.6.2 Pick-Up electrodes in the PSB 6
I.6.3 Scintillation screens 7
I.6.4 The apparatus for the measurement of the emittance of the 50 MeV beam of the Linac 7
I.6.5 The apparatus for the measurement of the energy dispersion of the 50 MeV beam of the Linac 7
I.6.6 BEAMSCOPE 7
I.6.7 The PSB target system 7

CHAPTER II: PHASE-PLANE TRAJECTORIES IN ALTERNATING-GRADIENT PROTON SYNCHROTRONS 9
II.1 BASIC ACCELERATOR THEORY 9
II.1.1 Transverse particle motion 9
II.1.2 Emittance and acceptance 10
II.1.3 Instability regions 12
II.2 INJECTION PROCESSES 14
II.2.1 Monoturn injection 15
II.2.2 Multiturn injection 17

CHAPTER III: MULTITURN INJECTION INTO THE PSB: MODEL CALCULATIONS AND MEASUREMENTS 18
III.1 GENERAL REMARKS 18
III.2 CALCULATION OF THE OPTIMIZED INJECTION PARAMETERS 22
III.3 THEORETICAL PREDICTIONS AND COMPARISON WITH MEASUREMENT 27
III.3.1 Results of the calculations for the model 27
III.3.2 Comparison of the model predictions with experiment 29
III.3.3 Investigation into the DS and optimized n_t values 31
III.3.4 Relative merits of this model 32
III.4 THE INFLUENCE OF SMALL FLUCTUATIONS IN THE INJECTION PARAMETERS ON THE MULTITURN INJECTION PROCESS 33
III.4.1 Injected beam parameters and their fluctuations 33
III.4.2 Fluctuations in the particle energy or in the magnetic field of the PSB 36
III.4.3 Influence of fluctuations in injection parameters on overall efficiency 37

CHAPTER IV: INCREASE OF MULTITURN INJECTION EFFICIENCY BY MEANS OF SKEW QUADRUPOLES 39
IV.1 INTRODUCTION 39
IV.2 COUPLING THEORY 40
IV.3 PRINCIPLES OF MULTITURN INJECTION WITH A HORIZONTAL–VERTICAL COUPLING TERM PRESENT 42
IV.4 EXPERIMENTAL RESULTS 43
IV.5 THEORETICAL CONSIDERATIONS 47

CHAPTER V: INFLUENCE OF THE SPACE-CHARGE FORCES ON THE MULTITURN INJECTION PROCESS 51
V.I INTRODUCTION 51
V.2 EXPERIMENTAL EVIDENCE FOR SPACE-CHARGE EFFECTS 51
V.3 CALCULATION OF SPACE-CHARGE EFFECTS AND THE LUMPED PARTICLE DISTRIBUTION 53
V.4 INVESTIGATION INTO THE CAUSE OF THE LARGE EFFECTIVE SEPTUM THICKNESS *DS* 56

CHAPTER VI: CONCLUSIONS 57

REFERENCES 59

APPENDIX I: CALCULATION OF *DI*, *DIP*, *AND* β_l FOR THREE-ANGLE PARTIAL ACCEPTANCE 62

APPENDIX II: CALCULATION OF *DI*, *DIP*, *AND* β_l FOR FOUR-ANGLE PARTIAL ACCEPTANCE 66

APPENDIX III: THE CALCULATION OF T_{IKS} 68

APPENDIX IV: EFFICIENCY CALCULATION 70

CHAPTER I

THE CERN PROTON SYNCHROTRON BOOSTER

I.1 INTRODUCTION

The Proton Synchrotron Booster (PSB) is a four-ring 800 MeV intermediate accelerator which was designed as the second stage of the improvement program initiated in 1964 for the 28 GeV/c Proton Synchrotron (PS) at CERN, Geneva. During a three-year period, 1973–76, the author was engaged in extensive studies to optimize the performance of this machine. As a part of these studies, a theory for the Multiturn Injection Process was conceived, which has been tested on the PSB. This is the subject of Chapter III. The method of increasing the injection efficiency, described in Chapter IV, is based on this theory.

The theory gives a good description of the injection process and could be used to define, more accurately than was previously possible, the required stability of the new Linac. At high injected beam intensities, space-charge forces are the main perturbations that cause deviations from the single-particle theory. Experiments done to estimate the influence of the space-charge forces on the PSB injection process are described in Chapter V.

To provide the necessary background information, a short history of the PSB is given in Chapter I, followed by a description of the parameters of the machine and of the measuring instruments used for the injection studies. In Chapter II the general accelerator principles needed for this study are discussed and various injection processes are explained, keeping in mind their application to the PSB.

I.2 A BOOSTER: WHY?

In 1965 the PS intensity was about 10^{12} protons per pulse[1]. At that time, and for a variety of reasons, there was a growing demand for increased beam intensity. In the first place it was essential for the study of interactions with low cross-sections, such as neutrino interactions and interactions yielding particles with high transverse momentum. Secondly, a higher beam intensity would facilitate the production of secondary particle beams with good intensity at higher energy. Finally, it would make the use of the PS more flexible, as more experiments could simultaneously be provided with a sufficient particle intensity. It was therefore envisaged to improve the repetition frequency of the PS by a factor of 2.5 to 3, depending on the cycle in use, and in addition to increase the intensity per pulse by a factor of 5.

The repetition rate was increased by installing a new main power supply and new accelerating cavities in the PS. A higher intensity per pulse was obtained by means of injection at a higher energy. The increase in intensity per pulse that can be obtained in this way can be calculated from Eq. (I.1)[2]. The equation gives the maximum number of particles N that can be accelerated per burst as a function of the machine parameters and the energy of the particles at injection:

$$N = CE_V(1+\sqrt{E_H/E_V})\tilde{B}_{PS}\beta^2\gamma^3 F \quad , \tag{I.1}$$

where

C is a constant which for the PS has the value $1.6 \times 10^{17}\,\mathrm{m^{-1}\,rad^{-1}}$;

E_H, E_V are the horizontal and the vertical emittances of the PS beam just after injection; the emittance is an important quantity for determining the maximum beam size, and is defined in Section II.1;

$\tilde{B}_{PS}$ is the bunching factor which enters into Eq. (I.1) because, during acceleration, bunches are formed (20 in the PS); this implies higher particle concentrations locally than with an unbunched coasting beam ($\tilde{B}_{PS} \approx 1/3$);

β is the velocity of the particle at injection divided by c, the velocity of light;

γ is the relativistic parameter $\sqrt{1/(1-\beta^2)}$;

F is a factor (≈ 1) to correct for image forces arising from the conducting vacuum chamber walls and the magnetic pole faces.

From this equation it can be seen that to increase the maximum PS intensity, E_H or E_V might be increased, but this would mean a total reconstruction of the CERN PS. The bunching factor $\tilde{B}$ is determined by the cycle time and the accelerating voltage at the RF cavities. The only practical way to obtain a higher pulse intensity is by injection at higher energies, as this increases the factor $\beta^2\gamma^3$.

Design studies showed that an increase by a factor of 5, which was to be expected when the injection energy was increased from 50 MeV to 200 MeV, could indeed be obtained with a 200 MeV injector Linac. The same result could be obtained by introducing an intermediate accelerator — a Booster — between the 50 MeV Linac and the PS. After a careful study of the relative merits of these two alternatives, it was finally decided to build a Booster Synchrotron, but of somewhat higher energy, 800 MeV. The reasons for this choice will be discussed in Section I.4.

I.3 DESCRIPTION OF THE 800 MeV BOOSTER

The Booster is a four-ring vertically-stacked proton synchrotron. Some of the design parameters are given in Table I.1. Its place in the PS accelerator complex is shown in Fig. I.1. The Linac produces a proton beam of 50 MeV with a pulse length of 100 μs. This beam can be injected either directly into the PS or into the PSB. The injection into the PSB and the recombination of the beams accelerated in the four rings will now be described in some detail.

Table I.1
Parameters of the 800 MeV Booster Synchrotron[3)]

Injection energy	50 MeV
Ejection energy	800 MeV
Number of rings	4
Number of bunches per ring	5
Acceleration time	620 ms
Design intensity	2.5×10^{12} protons per ring per pulse
Q_H value range[a)]	4.0–5.0
Q_V value range[a)]	4.0–5.5
Radius	25 m
Magnetic field at ejection	0.6 T
Vacuum pressure	2×10^{-8} Torr

a) Q_H,Q_V are defined in Section II.1 and represent the number of vertical or horizontal oscillations a particle will make during one revolution period.

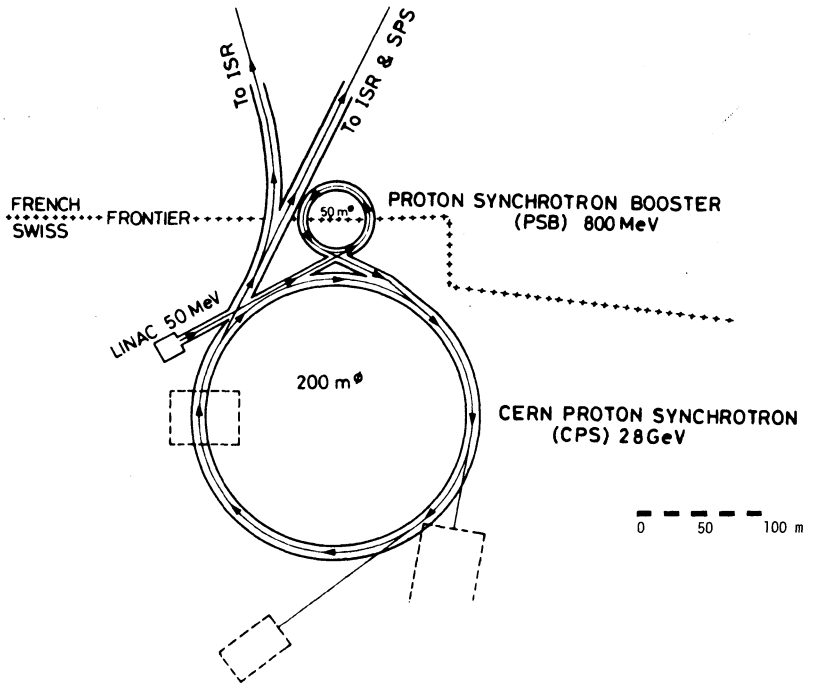

Fig. I.1 PS accelerator complex (from Ref. 1).

Before the beam enters the PSB, it is split vertically into four separate beams by a fast vertical distribution magnet (see Fig. I.2). The vertical divergence of these beams is increased by three vertical septum magnets, after which three vertical bending magnets align the beam horizontally into the levels of the four rings. The four superimposed beams are simultaneously accelerated to 800 MeV in about 620 ms. Each ring contains five bunches.

The four rings are synchronized such that the 4×5 bunches can be ejected successively with equal energy and equal time intervals between all the bunches (Fig. I.2), so that after the injection into the PS the 20 bunches are equally spaced along the circumference of the PS ring.

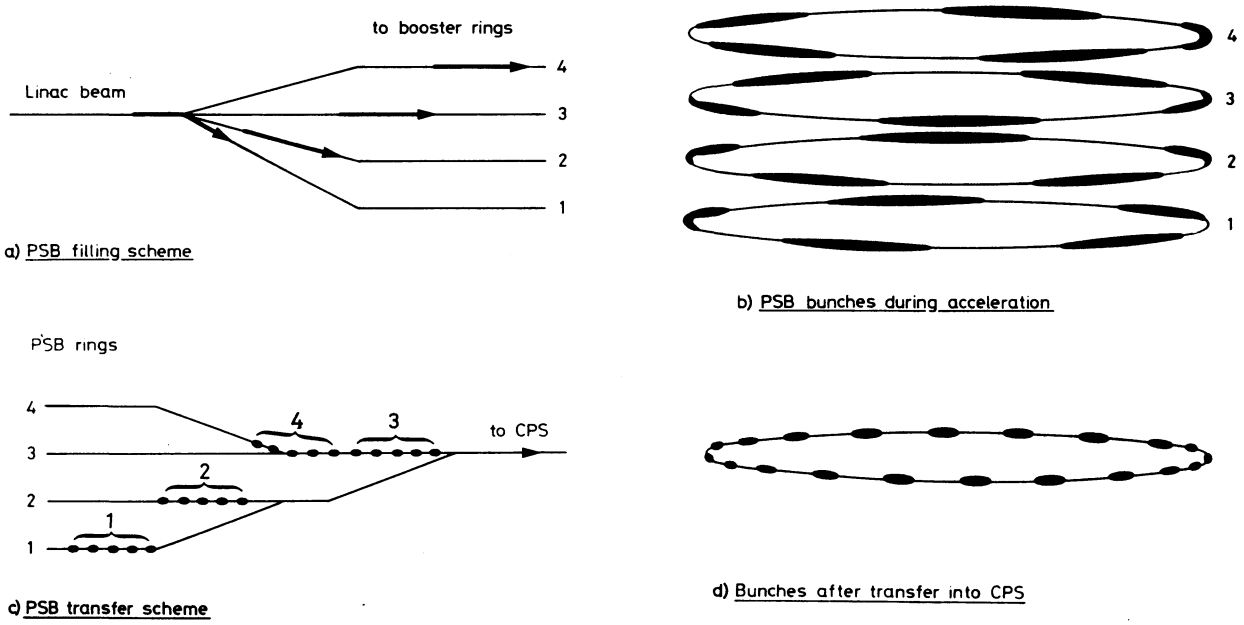

Fig. I.2 Injection into the PSB and the PS: sequence of events (schematic) (from PSB handbook[1]).

The recombination takes place by bending beam 4 towards beam 3 with the aid of a bending magnet. If the two beams are close enough, the angle between them is reduced with the aid of a septum magnet, and the final alignment of the two levels is done with a fast-pulsing vertical kicker magnet. Beams 1 and 2 and beams 1 + 2 and 3 + 4 are recombined in a similar manner.

In Fig. I.3a the relative position of the PSB with respect to the PS is shown, while in Fig. I.3b the superposition of the four PSB rings can be seen.

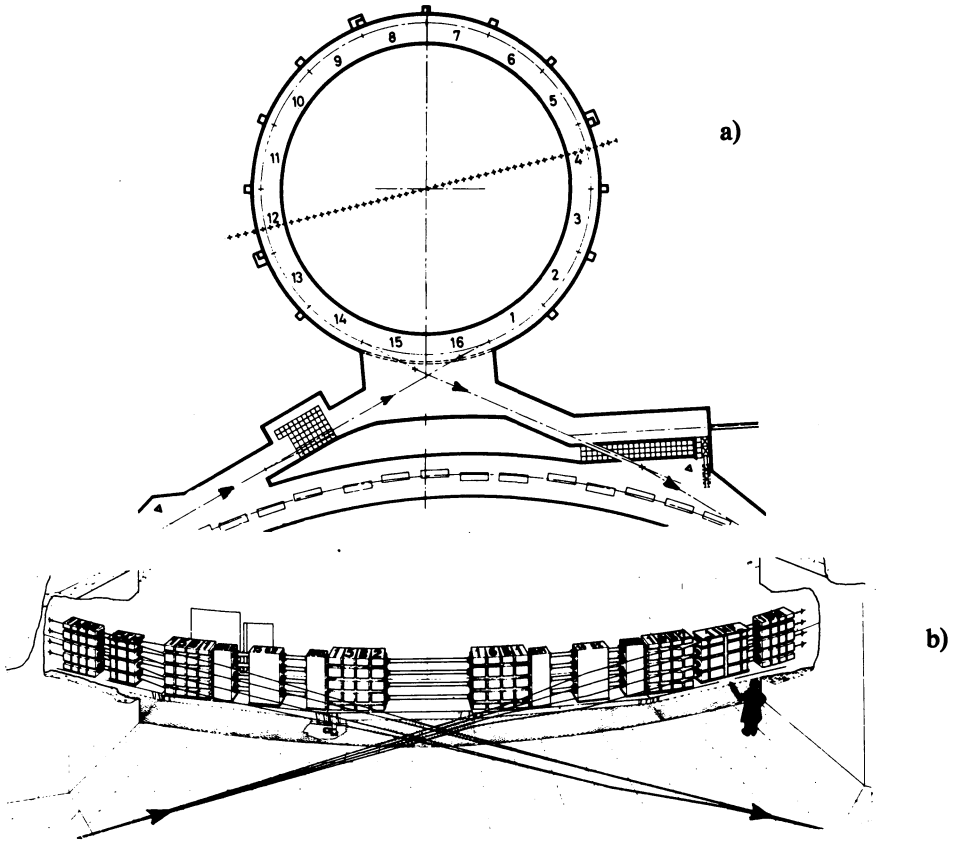

Fig. I.3 a) Plan view of the Booster in relation to the PS. The centre line of the ring is on the Franco-Swiss frontier. The numbers refer to the periodicity of the magnet structure[1].
b) Perspective view of the injection and extraction section of the Booster. B is a bending magnet; EM an ejection magnet; Q a quadrupole focusing magnet; and INF an inflector[1].

The PSB was constructed during the years 1968–72. The first injection into the PSB and the consecutive acceleration to 800 MeV of 5×10^{10} protons per pulse took place in May 1972. At the end of 1972, the first acceleration of particles injected from one PSB ring had taken place in the PS, and the recombination had been tested. At the end of 1973, the PSB was run as the PS injector during normal operation, and PS intensities of $5–6 \times 10^{12}$ protons per pulse were obtained[1,4].

In 1974 the 50 MeV Linac current was improved to 85 mA within the stability limits demanded by the Booster. However, owing to the stability problems in the Linac at high intensities, it was decided to build a new Linac adjacent to the old one. To have rebuilt the old Linac would have been just as expensive and would have meant a very long shutdown for the PS. At the end of 1974, 10^{13} protons were for the first time accelerated to 6 GeV in the PS. By the end of 1975 the design performance of 10^{13} protons per pulse within the required beam dimensions was achieved[4].

In 1980, with the introduction of the new Linac combined with several other improvements in the PSB, 2×10^{13} protons per pulse were accelerated to 800 MeV.

I.4 REASONS FOR CHOOSING AN 800 MeV BOOSTER

The first design for a PS Booster emerged as part of a study program for a 300 GeV accelerator. It was the so-called TART system[5], consisting of a two-ring, horizontally interlaced accelerator. When its merits were compared with those of a 200 MeV Linac, it turned out that for the same cost the TART system provided a more flexible instrument than did the 200 MeV Linac, so that the further studies were concentrated on the design of a Booster to increase the PS intensity.

The condition already mentioned in Section I.3, that it should be possible to inject into the PS either directly from the Linac or via the PSB, had important consequences for the design of the PSB, as the transverse properties of the PS beam at the end of the acceleration cycle should be independent of the mode of injection. Any change in the horizontal or vertical emittance (E_H or E_V) of the beam would affect the efficiency of the ejection system and the properties of the secondary beams[6–8].

In Section II.1 it is shown that throughout the acceleration E_H and E_V of the PS beam change according to the formula

$$E_{H,V}\beta\gamma = \text{const}, \tag{I.2}$$

where β and γ are the relativistic parameters of the beam particles. As E_H and E_V are required to have fixed values $E_H(T_{max})$ and $E_V(T_{max})$ when the PS beam particles have the maximum kinetic energy T_{max}, the values of the beam emittances required at any lower kinetic energy T are given by

$$\begin{aligned} E_H(T)(\beta\gamma)_T &= E_H(T_{max})(\beta\gamma)_{T_{max}}, \\ E_V(T)(\beta\gamma)_T &= E_V(T_{max})(\beta\gamma)_{T_{max}}. \end{aligned} \tag{I.3}$$

Formula (I.1) gives the number of particles of kinetic energy T that can be accepted in the PS inside emittances E_H and E_V. Substituting these emittances from Eqs. (I.3), one finds the maximum number of particles which, when injected at kinetic energy T, lie inside $E_H(T_{max})$ and $E_V(T_{max})$ when they have been accelerated to the maximum energy T_{max}:

$$N = CE_V(T_{max})\frac{(\beta\gamma)_{T_{max}}}{(\beta\gamma)_T}\left[\sqrt{1+\frac{E_H(T_{max})}{E_V(T_{max})}}\right](\beta^2\gamma^3)_T\tilde{B}_{PS}F \quad . \tag{I.4}$$

Therefore, to obtain an improvement of at least a factor of 5 in the number of particles per burst accelerated to T_{max}, the injection energy T should be sufficiently increased, with respect to the former injection energy of 50 MeV, to satisfy the relation

$$(\beta\gamma^2)_T/(\beta\gamma^2)_{50} \geq 5. \tag{I.5a}$$

A choice had to be made between a slow-cycling Booster or a fast-cycling Booster. To explain the difference, some of the properties of these two possible Booster-PS systems have to be discussed.

The total number of particles that can be accelerated in a synchrotron is independent of the radius. An increase in PS beam intensity can therefore be obtained only if the Booster can accelerate more than one batch of particles for every PS cycle.

A fast-cycling Booster is a one-ring Booster in which n_B batches of particles are accelerated to the injection energy of the PS and transferred, in n_B successive acceleration cycles of the Booster, to the PS. When all n_B batches are stacked in the PS, acceleration can take place.

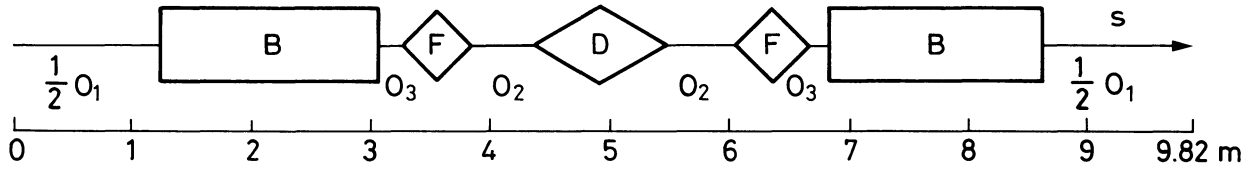

Fig. I.4 Schematic diagram of one magnet period of a PSB ring[3], B is a bending magnet; F and D are focusing and defocusing quadrupoles, respectively; O_1, O_2, and O_3 are field-free regions.

A slow-cycling Booster consists of n_B rings in which n_B particle batches are accelerated simultaneously and transferred to the PS within a time interval of the order of one PS revolution.

It was decided to build a slow-cycling synchrotron because it is cheaper[6–8], its bunching factor is higher (bunches are longer), and there are no long waiting-times during the filling of the PS, with all its attendant difficulties.

The bunching factor in the PSB ($\tilde{B}_B$) is different from the bunching factor in the PS ($\tilde{B}_{PS}$), i.e. $\tilde{B}_{PS} \approx 1/3$ while $\tilde{B}_B \approx 1/2$, which means that the ratio $\tilde{B}_B/\tilde{B}_{PS} \approx 1.5$. The differences in all other constants are an order of magnitude smaller. To obtain the improvement factor of 5 which can be accepted in the PS according to formula (I.5a), the following condition should be obeyed:

$$n_B\tilde{B}_B/\tilde{B}_{PS} \geq 5. \tag{I.5b}$$

As $n_B\tilde{B}_B/\tilde{B}_{PS}$ cannot be made large enough for a two-ring Booster, the three-ring and four-ring Boosters, each with one-turn ejection, were considered as serious candidates. More rings complicated the design of the machine too much.

It was readily decided to stack the rings vertically. Otherwise the rings must be interlaced horizontally, which leads to unwanted beam-beam interactions. When the rings are vertically stacked, more space is available for ejection, injection, and correcting devices[7].

A disadvantage of the three-ring type is that 21 bunches have to be accelerated, of which one bunch is lost because only 20 bunches are accepted in the PS.

These considerations, combined with the results of a design study for obtaining optimum ISR performance, led to the decision to build a four-ring, vertically stacked Booster with an ejection energy of 800 MeV[9–12]. Many possibilities were considered[13,14], with the restrictions $R_B = R_{PS}/4 = 25$ m, and five bunches per ring. In the design that was finally selected, $n_B\tilde{B}_B/\tilde{B}_{PS} \approx 6$ and $(\beta\gamma^2)_{800}/(\beta\gamma^2)_{50} \approx 8.5$. The latter factor was chosen somewhat larger than is strictly necessary so as to permit the injection, without loss of efficiency, of PS beams with unusual geometrical properties that are sometimes required for special-purpose ISR beams. An additional advantage is the future possibility of a further increase in the PS beam intensity.

A complete description of the final design is given elsewhere[3]. The total number of magnet periods in the ring is 16, and each period has the configuration shown in Fig. I.4. The tuning range of the PSB is $4 \leq Q_H \leq 5$, $4 \leq Q_V \leq 5.5$. The magnetic field could be kept low: 0.6 T at ejection. The vacuum is typically 2×10^{-8} Torr.

One period of a PSB ring consists of two bending magnets (B), two focusing quadrupole magnets (F), and one defocusing magnet (D). The straight sections have three different lengths (O_1, O_2, and O_3). The total length of one period is 9.82 m.

I.5 THE RELEVANCE OF THIS WORK TO THE PERFORMANCE OF THE PSB

When the work described here was started, the hope existed that, by increasing the knowledge of the influence of the parameters for the injection into the PSB, a method might be found to increase the intensity of the beam injected into the PSB. This increased injection efficiency must be obtained without seriously deteriorating the efficiency of other processes in the chain, in particular the injection efficiency into the PS which depends dramatically on the transverse dimensions of the beam in the PSB.

To understand thoroughly the interdependence of these efficiencies a much better understanding of the injection process, i.e. its detailed dependence on all the variables involved, was required. Improved knowledge might also help to reduce the setting-up time for the injection systems by eliminating the lengthy trial-and-error method needed to obtain the wanted beam quality.

Several computer programs were available to study the behaviour of the injection process:

i) A simulation program to calculate the injection efficiency for a given horizontal emittance as a function of eight adjustable injection parameters. However, the determination of the right values of these eight parameters for the optimum injection efficiency was a long and cumbersome process and gave very little insight into the way in which the optimum was obtained.

ii) A second simulation program to show the influence of the space-charge forces on the multiturn injection efficiency. This program solved, with the aid of a fast Fourier transform, the Poisson equation for the particle distribution in

the PSB, taking into account the conducting wall of the vacuum chamber. However, the detailed operation of this program was so hard to understand that it was very difficult to draw reliable information from it.

It seemed worthwhile to try and find a reliable formalism that would express the optimized injection parameters as a simple function of the parameters of the incoming beam and the accelerator. Several interesting qualitative ideas for improvements in existing optimization procedures were available, but none of them had been worked out quantitatively. The model presented here includes the following improvements:

i) a better insight into the influence of the value of the parameters on the multiturn injection efficiency,
ii) a possibility for application to other accelerators,
iii) some information about the influence of space-charge forces.

In parallel with the development of the model, an extensive program of experiments was set up to verify the underlying assumptions. From this emerged naturally a simple setting-up procedure. Differences between theory and practice pointed to eventual improvements in the theory or in the PSB setting. Another nice result was the information that was obtained about the value of the parameters required for the new Linac, concerning pulse length and stability in transverse and longitudinal planes which are dependent on the intensity of the beam.

I.6 SOME INSTRUMENTATION IN THE PSB

The instrumentation described in this section is that used for the multiturn injection studies during the period 1973–76. Since then new facilities have been added.

I.6.1 Beam-current transformers

A beam-current transformer consists of an annular core of high permeability magnetic tape, with n windings around it. The proton beam which passes through the core acts as a single-turn winding with current I_1, giving from n windings on the core an output of $I_2 = I_1/n$. Two types of transformers are used for multiturn injection studies:

- a fast transformer: 6 windings, bandwidth 100 MHz to 100 kHz,
- a slow transformer: 1000 windings, bandwidth 10^{-4} to 10 kHz.

They are installed in the same position in each ring[15].

The fast transformer is used for measuring the high-frequency time structure. The slow transformer has a large number of windings and is used, combined with an integrator wide-band amplifier, for low-frequency high-precision measurements. They are shielded against external magnetic fields, high-frequency magnetic fields, and low-frequency electrostatic fields. The signal of the slow beam transformer can be digitized at any moment during the cycle and is processed by the computer to give the number of protons in the ring.

There are also beam transformers in the injection line to measure the intensity time structure of the injected current. Their signal is integrated to obtain the total number of protons injected into a Booster ring.

I.6.2 Pick-Up electrodes in the PSB[16]

The purpose of the Pick-Up electrodes is the measurement of the form and the position of the closed orbit plus the eventual misalignment of the beam with respect to this closed orbit at injection. They are also needed for the measurement of the Q_H and the Q_V value of the beam[17,18].

The Pick-Up electrode is an electrostatic type of beam-position sensor containing pairs of ΔV and ΔH electrodes for vertical and horizontal position monitoring and a Σ electrode to measure the total charge. The electrodes for one Pick-Up station are designed such that their total area is small enough to put them together in the centre of a multipole correcting magnet[19].

Sixteen of these position sensors are available in each ring. The signal of each pair of electrodes is sent to the Main Control Room.

The differences between the charges induced on the pair of plates is a linear function of the beam displacement and the beam current. The total charge measured with the Σ electrode is used for the normalization of the position signals. In order to visualize simultaneously the position of the beam in the two planes of one ring at the location of the 16 Pick-Up stations, the signals are digitized and displayed on a console screen. Several integration times are provided according to the specific wishes of the user. Thus facilities exist for the measurement of the position of the beam during one turn or for the measurement of the closed orbit with several integration times. As the Pick-Up electrodes are placed inside the multipole magnets, all magnetic materials have been avoided in their construction.

To measure the Q_H value in the PSB the beam is deflected by a fast pulsing magnet, the Q kicker[20]. The coherent betatron oscillations excited in this way are observed by means of the Pick-Up electrodes. The ΔH signal of one station contains the frequency $f_H = |m_H - Q_H| f_{rev}$, where m_H is the integral part of the Q_H value and f_{rev} the revolution frequency. The number m_H must be derived from the currents in the focusing elements. To measure the function f_H the ΔH signal of the Pick-Up station is sent through a tuneable filter, so that the signal $0.55 f_{rev} \leq f_H \leq 0.95 f_{rev}$ is filtered out. This choice provides a sufficiently strong signal and a frequency range which is not too high. By measuring the f_{RF} value at the cavities, $f_{rev} = 0.2 f_{RF}$ is determined (5 bunches, see Section I.3). With the aid of f_H and f_{rev} the Q_H value can be determined. The same principle is used for the measurement of the Q_V value.

In one acceleration cycle 64 measurements can be made at minimum intervals of 3 ms. The kickers for either the horizontal or the vertical plane are kicked in all four rings simultaneously. The kick strength during the cycle is programmed such that the kick angle (0.21 mrad) stays constant during the whole acceleration period. The kick length is also programmed such that $\Delta t/\tau = 0.7$ (Δt = kick length, τ = revolution period). This means $\Delta t = 1.17\ \mu$s at 50 MeV and $\Delta t = 435$ ns at 800 MeV. Rise- and fall-times of about 80 ns are required. The number of measurements wanted, the interval between the measurements, the start of the measurements, and the choice of ring and plane can all be determined from the Main Control Room.

I.6.3 Scintillation screens[16)]

At the time of the multiturn injection measurements, the position of the beam in the injection line was measured with scintillation screens. These are mounted at critical points in the line to observe the position and the transverse form (envelope) at these points. They combine a good image with a good radiation resistance and low outgassing.

The image is recorded by a TV camera and sent directly to TV screens mounted in the Main Control Room. The precision is limited to ± 2 mm owing to interpretation problems and imperfections in the supporting structure[21)].

Later magnetic position monitors have been installed in the injection line[22)]. The beam trajectory is visualized at the main console graphic screen.

I.6.4 The apparatus for the measurement of the emittance of the 50 MeV beam of the Linac[23)]

For the measurement of the emittance of the Linac beam at 50 MeV, the beam is sent through a vertical slit so that a certain part of the beam is intercepted and only a beam of a certain horizontal width Δx is admitted. The beam slice passes through a quadrupole doublet, which is adjusted such that the measuring device — a horizontal line of Faraday cups plus grid — finds itself in the focal plane. Each Faraday cup and associated electronics is constructed such that a signal is given as soon as the collected charge surpasses an adjustable threshold. There are twenty cups, from which every 0.5 μs a signal pattern can be extracted. In front of the slit two kickers are placed which move the beam parallel to itself in the horizontal direction. One sweep of the beam in front of the slit takes 10 μs. An acquisition of the above described signal every 0.5 μs yields a 20 × 20 matrix with on the vertical axis (the line of Faraday cups) the divergence, and on the horizontal axis (the horizontal sweep of the beam in time) the position with respect to the beam centre. The line enclosing all the points for which the number of particles exceeds a certain threshold can be approximated by an equidensity ellipse in the horizontal phase plane. The same can be done for the vertical plane by a vertical movement of the beam in front of a horizontal slit and turning the line of Faraday cups through 90°. By varying the adjustable threshold one obtains a plot of the particle density in the phase plane versus the beam emittance.

I.6.5 The apparatus for the measurement of the energy dispersion of the 50 MeV beam of the Linac[16)]

By using a vertical bending magnet with edge focusing and a bending radius of 1.2 m the Linac beam is bent upwards through 54°. A detector consisting of nineteen secondary emitting nickel strips 1 mm wide, separated by 0.2 mm, is placed in the image of the slit. The resolution can be varied by turning the device. The best resolution, 30 keV, is obtained at an angle of 25° to the normal axis. The strips are sandwiched between two aluminium foils with a 100 V bias with respect to the strips to collect the emitted electrons. The output signals of the nineteen strips are displayed in histogram form on a TV screen mounted in the Main Control Room. The time of the measurement can be determined at will. Each measurement takes 0.5 μs, which is short compared to the beam length of 100 μs.

I.6.6 BEAMSCOPE[24,25)]

The BEAMSCOPE permits the measurement of the particle distribution in the PSB beam. With the aid of three dipole magnets, a well localized closed-orbit distortion is created that brings the beam onto scrapers. All particles with transverse oscillation amplitudes larger than the distance from beam centre to scraper edge are lost. When the current of the dipoles is changed linearly with time (first part of a sine function) a certain loss pattern will be observed on the slow beam transformer. The differentiated signal is proportional to the loss rate of the beam and this again is proportional to the betatron amplitude distribution. This device is very useful in determining relatively fast changes in the amplitude distribution of the beam, which gives some insight into the mechanism of some of the beam blow-ups observed in the PSB.

I.6.7 The PSB target system[16)]

The beam size is important for the Booster-PS transmission efficiency and is an indication of the quality of the beam. The booster target system provides more accurate information about the beam size than the BEAMSCOPE.

To measure the horizontal width and horizontal position of the beam a target system is used consisting of two arms, one of which can be shot quickly into the beam from the inside and the other simultaneously from the outside. First the position of the inside arm is adjusted by observing the slow beam transformer signal until exactly 5% of the beam is lost. This operation is then repeated with the outside arm.

The average of the final positions of the arms gives the position of the centre of the beam, the difference of the positions its horizontal width. The vertical position and vertical width of the beam are determined in the same way with a second target system.

The plunging and extraction of the target arms takes place with a controlled velocity. The time from fully out to fully in and vice versa amounts to 45 ms. The targets stay in for 15 ms. Owing to changes in the betatron amplitude during acceleration, precisions of $\pm 1\%$ horizontally and $\pm 4\%$ vertically are obtained[26].

CHAPTER II

PHASE-PLANE TRAJECTORIES IN ALTERNATING-GRADIENT PROTON SYNCHROTRONS

II.1 BASIC ACCELERATOR THEORY

In this chapter the parameters used for the description of the particle behaviour in the synchrotron are described in some detail.

An accelerator has a periodical structure, as a certain magnet configuration is repeated along the circumference of the machine. This means that the particle trajectories in the accelerator can be calculated when the properties of one unit cell are known.

In the accelerator an equilibrium orbit (closed orbit) exists which is a particle trajectory that is closed. When no perturbation is present, the closed orbit coincides with the symmetry axis of the magnetic fields. Around this path the real beam particles will oscillate with a certain amplitude and frequency in the horizontal (x) and the vertical (z) direction (betatron oscillations). This motion will be discussed in Section II.1.1.

The particles are accelerated by the RF cavities, which produce electric fields. Their variation with time has the form of a sine function. During the acceleration of the particles the accelerating field radio frequency (RF) and the magnetic field must be precisely adjusted with respect to each other to keep the beam in the centre of the vacuum chamber. With respect to the RF a stable phase ϕ_s exists, around which the phase ϕ of the particle will perform synchrotron oscillations. This subject will not be treated here as it is not essential to the understanding of the multiturn injection process.

The formulae derived in this chapter will establish a consistent notation to be used throughout this work and will form the basis for the discussion in the following chapters. The particle trajectory will be described in the six-dimensional space (x, x', z, z', ϕ, ϕ'), where x, z, and ϕ are the coordinates of the particle with respect to the equilibrium orbit and the RF phase. The prime denotes differentiation with respect to s, the coordinate along an equilibrium orbit. The motion of a particle can be decoupled into motions in the horizontal, vertical, and longitudinal phase planes separately, as the accelerator is constructed such that forces which might couple these motions are as small as possible.

II.1.1 Transverse particle motion

The motion of the particle with respect to the equilibrium orbit is described by the coordinates x and z, for the horizontal and vertical motions, respectively. When the formulae apply to the transverse motion in general, either horizontal or vertical, the coordinate y is used.

The Lorentz force acting on a particle which moves on an equilibrium orbit through quadrupole fields is given by

$$\begin{aligned} \frac{dp_z}{dt} &= +ev\frac{\partial B_x(s,z)}{\partial z}z \\ \frac{dp_x}{dt} &= -ev\frac{\partial B_z(s,x)}{\partial x}x \quad , \end{aligned} \tag{II.1}$$

where v is the component of the particle velocity along the machine circumference. The corresponding longitudinal momentum component will be denoted by p. Assuming that no acceleration takes place and using the variable s, a periodic function $K_y(s)$ can be defined:

$$K_z(s) = -\frac{e}{p}\frac{\partial B_x(s,z)}{\partial z} \quad , \quad K_x(s) = \frac{e}{p}\frac{\partial B_z(s,z)}{\partial x} \quad . \tag{II.2}$$

The equation of motion of a particle around the equilibrium orbit in an accelerator can be given by [27]

$$d^2y/ds^2 = -K_y(s)y \quad , \qquad K_y(s+L) = K_y(s) \quad , \qquad L = C/N \quad , \tag{II.3}$$

where

N = number of unit cells in the accelerator

C = circumference of the accelerator.

Equation (II.3) is a type of Hill's equation. For special functions $K_y(s)$ the solutions are bounded and can be described by a pseudoharmonic oscillation with periodically varying amplitude. They can be written in the form

$$y(s) = aw(s)\cos\{\psi(s) + \chi\}, \tag{II.4}$$

where a and χ are arbitrary constants determined by the initial conditions.

The functions $w(s)$ and $\psi(s)$ must satisfy the equations:

$$\frac{d^2w}{d^2s} + K_y w - \frac{1}{w^3} = 0 \tag{II.5}$$

and

$$d\psi/ds = 1/w^2. \tag{II.6}$$

This is easily verified by substituting Eq. (II.4) into Eq. (II.3).

The particle accelerator must be constructed such that the function $K_y(s)$ generates bounded solutions for the particle trajectories. The function $w(s)$, which is solely determined by $K_y(s)$, is periodic with period L and independent of the initial conditions of the particle. The function $\psi(s)$ is in its turn determined by $w(s)$.

The functions $w(s)$ and $\psi(s)$ are, of course, different for the horizontal and the vertical motion. Only when there is a cause for confusion will an extra index be used.

Instead of $w(s)$ the function

$$\hat{\beta}(s) = w^2(s) \tag{II.7}$$

is commonly used in accelerator theory. In terms of $\hat{\beta}(s)$ the solution (II.4) takes the form

$$y(s) = a\sqrt{\hat{\beta}(s)}\cos\{\psi(s) + \chi\}, \tag{II.8}$$

where, according to Eq. (II.6),

$$\psi(s) = \int_0^s \frac{ds^*}{\hat{\beta}(s^*)}. \tag{II.9}$$

A very important parameter is the number of betatron oscillations Q per complete revolution:

$$Q = \{\psi(C + s) - \psi(s)\}/2\pi. \tag{II.10}$$

Using Eq. (II.9), the Q values for the horizontal and vertical motions, Q_H and Q_V, respectively, can be expressed in the form

$$Q_H = \frac{1}{2\pi}\int_0^C \frac{ds}{\hat{\beta}_H(s)} \tag{II.11}$$

$$Q_V = \frac{1}{2\pi}\int_0^C \frac{ds}{\hat{\beta}_V(s)}. \tag{II.12}$$

The function $\hat{\beta}(s)$ can therefore be described as the instantaneous betatron wavelength of the transverse particle motion divided by 2π.

II.1.2 Emittance and acceptance

So far only the transverse motion of a single particle with respect to the closed orbit has been considered. A particle beam in the accelerator consists of many particles, all moving according to Eq. (II.8), but with different initial conditions. The behaviour of the particle beam as a whole can be conveniently described in terms of the image points (y, y') of the particle trajectories in the transverse phase plane.

Two new functions $\hat{\alpha}(s)$ and $\hat{\gamma}(s)$ are defined:

$$\begin{aligned} \hat{\alpha}(s) &= -\hat{\beta}'(s)/2 \\ \hat{\gamma}(s) &= \{1 + \hat{\alpha}^2(s)\}/\hat{\beta}(s). \end{aligned} \tag{II.13}$$

Together with $\hat{\beta}(s)$ the functions $\hat{\alpha}(s)$ and $\hat{\gamma}(s)$ are called the Twiss parameters.

It can be shown by direct substitution of the general solution (II.8) that for each individual beam particle the expression $\hat{\gamma}y^2 + 2\hat{\alpha}yy' + \hat{\beta}y'^2$ has a constant value a^2 throughout the motion. The equation

$$I(y, y') = \hat{\gamma}(s)y^2 + 2\hat{\alpha}(s)yy' + \hat{\beta}(s)y'^2 = a^2 \tag{II.14}$$

is the equation of an ellipse in the (y, y') plane. The area πa^2 of the ellipse is determined by the initial conditions of the particle considered. $I(y, y')$ is called the Courant-Snyder invariant[27]. The area of the ellipse is independent of s, but its form and orientation depend on $\hat{\beta}(s)$ and are thus determined by the magnet configuration. The change in form and orientation along the machine circumference is consequently periodic with period L.

To a certain beam particle and a fixed point p on the machine circumference corresponds one fixed ellipse in a phase plane. After each machine revolution the image point of the particle reappears at p on this same ellipse, but in general with a different phase.

The beam particle with the largest oscillation amplitude at any given point around the machine circumference lies on the ellipse with the largest area. This ellipse envelops the image points of all other beam particles. The area defined by this ellipse is called the emittance E of the beam. Therefore one can write:

$$E = \pi a_{\max}^2. \tag{II.15}$$

The emittance is the area in the phase plane within which all beam particles lie. Together with $\hat{\beta}(s)$ the beam width is determined at every point s along the machine circumference. In Fig. II.1 the ellipse is shown that corresponds to the particle with $I(y, y') = a_{\max}^2$ at a point s. The maximum amplitude and thus half the beam diameter (y_m) at s is given by[28]

$$y_m = a_{\max}\sqrt{\hat{\beta}(s)} = \sqrt{\frac{E\hat{\beta}(s)}{\pi}}. \tag{II.16}$$

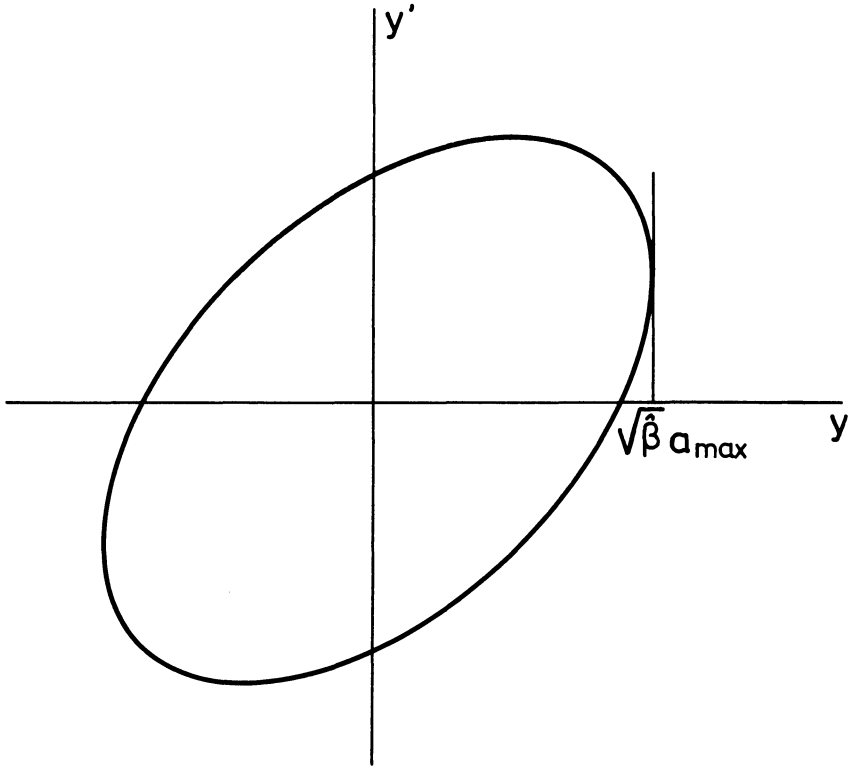

Fig. II.1 Courant-Snyder ellipse in (y, y') phase space. $\sqrt{\beta}\, a_{\max}$ is the maximum amplitude for a particle moving on the ellipse at this particular point in the accelerator.

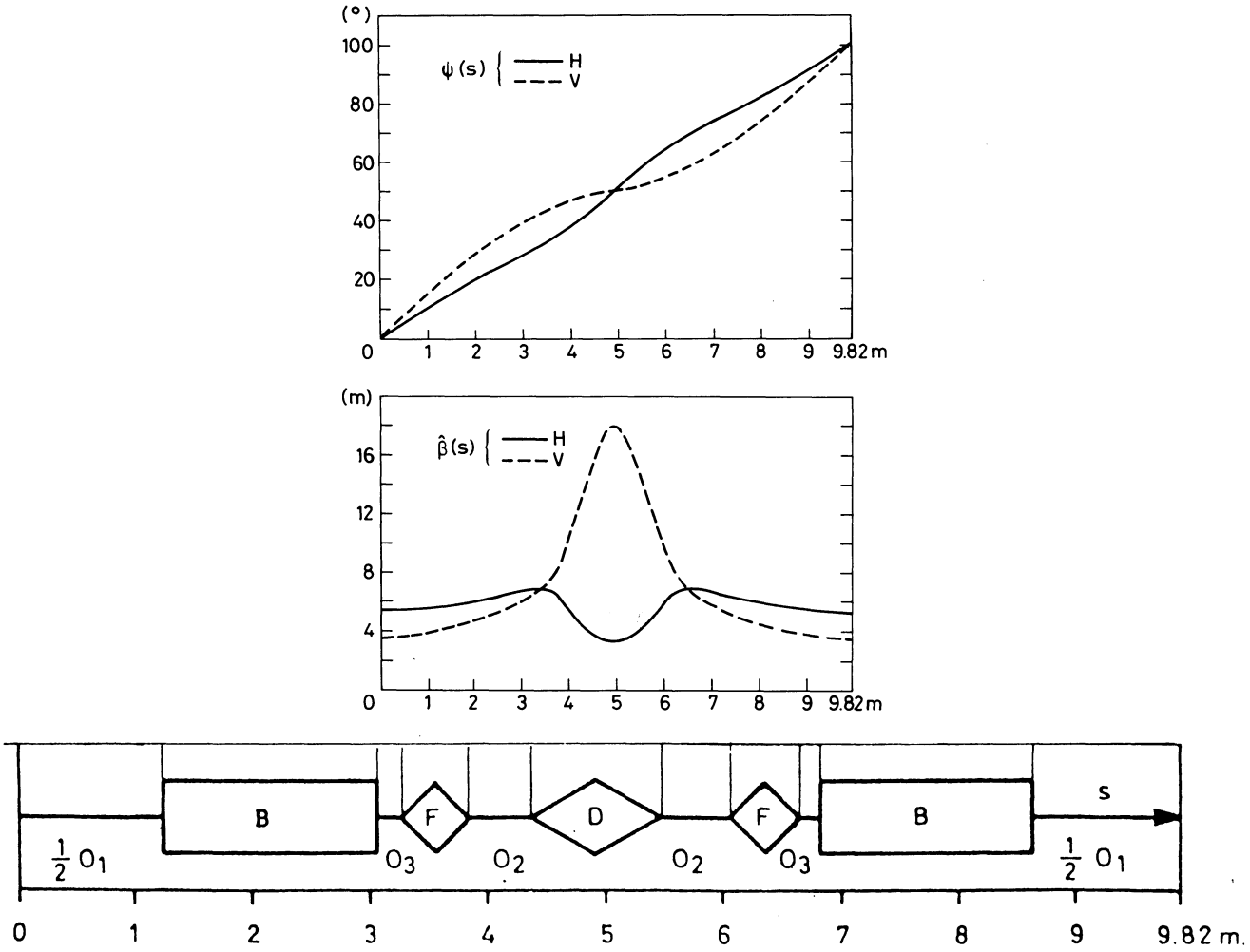

Fig. II.2 Phase advance $\psi(s)$ and betatron functions $\beta_H(s)$ and $\beta_V(s)$ along one PSB period[3].

The admittance (or acceptance) A of the accelerator is the largest area in phase space that can be accepted in the machine. When $r(s)$ is the smallest of the distances between the equilibrium orbit and the opposite walls of the vacuum chamber, a particle can only be accepted if

$$a\sqrt{\hat{\beta}(s)} < r(s) \quad \text{or} \quad a < r(s)/\sqrt{\hat{\beta}(s)} \quad .$$

From this it follows that

$$A = \min\left\{\frac{\pi r^2(s)}{\hat{\beta}(s)}\right\} \quad , \quad 0 \leq s \leq NL \quad . \tag{II.17}$$

In Fig. II.2 the functions $\hat{\beta}_H(s)$, $\hat{\beta}_V(s)$, $\psi_H(s)$, and $\psi_V(s)$ are plotted for one period of the PSB. The effect of Eq. (II.9) can be clearly seen: the phase advance $\Delta\psi$ per unit length increases when $\hat{\beta}$ decreases. In the lower part of the figure the magnet configuration of the PSB unit cell is shown on the same s scale.

From the ψ plot the Q_H and Q_V values of the machine can be derived. According to the figure, the phase advance $\Delta\psi$ per unit cell is 104° for both the horizontal and the vertical phase plane. There are 16 unit cells in the PSB and thus one obtains

$$Q_V = Q_H \approx \frac{16 \times 104}{360} \approx 4.62 \quad .$$

II.1.3 Instability regions

The formulae derived in this section are only valid when there is no coupling between the horizontal and the vertical motion and when Eqs. (II.3) apply. In an actual accelerator neither of these conditions is fulfilled, because higher order perturbation fields are present.

It can be shown that, even when the horizontal and vertical motions are completely decoupled, the motion is unstable when the value of either Q_H or Q_V is integral or half-integral, because in that case the transverse motion is in resonance with the recurrence of the magnetic field errors.

When, in addition, a residual coupling between the horizontal and vertical motions is present, instabilities may occur for any pair of values of Q_H and Q_V for which

$$n_1 Q_H + n_2 Q_V = n_3, \tag{II.18}$$

where n_1, n_2, and n_3 are positive or negative integers. It depends on the individual properties of each particular accelerator whether for a given set of values of n_1, n_2, and n_3 the motion is really unstable. In Fig. II.3 a Q_H–Q_V diagram is shown with the most important resonance lines observed in the PSB.

When no correcting lenses are available it is important to stay away from these lines. As the PSB is built up of 16 periods, the 16th harmonic is consequently present. Nevertheless the line $3Q_V = 16$ is partially compensated, as is $Q_H + 2Q_V = 15$ [29,30].

In the same figure the PSB working point used during the multiturn injection studies (1973–76) is shown. From the point A (injection) the working point moves to B in $\approx$20 ms. From there it moves in $\approx$ 600 ms to point C (ejection). The reasons for programming the working point in this way will be explained in Chapters IV and V.

After the installation of the correcting elements in the PSB and the use of other techniques to improve the beam intensity[30], another working point was chosen which in 1980 permitted the acceleration of 2×10^{13} protons to 800 MeV. From the point A' the working point moves in 100 ms to the point B'; ejection takes place after 600 ms at point C.

Finally a remark should be made on the evolution of the emittance of the beam during the acceleration of the particles. At the end of Section II.1 the remark was made that, owing to the machine design, no appreciable coupling exists between the horizontal, vertical, and longitudinal components of the particle motion. The particles therefore move in each of the transverse planes under the influence of only the linear focusing forces acting in that plane.

Equations (II.1) are canonical with

$$p_x = m_0 \gamma \frac{dx}{dt}$$
$$p_z = m_0 \gamma \frac{dz}{dt} \tag{II.19}$$

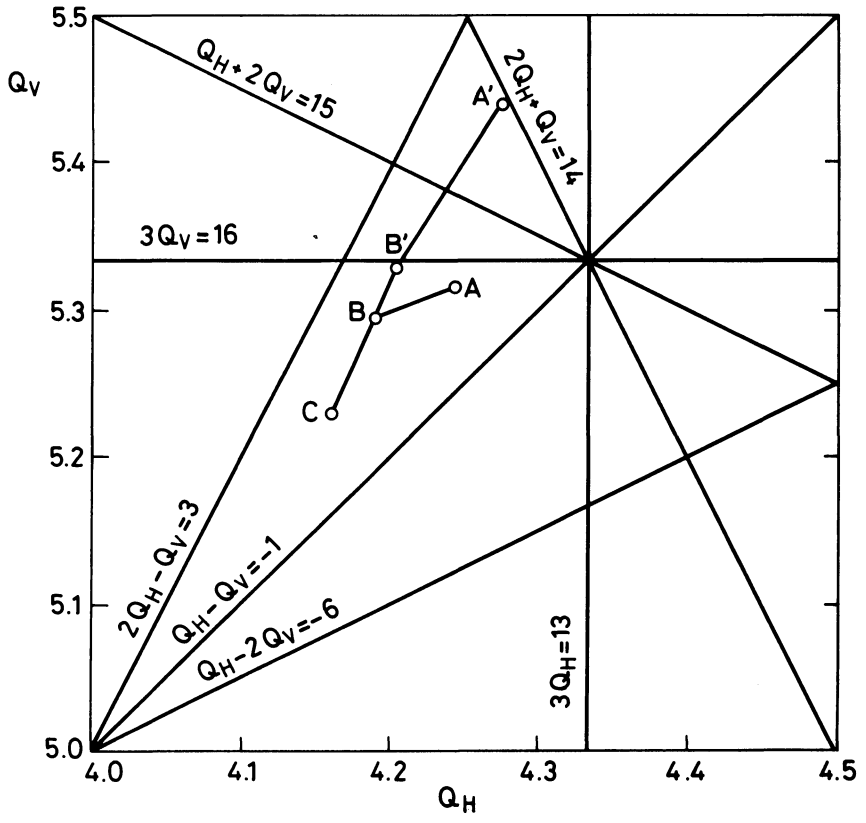

Fig. II.3 Q_H–Q_V diagram with the most important resonance lines in the PSB. The movements of the working point in 1976 (line A, B, C) and in 1981 (line A', B', C) are shown. A, A': injection points, C: ejection point.

and Liouville's theorem can be applied, i.e. the area S in (p_y, y) phase plane occupied by the beam particles is constant throughout the acceleration. S can be written as

$$S = \int p_y \, dy = m_0 \gamma \frac{ds}{dt} \int \frac{dy}{ds} \, dy = m_0 \gamma \beta c E \quad , \tag{II.20}$$

where β and γ are the relativistic parameters and m_0 is the rest mass of the beam particles. Because S is constant the emittance E of the beam must change during the acceleration according to the formula[31]

$$E \beta \gamma = \text{const.} \tag{II.21}$$

II.2 INJECTION PROCESSES

Several types of injection processes are in use depending on the particular design of an accelerator. The choice of the injection parameters depends critically on the machine configuration and the technological development at the time of the design of the machine.

To inject protons properly into a circular accelerator two main problems must be solved:

a) The incoming beam must be aligned on the equilibrium orbit, which is difficult because the fields of the guiding magnets deflect the protons such that they will always arrive on the equilibrium orbit at an angle, unless something special is done to align the incoming particles on the equilibrium orbit.

b) The incoming beam must be matched to the transverse and longitudinal phase-plane properties of the beam in the accelerator.

An attractive method to solve the first problem is injection with negatively charged hydrogen ions. As H^- ions are deflected by the bending magnets in a direction opposite to that of the circulating protons it is easy to align the H^- beam directly on the equilibrium orbit. At the position where the H^- ions move tangentially to the proton orbit a stripper foil is positioned which removes the electrons from the H^- ions so that after the stripper foil an aligned proton beam moves along the equilibrium orbit (Fig. II.4). In this way it is, in principle, possible to increase the circulating proton current by simple injection during any wanted number of machine revolutions[32,33]. H^- injection has been put into operation at Fermilab[34] and will soon be implemented at BNL.

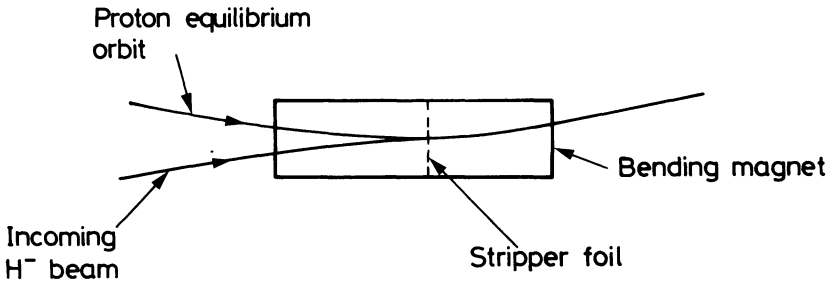

Fig. II.4 H^- injection (schematic).

However, this injection method was considered to be unsuitable for the PSB, mainly because at the time of the construction of the PSB the existing H^- sources could not produce sufficient H^- ions per time interval. Additional disadvantages are the short lifetime of the stripper foil due to radiation damage, and the increase in beam size due to multiple scattering in the foil.

For these reasons, classical schemes, based on the direct injection of protons, were chosen for the PSB. However, in the light of experience gathered at other places[31] with improved H^- sources, this scheme may become interesting for the PSB at some later stage.

The simplest method, which is also available in the PSB, is the monoturn injection. The injection is started at a certain moment and ends when the first injected protons have made one full turn. The whole circumference of the accelerator is thus filled, except for a small gap; its size is determined by the switching off time of one of the injection magnets. This is a straightforward method but lacks versatility.

The multiturn injection process, in which the injection extends over a much longer period, yields higher intensities, but is also more complicated. Multiturn injection is used in the PSB for normal operation, but monoturn injection is more suitable when particle trajectories at injection have to be studied, as this injection method can produce a beam which is longitudinally sufficiently modulated in intensity to obtain good signals from the Pick-Up electrodes. To make monoturn injection into the PSB possible, if required, an extra magnet was installed in addition to the injection magnets needed for multiturn injection.

Both injection methods will be discussed in the following sections, taking the PSB as an example.

II.2.1 Monoturn injection

To describe the motion of the injected beam particles let us again split it into two components: the longitudinal motion along the centre line of the beam and the transverse motion of the particles with respect to this centre line. A particle moving along the centre line will be referred to as a central particle. The transverse motion of the particles with respect to the centre line of the injected beam can be conveniently described again in terms of the ellipse enveloping all injected beam particles in the horizontal or the vertical phase plane.

As the injection takes place in the horizontal plane, the motion of the particles in this plane is of prime interest. Most of the discussion of injection processes will therefore concern the horizontal motion, and the variables and parameters used in the remainder of this chapter will refer to the horizontal motion unless otherwise specified.

The principle of monoturn injection is schematically shown in Fig. II.5. The numbers in the figure apply to the PSB. The incoming beam approaches the PSB at an angle of 66 mrad to the equilibrium orbit. At a distance of 50 mm from this orbit the angle is reduced to zero by a very thin septum magnet, which deflects the incoming beam but leaves the circulating proton beam undisturbed. The exit of this magnet will be called the injection point S. After the septum magnet the centre line of the injected beam traverses a quarter betatron wavelength before crossing the equilibrium orbit at point K, where a fast kicker magnet aligns the injected beam on the closed orbit.

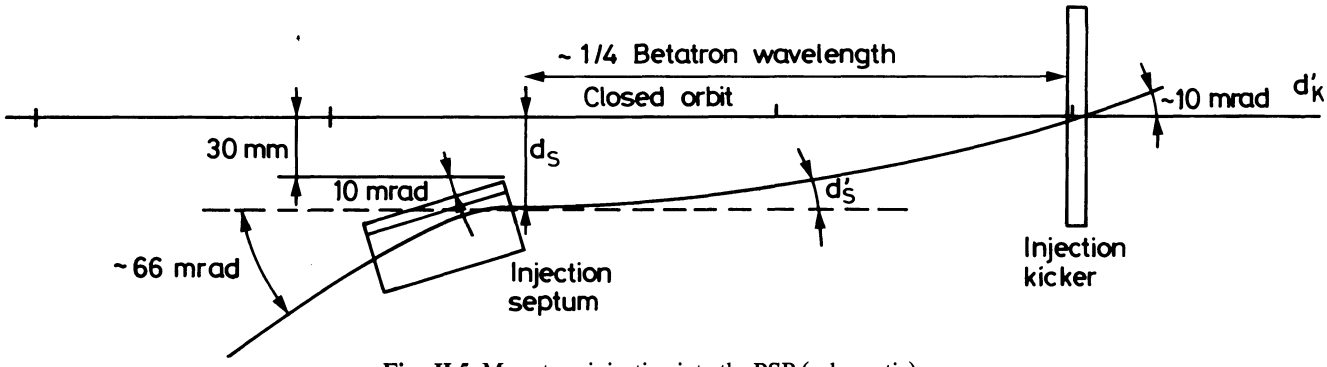

Fig. II.5 Monoturn injection into the PSB (schematic).

The injection point S is situated such that $\hat{\beta}_s'$, the derivative of the betatron function in S, vanishes (Fig. II.2). Assuming that a central injected beam particle leaves the injection septum parallel to, and at a distance d_s from, the closed orbit, the Courant-Snyder invariant for this particle is given by

$$I = d_s^2/\hat{\beta}_s, \tag{II.22}$$

from Eqs. (II.13), (II.14) and the condition $\hat{\beta}_s' = 0$.

The deflection angle required from the kicker magnet can now be easily calculated. The quantity I is conserved and therefore the deflection angle $\Delta x_k'$ required from the kicker is found to be

$$\Delta x_k' = \sqrt{\frac{I}{\hat{\beta}_k}} = d_s\sqrt{\frac{1}{(\hat{\beta}_s\hat{\beta}_k)}} \quad . \tag{II.23}$$

For the PSB, $\Delta x_k' \approx 10$ mrad.

Before the first injected particles return to K after having made one revolution, the current in the kicker magnet must be reduced to zero because otherwise these particles are lost. In the PSB a time interval of 70 ns is required to reduce this current to zero. As 1.66 μs is the period of revolution, 96% of the beam can be precisely aligned on the equilibrium orbit.

The final aim of the injection process is the injection of the largest possible fraction of the incoming beam into the smallest possible horizontal and vertical phase-space area of the accelerator. For this the following two conditions must be satisfied:

- The phase-space properties of the injected beam must match the phase-space structure of the accelerator beam at the injection point S.
- The injected beam must be aligned precisely along the closed orbit of the accelerator.

First the effect of a mismatch in phase space will be considered, assuming perfect alignment. This case is illustrated in Fig. II.6a. Curve 2 is an equidensity line of the incoming beam in the transverse plane at the injection point, enveloping the particles of the injected beam. To a good approximation this equidensity line can be assumed to be an ellipse. Curve 1 is a Courant-Snyder ellipse of the accelerator with the same area as ellipse 2.

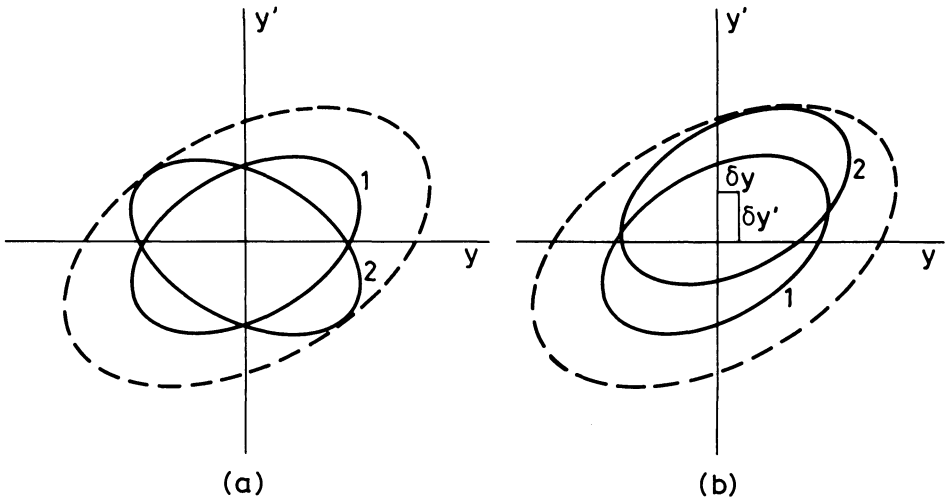

Fig. II.6 a) Emittance increase due to a mismatch of the incoming beam.
b) Emittance increase due to a misalignment of the incoming beam.

If ellipse 2 had had the same form and orientation as ellipse 1 the two ellipses would have coincided and the injected beam particles would still have been found within ellipse 1 after several turns in the accelerator. In actual fact there is a mismatch and therefore the envelope of the injected particles after a few revolutions is the dotted ellipse, which has an area considerably larger than ellipse 1.

The matching of the incoming Linac beam equidensity ellipses to the Courant-Snyder ellipses at the injection point of the PSB is achieved by adjusting several quadrupole magnets placed in the injection beam line from the Linac. These quadrupoles focus the Linac beam, and with their aid the form of the equidensity ellipses in the vertical and horizontal phase planes can be modified while their area stays constant.

The second case, misalignment of an injected beam that is perfectly matched to the phase-space structure of the accelerator, is shown in Fig. II.6b.

The ellipse 2, the envelope of the injected beam, has a form and orientation that matches ellipse 1, the Courant-Snyder ellipse of the machine at the injection point. But, owing to a misalignment, the centre of ellipse 2, which represents the centre line of the injected beam, is displaced by an angle $\partial y'$ and a distance ∂y with respect to the centre of ellipse 1. The emittance of the accelerator beam corresponding to this injected beam after several turns in the machine is the dotted ellipse, which circumscribes the injected particles. It has a form determined by the machine geometry, and an area larger than ellipse 1 which would be the emittance of the accelerator beam if no misalignment had taken place.

If the surface of the dotted ellipse is larger than the area of the acceptance of the accelerator the particles falling outside the acceptance ellipse will be lost on the vacuum chamber walls.

In the vertical plane the alignment is done with two dipoles, placed in the injection channel, which determine the angle and the position of the beam with respect to the equilibrium orbit.

In conclusion, from Figs. II.6a and II.6b it can be seen that a misalignment of the incoming beam with respect to the equilibrium orbit or a mismatch of the incoming beam emittance with respect to the Courant-Snyder ellipse at the injection point leads to an unwanted increase of the accelerator beam emittance in both planes. If the resulting emittances are larger than the corresponding accelerator acceptances, the outer particles are lost until the resulting accelerator beam emittances are equal to the corresponding acceptances.

Extensive calculations on the changes in the particle distribution caused by the misalignment or the mismatch of the incoming equidensity ellipses with respect to the Courant-Snyder ellipses can be found elsewhere[35,36].

For a good injection into the PS, the emittance of the PSB beam at 800 MeV should fit the acceptance of the PS in both transverse planes. Too small an emittance means a low intensity (see Section II.2.2) and too large an emittance causes unacceptable irradiation of the accelerator components. In 1976 this fixed the emittance of the 50 MeV PSB beam at 130 π mm · mrad for the horizontal and 40 π mm · mrad for the vertical plane. Later, in 1980, larger emittances were tolerated ($E_H = 230\,\pi$ mm · mrad, $E_V = 120\,\pi$ mm · mrad), but they do not modify the arguments developed in this chapter.

The emittance of the Linac beam containing 95% of the particles at 50 MeV is 30 π mm · mrad in both planes. It is therefore not possible to fill the required horizontal emittance of the PSB beam by monoturn injection. The multiturn injection process that was actually used is described in the next section and the following chapters.

II.2.2 Multiturn injection

A schematic diagram of multiturn injection into the PSB is shown in Fig. II.7. The main features, in particular the position of the incoming Linac beam and the septum magnet, are the same as for monoturn injection (Fig. II.5). However, instead of the one kicker magnet used in monoturn injection there are now four kicker magnets. With these magnets a 6 m long section of the closed orbit around the injection point can be shifted parallel to itself in the median plane of the PSB.

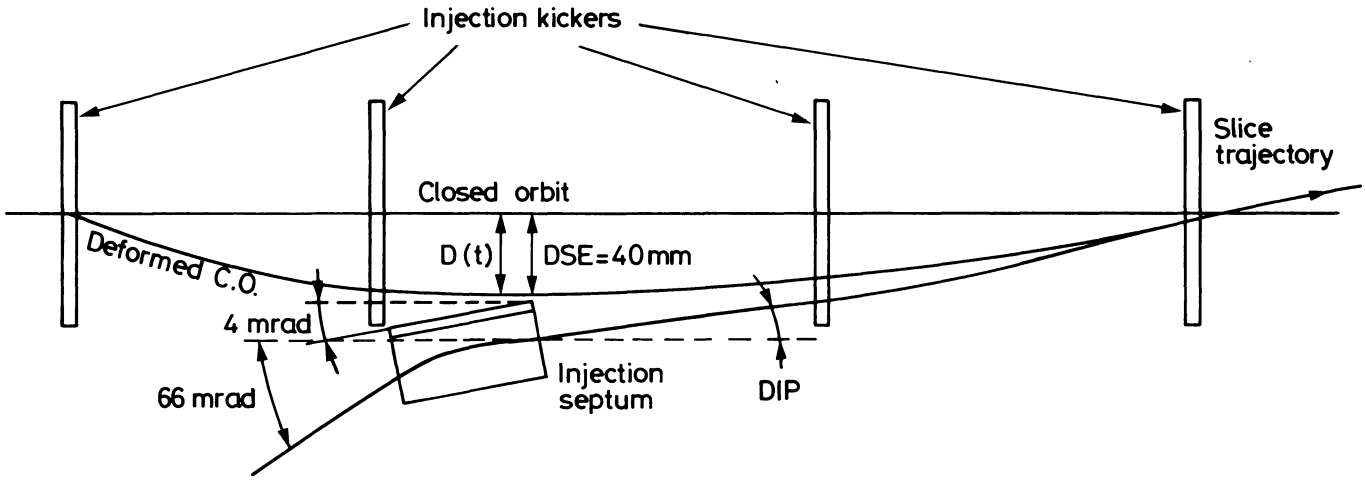

Fig. II.7 Multiturn injection into the PSB (schematic).

At the start of the injection the displacement $D(t)$ of the closed orbit is so large that near the injection point the closed orbit and the injected beam almost coincide. From this moment onwards the displacement of the closed orbit decreases linearly with time.

The first injected particles move almost on the closed orbit and thus have a small horizontal betatron amplitude. If the closed orbit did not move, the particles would inevitably return to their original position on the outside of the septum after a number of revolutions and would therefore be lost. But because in fact the closed orbit moves towards the centre of the machine, a fraction of the particles will be able to pass the septum on the inside and will thus be bent in the machine. At the end of the injection the first injected particles have typically made 10 to 15 revolutions.

As the closed orbit moves away from the septum the betatron amplitude of the injected particles increases. The ellipse in horizontal phase space corresponding to an emittance of $130\ \pi$ mm · mrad is gradually filled in this manner, starting from the centre and moving outwards. When the edge of the ellipse is reached the injection is terminated.

Vertically the beam is aligned and matched in the same way as is done for monoturn injection.

In Chapter III the multiturn injection process is analysed in detail. First the evolution of one single injected beam slice during the injection period is calculated. A beam slice is a group of particles injected within a small time interval Δt. The slice loses particles because in the course of the first turns in the PSB it always passes a few times so close to the injection septum that part of it is cut off. In the horizontal phase plane the successive cuts show up as straight lines that enclose an area, the partial acceptance of the slice, which contains all the particles that are finally accepted and accelerated. The partial acceptance of the slice depends on the moment of injection, on the PSB machine parameters, and on the properties of the incoming beam.

Using the expressions for the partial acceptance of a slice in terms of the various parameters, a total injection efficiency can then be calculated and the values of the parameters that correspond to the maximum total PSB beam intensity can be determined.

CHAPTER III

MULTITURN INJECTION INTO THE PSB: MODEL CALCULATIONS AND MEASUREMENTS

III.1 GENERAL REMARKS

Although the principles of multiturn injection are well known[37–42], there has never been an attempt to describe the process with the aid of simple equations for any given Q_H value. The estimate of the value of the critical parameters has been done with the aid of simulation programs, which are cumbersome to handle owing to the lengthy trial and error optimization procedure[43,44].

In this chapter a multiturn injection process will be considered where the closed orbit movement is excited by means of kicker magnets. This procedure, which was described in Section II.2.2, is used in alternating-gradient (AG) proton synchrotrons in general and consequently also in the PSB. The deviation is created in the PSB by four simultaneously pulsed kicker magnets per ring. Just before the injection starts, at the time $t = 0$, the magnets give the closed orbit near the injection point a parallel displacement DO over a length of 6 m. The displacement is programmed to decrease linearly during injection according to the formula

$$D(t) = DO(1 - t/T_{IKS}), \tag{III.1}$$

where $D(t)$ is the instantaneous closed-orbit displacement at the time t. The constant T_{IKS} determines the speed of movement of the closed orbit.

The amplitude DO is the same for the four rings, but the time $t = 0$ can be chosen for each ring separately. To achieve maximum injection efficiency the beam can be injected during 15 machine revolutions of 1.66 μs each. The Linac pulse was therefore made 100 μs long to allow injection of the beam during 25 μs into each of the four levels of the PSB.

The purpose of the multiturn injection process in the PSB is to inject as many particles as possible into a fixed horizontal emittance E_H at 50 MeV, using a Linac beam with definite properties. During the injection studies (1973–76), E_H was set at 130 π mm · mrad. Later (1981), owing to all kinds of improvements[29,30], a larger E_H of 240 π mm · mrad was used. The value 130 will be used throughout this chapter, but the value 240 does not significantly change the arguments developed in this chapter.

How large a fraction of the injected particles will actually be accelerated in the PSB depends on a large number of parameters: the PSB machine parameters, the parameters related to the injection apparatus and the injection timing, and the parameters defining the properties of the injected beam.

Some of these parameters are fixed, i.e. they cannot be changed or they are never changed in optimizing the injection process. Examples are (Fig. III.1):

t_{rev} the revolution period at injection (1.66 μs)
DSE the distance between the inner septum edge and the undisplaced closed orbit (40 mm)
DS the effective septum thickness (1.5 mm)
DO the maximum displacement of the closed orbit (48 mm)
E_H the nominal horizontal emittance of the PSB beam at 50 MeV (130 π mm · mrad)
β_s the value of the horizontal betatron function at the injection point (typically 5.8 m, weakly dependent on Q_H)
$\beta_s' = d\beta_s/ds = 0$.

Because β_s and β_s' are constant parameters, the Courant-Snyder ellipses in the horizontal phase plane for the PSB at the injection point can be represented by

$$x^2/\beta_s + \beta_s x'^2 = \text{const}. \tag{III.2}$$

Variable parameters can be changed in the course of the injection studies. However, even the variable parameters are constant during each injection cycle, unless otherwise specified.

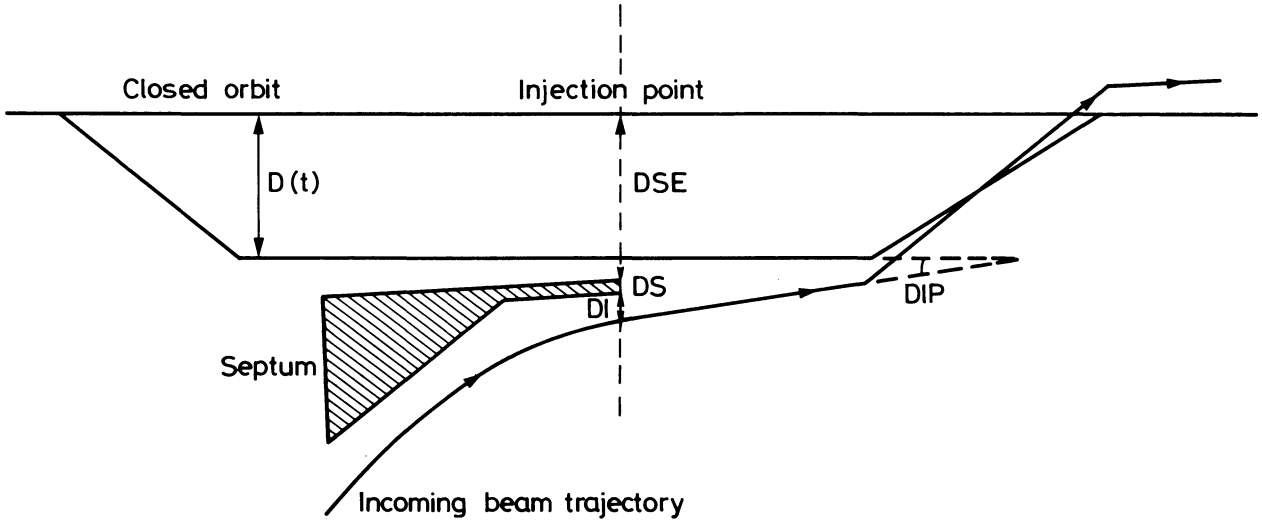

Fig. III.1 Principal parameters for the multiturn injection.

The most important variable machine parameter is the Q_H value of the PSB at injection. A change in the Q_H value has a profound influence on the entire injection process.

Variable parameters related to the timing of the injection are T_{IKS}, the parameter that determines the speed of the transverse motion of the closed orbit, and n_t, the numbers of turns injected.

The other three variable parameters, *DI*, *DIP*, and β_l, determine the properties of the injected beam when it enters the PSB at the injection point.

The parameter *DI* is the distance between the centre of the beam entering the PSB and the outer septum edge; the angle between the closed orbit and the incoming beam direction at the exit of the injection septum is denoted by *DIP* (Fig. III.1).

The parameter β_l is connected with the properties of the injected beam in the horizontal phase plane at the injection point. These properties are best defined by specifying the distribution of the image points of all injected beam particles in this phase plane. The equidensity lines of this distribution are ellipses. The form of these ellipses should match the symmetry properties imposed by the septum magnet and the form of the Courant-Snyder ellipses at the injection point of the PSB, i.e. the focusing magnets in the injection beam line should be adjusted such that the main axes of the equidensity ellipses are parallel to the x and x' axes in the horizontal phase plane[42]. The equation of the equidensity ellipses in the horizontal phase plane of the PSB at the injection point can then be written as

$$\frac{(x - x_c)^2}{\beta_l} + \beta_l(x' - x_c')^2 = \frac{\varepsilon}{\pi} \quad , \tag{III.3}$$

where (x_c, x_c') are the coordinates of the incoming beam centre with respect to the closed orbit. The area of the ellipse — or the horizontal emittance of the incoming beam inside this ellipse — is ε, and β_l is a variable parameter.

Beam measurements, using the methods described in Section I.6.3, have been made to determine experimentally the number of particles $I(\varepsilon)$ inside ellipse (III.3) as a function of ε. To a good approximation $I(\varepsilon)$ is found to follow the relation

$$I(\varepsilon) = I_0(1 - e^{-\varepsilon/\varepsilon_0}) \quad . \tag{III.4}$$

The fixed parameter $\varepsilon_0 = 10\,\pi$ mm · mrad is the area of the ellipse containing $\approx 63\%$ of the injected beam particles. The maximum value of I_0 was 85 mA at the time of the experiments (raised to 120 mA in the meanwhile). The particle density in phase space is thus seen to decrease exponentially from the centre of the injected beam outwards. This is actually true for both the horizontal and the vertical direction.

In this chapter the optimum values for the variable parameters are calculated and the results of the calculation are compared with measurements on the PSB beam. The calculation is based on the determination, for given values of Q_H and n_t, of those values of $DI(t)$, $DIP(t)$ and $\beta_l(t)$ for which the largest fraction of the particles in a beam slice is injected at time t into the PSB.

The condition that at the end of the injection 95% of the injected particles should lie within a horizontal emittance of $130\,\pi$ mm · mrad then determines the value of T_{IKS} as a function of the other five variable parameters.

In Fig. III.2 the history of an incoming beam slice, injected at time t, is shown in the horizontal phase plane during the first four revolutions in the PSB. Instead of (x, x') the coordinates $(x, \beta_s x')$ are used. In terms of these coordinates the Courant-Snyder ellipses of the PSB at the injection point are circles and this is convenient for some of the

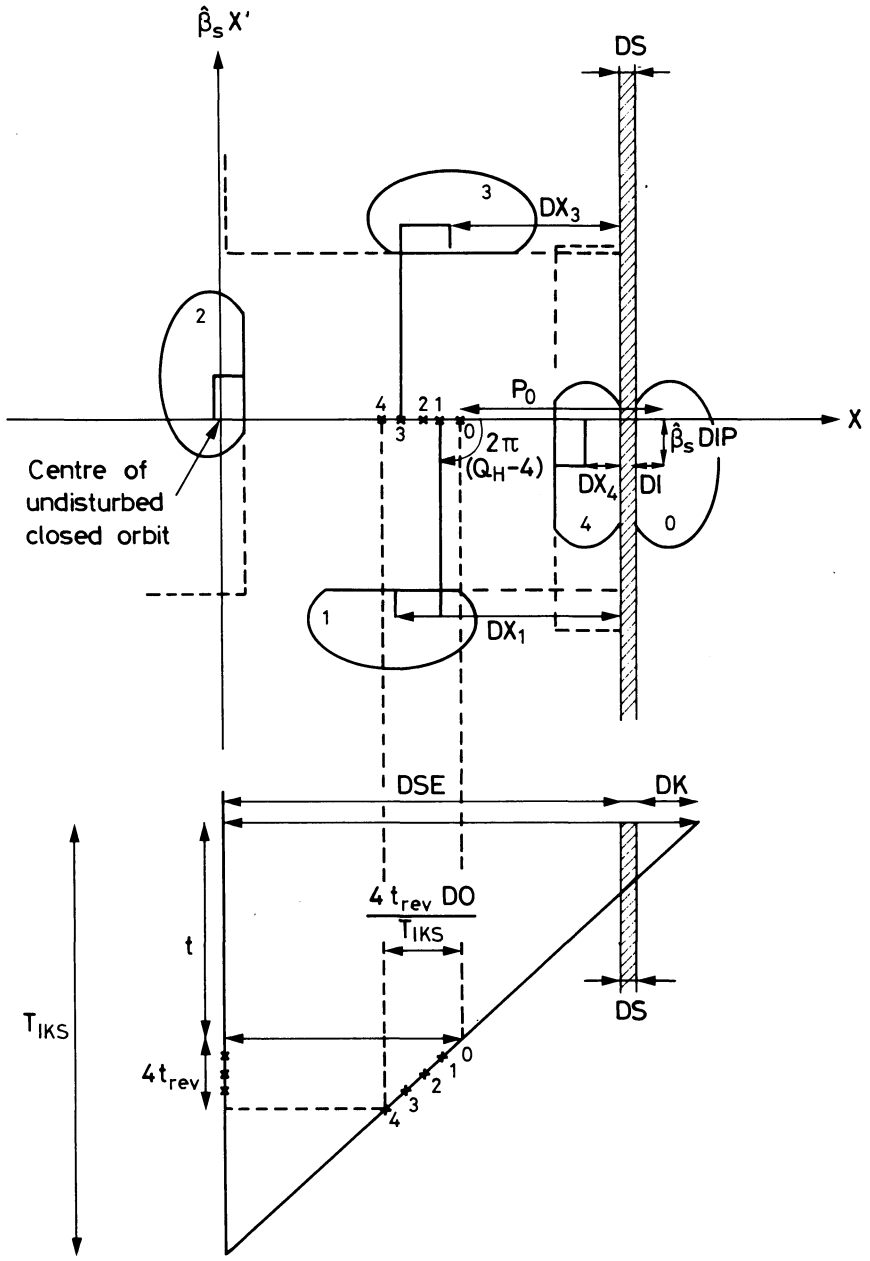

Fig. III.2 Evolution of a slice injected at point zero. Points 1, 2, 3, and 4 show the position of the slice after 1, 2, 3, or 4 turns, respectively, when $Q_H = 4.25$ (the value 4.25 is chosen to simplify the drawing).

calculations. The form of the ellipse representing the incoming beam slice at injection is given by Eq. (III.3). In the coordinate system $(x, \beta_s x')$ this equation can then be written as

$$(x - DSE - DS - DI)^2 + (\beta_t^2/\beta_s^2)(\beta_s x' - \beta_s DIP)^2 = \varepsilon\beta_t/\pi\,. \tag{III.5}$$

The figure is drawn for $\beta_t = 3.1$ and $\varepsilon = \varepsilon_0$, so that the ellipse envelops 63% of the particles in the slice. After each revolution the centre of the beam slice reappears at the injection point on a circle with constant radius $P_0(t)$. The centre shifts each turn a distance $t_{rev}DO/T_{IKS}$ further towards the position of the undisturbed closed orbit. During each revolution the particles of the slice perform Q_H horizontal oscillations. In the figure $Q_H = 4.25$. This means that the centre of the beam slice ellipse has moved after each revolution over an angle of $0.25 \times 2\pi = 0.5\,\pi$ along the circle in the clockwise direction.

The orientation of the slice and the distance DX_t between the centre of the slice and the inner septum edge after the i^{th} revolution determine how many particles of the slice are removed. The successive septum cuts — assumed to be straight lines[45] — into the same incoming beam slice determine a polygon in the horizontal phase plane that encloses an area, the partial acceptance of the slice, in which the particles of this particular slice must lie in order to be accepted and preserved in the accelerator. When n_t turns have been injected, a slice of PSB beam is constituted by n_t partial

acceptances lying in a spiral in the horizontal phase plane such that the earliest injected particles lie in the partial acceptance closest to the centre of the beam and the last injected particles in the partial acceptance closest to the edge of the beam. All partial acceptances are separated by a distance determined by the septum thickness DS. The resulting situation in the horizontal phase plane is shown in Fig. III.3 for a Q_H value of 4.25. Although the area of the partial acceptance increases considerably towards the edge of the beam the number of particles in the partial acceptance obviously increases slowly as soon as its area exceeds ε_0.

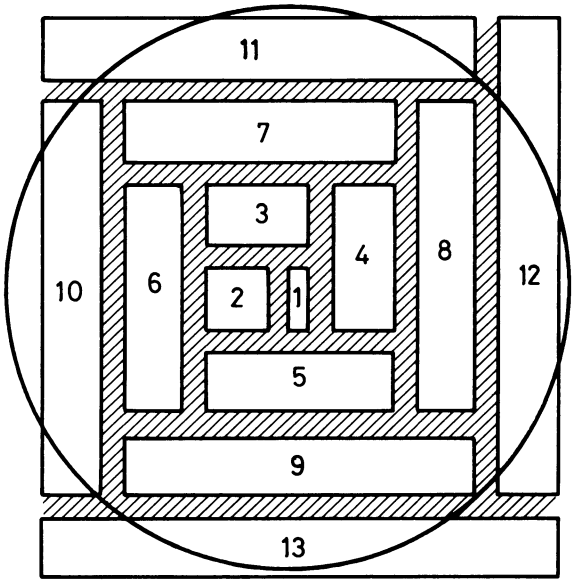

Fig. III.3 Filling of the horizontal phase plane by 13 slices when $Q_H = 4.25$. Shaded area is the septum shadow.

The minimum number of cuts to determine the partial acceptance is three. However, if two of the cuts are almost parallel, four cuts are needed. Further cuts are usually of no importance because they fall outside the area already determined by the three- or four-angle configuration. For this reason no partial acceptance configurations with more than four cuts have been considered.

The calculation of the values of the optimized parameters is therefore based on the distinction of the following two cases:

i) three-angle partial acceptance (determined by three cuts)
ii) four-angle partial acceptance (determined by four cuts).

Which of the two cases is appropriate can be determined for each individual slice of beam.

In Fig. III.4 the partial acceptance is shown for an early slice (a) and a later slice (b) after ten revolutions and for a Q_H value of 4.20. In this figure the ellipse in the horizontal phase plane is shown in fixed orientation. The position of the

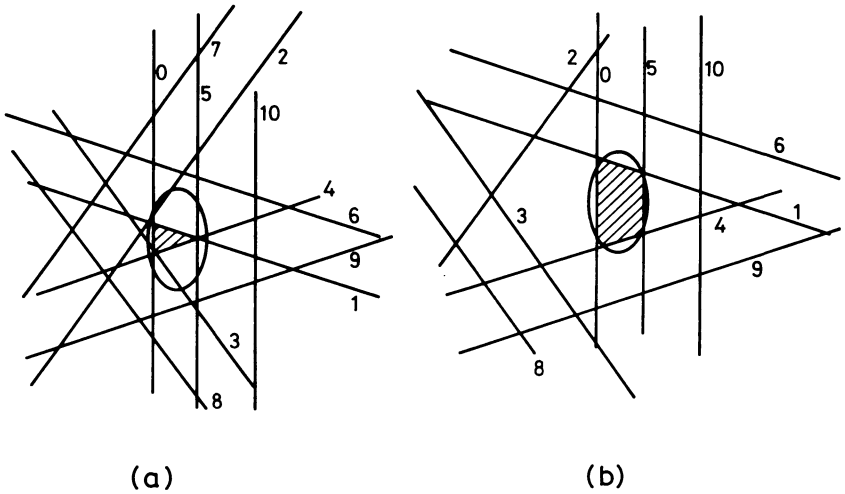

Fig. III.4 Layout of the septum cuts in the horizontal phase plane of two slices injected, with $Q_H = 4.20$. The slice of (a) is injected at the start of the injection, while the slice of (b) is injected at the end.

inner septum edge after 1, 2, ..., 10 revolutions is shown with respect to this fixed ellipse. The number 0 corresponds to the cut made by the outer septum edge at injection. Each revolution of the slice in the PSB corresponds to 4.20 betatron oscillations.

After each revolution the inner septum edge therefore reappears $0.20 \times 360 = 72°$ further counter-clockwise. After five revolutions the cut has gone full circle and is again parallel to cut 0.

Although the angle of the successive cuts with respect to the ellipse is the same in the cases shown in Figs. III.4a and III.4b, the distance of the cuts to the centre of the ellipse is different in the two cases because the moment of injection is different. In Fig. III.4a this results in a three-angle partial acceptance determined by cuts 0, 1, and 4, whereas in Fig. III.4b the partial acceptance happens to be of the four-angle type determined by cuts 0, 1, 4, and 5. The program that calculates the partial acceptance areas is able to recognize these two configurations.

III.2 CALCULATION OF THE OPTIMIZED INJECTION PARAMETERS[46)]

The efficiency of the injection process is defined as the total number of particles which are kept in the synchrotron after the completion of the injection process divided by the total number of particles coming from the injector within the time interval that the beam is injected.

The efficiency of a slice injected at time t is defined as the number of particles in this slice kept in the accelerator divided by the total number of particles in this slice coming from the injector.

The purpose of the theoretical model for the multiturn injection process developed here is the calculation of the over-all injection efficiency in terms of the variable parameters $DI(t)$, $DIP(t)$, $\beta_l(t)$, Q_H, n_t, and T_{IKS}. The method of calculation is based on finding the values for $DI(t)$, $DIP(t)$, and $\beta_l(t)$ that will maximize the efficiency for the beam slice injected at time t for given values of Q_H, n_t, and T_{IKS}. It will be shown that $DI(t)$, $DIP(t)$, and $\beta_l(t)$ are in general linear functions in t. By integrating over all slices the total injection efficiency can then be found for the given set of values for Q_H, n_t, and T_{IKS}.

Of the last three variable parameters only Q_H can be freely chosen within certain limits owing to space-charge-induced detuning. The parameter n_t, the number of turns injected, was fixed within the range $n_t \leq 15$ by the properties of the Linac beam. It turned out that the overall efficiency has a flat maximum between $n_t = 13$ and $n_t = 15$. In most of the calculations $n_t = 13$ was used, but $n_t = 15$ was also taken in a few cases.

The parameter T_{IKS} is determined by the condition that after injection 95% of the PSB beam should lie within $E_H = 130\ \pi$ mm · mrad. The 5% of particles outside E_H are used for measuring the position and the width of the beam by plunging in targets. This method was described in Section I.6.7. The result of the efficiency calculations depends strongly on the value of T_{IKS}. A reliable and accurate calculation of T_{IKS} for given values of the other variable parameters is therefore required.

The most important results of the model calculations can be summarized as follows:

i) The injection efficiency is calculated as a function of Q_H under two different assumptions:
   a) $DI(t)$, $DIP(t)$, and $\beta_l(t)$ vary with time in accordance with the best theoretical values.
   b) DI, DIP, and β_l have fixed average values $\overline{DI}$, $\overline{DIP}$, and $\overline{\beta_l}$ during injection.
   It will be shown that the gain in efficiency obtained by varying the beam parameters with time is not sufficiently important to justify installation of the expensive and complicated additional apparatus in the injection beam line that would be required to change DI, DIP, and β_l during injection.

ii) By studying the variation of the total injection efficiency and the best values of $\overline{DI}$, $\overline{DIP}$, and $\overline{\beta_l}$ as a function of Q_H at injection, the relative merits of possible working points for the PSB can be evaluated, taking into account the influence of the choice of the Q_H value on the behaviour of the PSB beam after injection.

iii) The dependence of the total injected beam intensity on the number of injected turns n_t, for a preselected Q_H value, can be reliably calculated. The final choice of the n_t value can be justified on the basis of this result.

The derivation of the functions $DI(t)$, $DIP(t)$, and $\beta_l(t)$, which correspond to maximum efficiency over the entire injection period for a beam slice injected at time t, is rather complicated. Only the basic method of calculation and the results are presented here. A more detailed account is given in Appendix I for the case of a three-angle partial acceptance and in Appendix II for the four-angle case. Only the three-angle case will be treated here. The four-angle case is completely analogous.

To explain the principles involved, the best starting point is a diagram of the type presented in Fig. III.2, where the history of an incoming beam slice is shown in the horizontal phase plane at the injection point. The beam slice is represented by an equidensity ellipse, the coordinates are $(x, \beta_s x')$, and the equation of the ellipse at injection is given by Eq. (III.3). During injection the beam slice reappears four times at the injection point and the position of the ellipse in the phase plane after each turn is shown in the diagram.

Only the relative position of the equidensity ellipse and the inner septum edge after each turn is important for the present problem. This information is collected for the whole injection period in Fig. III.4, where the position of the ellipse and the septum edge after each revolution is shown in a coordinate system fixed to the ellipse and which therefore jumps to a new position in the horizontal phase plane after each revolution. Figure III.4a for the three-angle partial

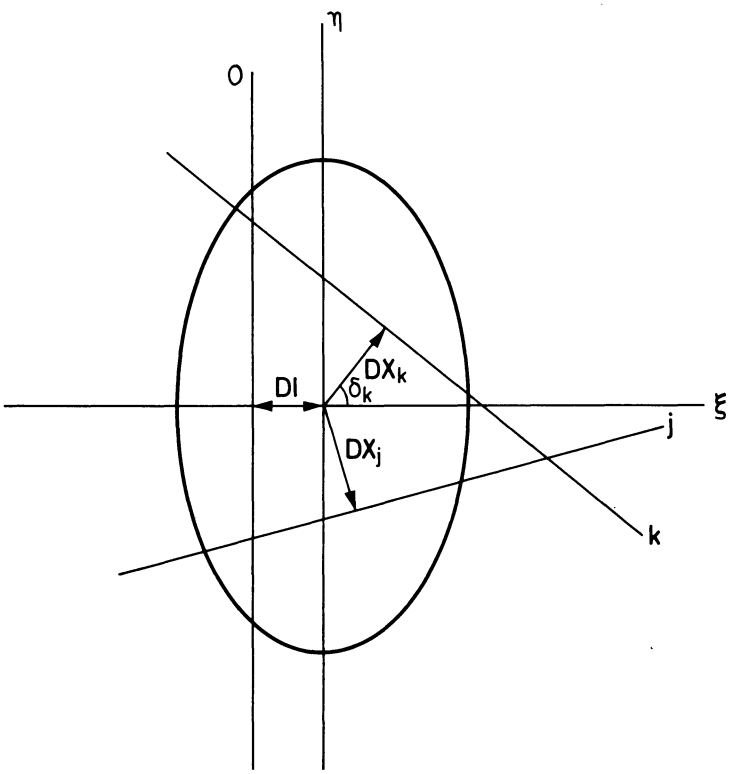

Fig. III.5 Representation of the three-angle partial acceptance determined by the cuts 0, j, and k. Their respective distances from the slice centre are DI, DX_j, and DX_k.

acceptance is shown on a larger scale in Fig. III.5. The coordinates in phase plane are denoted by (ξ, η), the origin of the coordinate system is the centre of the equidensity ellipse, and the direction of the axes is along the main axes of the ellipse. In these coordinates the equation of the ellipse can, according to Eq. (III.5), be written as

$$\xi^2 + \frac{\beta_l^2}{\hat{\beta}_s^2}\eta^2 = \frac{\varepsilon\beta_l}{\pi} \quad , \tag{III.6}$$

where ε is the surface area of the ellipse. Only the three cuts that determine the partial acceptances are shown. These cuts are labelled 0, j, and k, according to the number of revolutions after which the cut was made by the injection septum. The distances from the centre of the ellipse to the cuts 0, j, and k are DI, DX_j, and DX_k, respectively, where the symbols have the same meaning as in Fig. III.2.

By comparing with Fig. III.2, it is also easily seen that the angle δ_l, determining the direction of the cut, obeys the relation

$$\delta_l = 2\pi Q_H i \, . \tag{III.7}$$

The efficiency of a given beam slice will be high when the most intense part of the incoming beam is well centred in its partial acceptance. For the particle density distribution given by Eq. (III.4) it is reasonable to assume that for maximum efficiency the three cuts determining the partial acceptances should be tangents of the same equidensity ellipse of the slice. This situation, shown in Fig. III.6a, can, for given β_l, always be obtained by adjusting the parameters DI and DIP.

The parameter β_l determines the shape of the inscribed ellipse. Among the inscribed ellipses corresponding to different β_l values there is one with the largest area. The β_l value for this ellipse is that value for which the incoming beam slice will have the highest efficiency.

The condition that the three cuts determining the partial acceptance should be tangents of the same equidensity ellipse of the beam slice is equivalent to two relations between the six variable parameters. This can be seen by transforming Fig. III.6a to a new system of coordinates (ξ^n, η^n), connected to the coordinate system (ξ, η) by the relations

$$\begin{aligned} \xi^n &= \xi \\ \eta^n &= \frac{\beta_l}{\hat{\beta}_s}\eta \end{aligned} \quad . \tag{III.8}$$

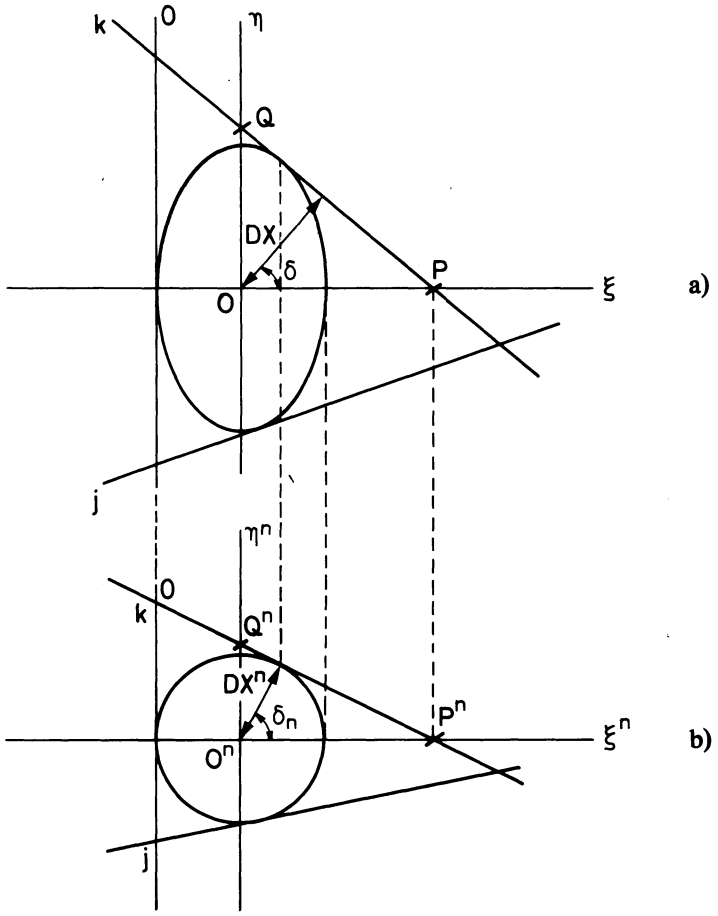

Fig. III.6 Transformation of the distances DX to the normalized distances DX^n. The relation between DX and DX^n is found as follows:

$$DX = (OP)\cos\delta$$

$$DX^n = (O^nP^n)\cos\delta_n = \frac{(O^nP^n)}{\sqrt{1+\mathrm{tg}^2\delta_n}} = \frac{(O^nP^n)}{\sqrt{1+(O^nP^n)^2/(O^nQ^n)^2}}$$

$$= \frac{(OP)}{\sqrt{1+\left(\hat{\beta}_s^2/\beta_l^2\right)[(OP)^2/(OQ)^2]}}$$

or

$$DX^n = \frac{DX}{\sqrt{\cos^2\delta+\left(\hat{\beta}_s^2\sin^2\delta\right)/\beta_l^2}}$$

The result of this transformation is shown in Fig. III.6b. The equidensity ellipse is transformed into a circle, as can be easily verified by writing Eq. (III.6) in terms of ξ^n and η^n.

The condition that the three cuts are tangents to the ellipse in Fig. III.6a can now be replaced by the equivalent condition that the centre of the circle in Fig. III.6b lies at equal distance from the three cuts. These distances after transformation are called the normalized distance DX_i^n. It is shown in Fig. III.6 that

$$DX_i^n = \frac{DX_i}{F(iQ_H)} \tag{III.9}$$

with

$$F(iQ_H) = \sqrt{\frac{\hat{\beta}_s^2}{\beta_l^2}\sin^2(2\pi Q_H i) + \cos^2(2\pi Q_H i)} \quad . \tag{III.10}$$

In terms of the normalized distances the required condition for maximum efficiency of the slice can be written in the form

$$DI(t) = DX_j^n = DX_k^n \tag{III.11}$$

or

$$DI(t) = \frac{DX_j}{F(jQ_H)} = \frac{DX_k}{F(kQ_H)} \quad . \tag{III.12}$$

By considering the geometry in Fig. III.2 the following expression can be derived for DX_i:

$$DX_i = P_0(1 - \cos 2\pi Q_H i) - DI - DS + \frac{it_{rev}}{T_{IKS}} - \hat{\beta}_s DIP \sin 2\pi Q_H i \tag{III.13}$$

with

$$P_0 = DI + DS + DSE - DO + \frac{DO}{T_{IKS}}t = DI - DK + \frac{DO}{T_{IKS}}t \quad . \tag{III.14}$$

By substituting Eqs. (III.13) and (III.14) in (III.12) and solving for DI and DIP, the functions $DI(t)$ and $DIP(t)$ are found for which the slice injected at time t has the highest efficiency for given values of β_l, Q_H, n_t, T_{IKS}, and of the fixed parameters. This calculation is carried out in Appendix I and leads to the result:

$$DI(t) = \frac{A_{DI}}{T_{IKS}}t + \frac{B_{DI}}{T_{IKS}} + C_{DI} \tag{III.15}$$

$$DIP(t) = \frac{A_{DIP}}{T_{IKS}}t + \frac{B_{DIP}}{T_{IKS}} + C_{DIP} \quad , \tag{III.16}$$

where the dependence on T_{IKS} is explicitly shown and the coefficients depend on all the other parameters.

Finally the value of β_l must be determined for which the equidensity ellipse in Fig. III.6a has the largest area. The equation of this ellipse is given by Eq. (III.6). Because the point $(-DI, 0)$ must always lie on the ellipse the relation

$$\varepsilon = \frac{\pi DI^2}{\beta_l} \tag{III.17}$$

must hold. The area is therefore largest when $d\varepsilon/d\beta_l = 0$ or

$$\frac{d}{d\beta_l}\left\{\frac{DI^2(t)}{\beta_l}\right\} = 0 \quad .$$

The optimum value for β_l that follows from this condition is calculated in Appendix I. The best value of β_l is, surprisingly, independent of t and can be approximated by

$$\beta_l(t) = \frac{\sqrt{0.9}\,\hat{\beta}_s\,|\mathrm{tg}(2\pi Q_H j)|}{\left\{0.738 + \left[\frac{\cos(2\pi Q_H k)}{\cos(2\pi Q_H j)}\left|\frac{\sin(2\pi Q_H j)}{\sin(2\pi Q_H k)}\right| + 0.4\right]^2\right\}^{1/2}} \quad . \tag{III.18}$$

This expression therefore gives the best value for the ratio of the main axes of the ellipse as a function of the partial acceptance geometry.

The best values for $DI(t)$, $DIP(t)$, and $\beta_l(t)$ in the case of the four-angle partial acceptance are calculated in Appendix II. The partial acceptance is now determined by four cuts $0, j, k$, and l. As cut j is almost parallel to cut 0 and therefore $\sin 2\pi Q_H j \approx 0$, $DI(t)$ is decoupled from $DIP(t)$ so that small changes in $DIP(t)$ affect $DI(t)$ only in a second-order approximation and vice versa. The condition for maximum efficiency of the slice in this configuration is

$$DI(t) = DX_j^n = DX_k^n = DX_l^n. \tag{III.19}$$

It leads to the same equations (III.15) and (III.16) for $DI(t)$ and $DIP(t)$ as in the three-angle case, but the coefficients are different functions of the other injection parameters.

The best β_l value is for the four-angle partial acceptance given by the relation

$$\beta_l(t) = \frac{\hat{\beta}_s}{2} \frac{DI(T_B) + DI(T_E)}{At + B} \quad , \tag{III.20}$$

where A and B (see Appendix II) are again functions of the injection parameters. T_B is the time at the start and T_E the time at the end of the injection of the beam into the accelerator.

In the preliminary discussion at the beginning of this section, attention was already drawn to the importance of an accurate calculation of the value of the parameter T_{IKS} for which 95% of the PSB beam lies within an emittance $E_H = 130\ \pi$ mm · mrad just after injection. Only the general principles underlying the injection timing will be discussed here. It is also shown how the correct value for T_{IKS} can be found in first approximation.

First the time T_B for the start of the injection must be chosen. If T_B is chosen too early the first part of the incoming beam is lost, if T_B is chosen too late the centre of the horizontal emittance of the PSB beam is not filled. These undesirable conditions are avoided if T_B is chosen to obey the relation

$$T_B = \frac{DK}{DO} T_{IKS} - t_{rev} \quad . \tag{III.21}$$

The injection is then started one revolution period before the closed orbit coincides with the outer septum edge. Consequently the beam is well filled from the centre. The purpose of the further calculation is to find a T_{IKS} value which best accommodates an injection into E_H for a fixed n_t (no holes in the centre).

The time for the end of the injection T_E is fixed by T_B and n_t:

$$T_E = T_B + n_t t_{rev} = \frac{DK}{DO} T_{IKS} + (n_t - 1) t_{rev} \quad . \tag{III.22}$$

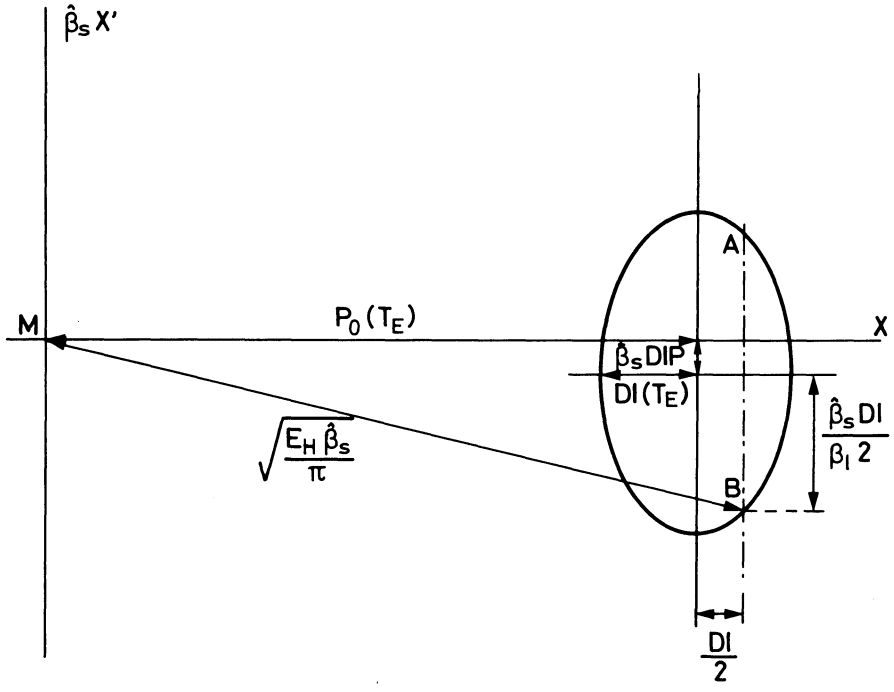

Fig. III.7 The position of the horizontal emittance limitation within the slice injected at time T_E.

The fraction of the PSB beam lying outside E_H after the injection is strongly influenced by the value of T_E. When T_B is chosen according to Eq. (III.21), T_E is determined by two variable parameters only: T_{IKS} and n_t. The value of T_{IKS} depends on n_t and E_H, which means that all injection timings are determined by the values of E_H and n_t.

When T_E is chosen such that for the beam slice injected at time T_E the configuration in phase space shown in Fig. III.7 is realized, very nearly 5% of the PSB beam lies outside E_H after injection. This can be shown by carrying out the calculation for a number of values of the various injection parameters. The coordinate system in Fig. III.7 is the same as in Fig. III.2, but the figure is drawn for a time so long after the end of the injection that the closed-orbit displacement has gone back to zero. The large circle corresponds to $E_H = 130\ \pi$ mm · mrad. The ellipse is the inscribed ellipse of the partial acceptance of the slice injected at time T_E. It is similar to the ellipse in Fig. III.6a. For convenience the angle $2\pi Q_H i$ is taken to be an integral number times 2π.

The line AB is parallel to the long axis of the ellipse and halves the short axis. Of the area of the ellipse $\approx$20% lies on the right-hand side of AB. The time T_E is determined by the fact that for the slice injected at time T_E the following relation should hold:

$$MB = \sqrt{\frac{\hat{\beta}_s E_H}{\pi}} \tag{III.23}$$

or

$$\{P_0(T_E) + DI(T_E)/2\}^2 + \hat{\beta}_s^2 \{DIP(T_E) + DI(T_E)/(2\beta_l)\}^2 = E_H \hat{\beta}_s \quad . \tag{III.24}$$

By substituting in this formula the expressions for P_0, DI, DIP, and β_l, using the Eqs. (III.14), (III.15), (III.16), and (III.18), respectively, a relation is obtained between T_{IKS}, Q_H, and n_t. Solving for T_{IKS} the value T_{IKS}^c is obtained for which to a good approximation 5% of the PSB beam lies outside an emittance E_H after injection. The result of this calculation can be found in Appendix III.

In some special situations the above-mentioned method of estimating T_{IKS} is not precise enough. By linearizing the efficiency behaviour around T_E, using the above calculated T_{IKS} value as first approximation, a more accurate value for T_{IKS} can be obtained. This procedure is also described in Appendix III.

Finally the efficiency of the whole injection process can now be calculated for a specific Q_H value. First the efficiency of a number of beam slices injected at regular time intervals is computed. The partial acceptance of each of these slices is divided up into small rectangles. Using the known particle-distribution function in phase space the number of particles in each rectangle can then be found. A summation over all rectangles in the partial acceptance then yields the total number of accepted particles in the slice and hence the efficiency.

The overall efficiency is then obtained by an integration in time, using Simpson's rule, based on the calculated efficiency of the set of selected slices. More details of this calculation are given in Appendix IV.

III.3 THEORETICAL PREDICTIONS AND COMPARISON WITH MEASUREMENT[46)]

III.3.1 Results of the calculations for the model

The results of the calculations for the variable parameters DI, DIP, β_l, and T_{IKS} are shown in Figs. III.8a, b, c, and d, respectively. The best values of the parameters are plotted as a function of Q_H for $n_t = 15$. The resulting efficiency is shown in Fig. 8e. The dots in the efficiency plot represent the calculated efficiency when the time-dependent optimized parameters $DI(t)$, $DIP(t)$, and $\beta_l(t)$ are used in the efficiency calculation instead of the averaged values. The gain is seen to be only marginal, so that investment in expensive equipment in order to change the parameters during injection is certainly not justified. Qualitatively it can easily be understood that the gain is so small; when the partial acceptance is large compared to ε_0 the efficiency is not sensitive to small variations of the parameters and in the case where the partial acceptance is relatively small the number of particles involved is only a small fraction of the total beam current.

From the Figs. III.8a to III.8e immediately several features show up. The efficiency is relatively independent of the Q_H value, with three dips around $Q_H = 4.33$, 4.5, and 4.67. These low efficiencies are accompanied by large T_{IKS} values, which indicates that the partial acceptance configuration favours the particles with relatively large horizontal betatron amplitudes. To compensate for this the movement of the closed orbit has to be slowed down to keep 95% of the particles within the wanted horizontal emittance. These two Q_H values are also marked by relatively large DIP and low DI values.

To illustrate this in more detail, the partial acceptance for the Q_H value 4.33 is shown in Fig. III.9. Cut 0 is almost parallel to cut 3. The partial acceptance is long and thin, which translates itself into the small DI and β_l values calculated. As a consequence of the angle of cut 3 with respect to cut 0, the best efficiency is obtained when the DIP value is significantly different from zero at the end of the process. The cut 1 moves relatively fast away from the centre of the figure while cut 3 moves only slowly. The same explanation is valid for the DIP values around 4.1 and 4.9.

As a consequence of the relatively low β_l and large DIP values, many particles will have relatively large horizontal amplitudes around the Q_H values 4.33 and 4.67. However, a beam with a horizontal emittance of 130 π mm · mrad is wanted, and consequently the T_{IKS} value must be larger than is needed for the other Q_H values.

For this reason low efficiencies are predicted around the Q_H values 4.33, 4.67, and 4.5.

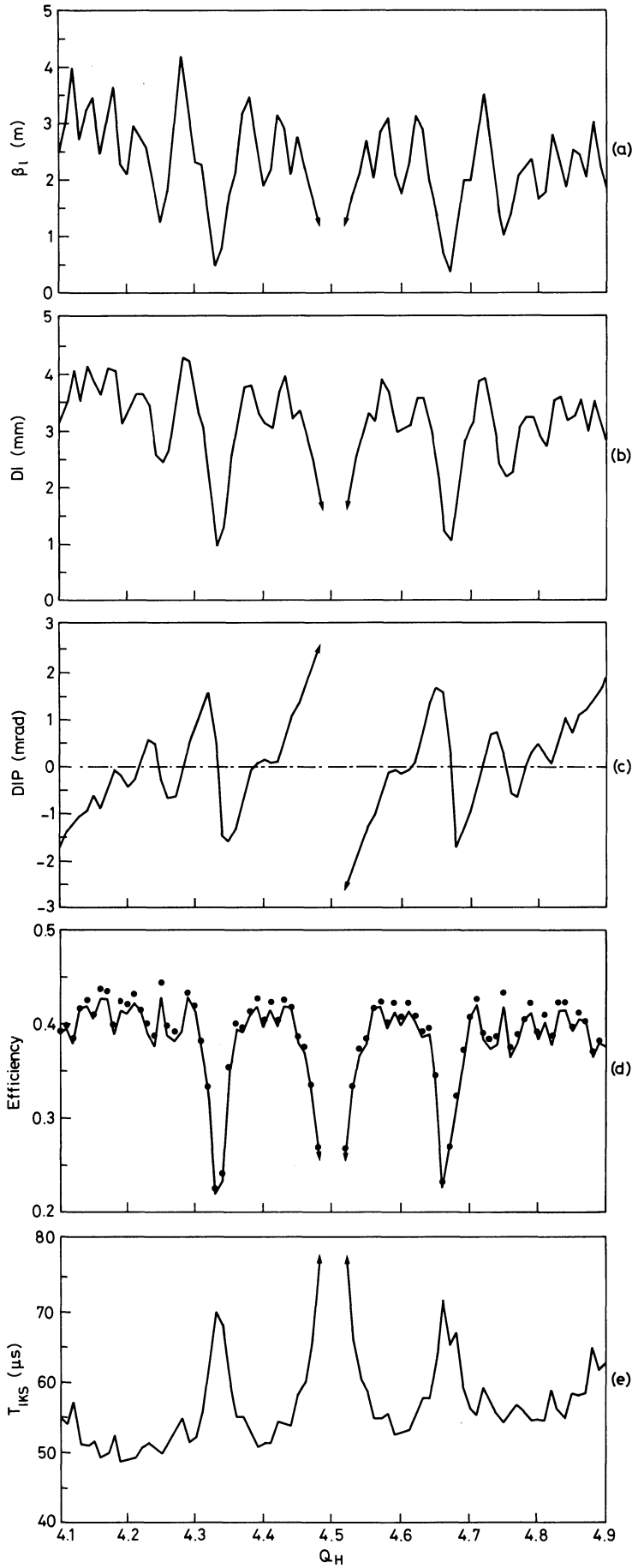

Fig. III.8 Plots of the calculated optimized parameters versus Q_H for 15 injected turns and DS= 1.5 mm. The dots in (e) represent the efficiency when DI, β_l, and DIP are optimized functions of t.

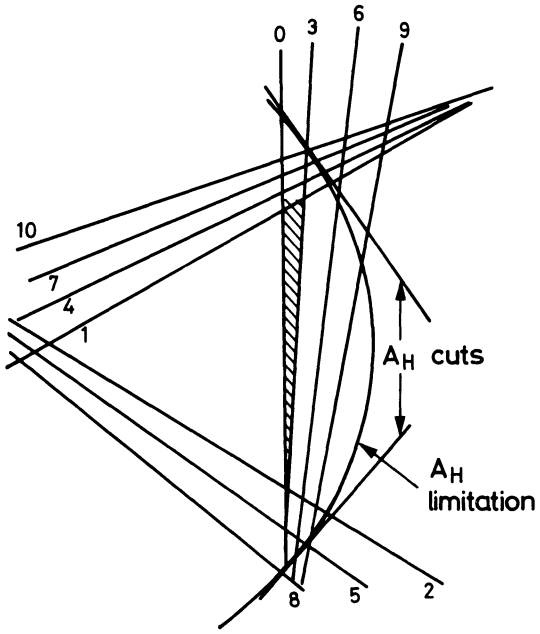

Fig. III.9 The influence of the horizontal acceptance (A_H) on the partial acceptance when $Q_H = 4.33$.

For the same reason one would expect low efficiencies around $Q_H = 4.25, 4.75, 4.2, 4.4, 4.6$, and 4.8. This is not the case for the PSB, since the partial acceptances are more symmetric and the distance from cut 0 to cut 4 in the case of $Q_H = 4.25$ and 4.75, and to cut 5 in the other four cases, is sufficiently large to obtain a partial acceptance which allows more particles to be injected with small *DIP* and large *DI* values.

III.3.2 Comparison of the model predictions with experiment

III.3.2.1 Methods used for the measurement of the injection parameters

Below, the methods of measuring Q_H, *DI*, *DIP*, and the efficiency will be discussed.

The Q_H values are measured with the Q kickers described in Section I.6.2. In the curves of Fig. III.10 the measurements are corrected for space-charge forces and the error is determined by the jitter in the measured value of the coherent Q_H value and the spread and shift in the incoherent Q_H value (see Section III.2).

The measurements of the values of *DI* and *DIP* are carried out in an indirect way, because during the injection of the beam many particles are lost on the septum, and the Pick-Ups placed directly after the injection septum are sprayed with particles thus rendering their signal unreliable. As a consequence, the position and the angle of the beam immediately after the septum cannot be measured directly.

DI has been measured indirectly in the following way. By moving the injection septum in a parallel way away from the vacuum chamber axis (increasing *DSE*) less beam will enter the vacuum chamber and the cut 0 shown in Fig. III.4b will move from the left to the right when the alignment of the incoming beam is not changed in the meantime. The position of the septum with respect to the vacuum-chamber centre is known with a precision of 0.1 mm and for a slice of incoming beam a plot can be made (*DI*, *DIP*, and β_l constant) of the current entering the PSB at the injection point versus the injection septum position. Per definition 50% of the beam enters the PSB when *DI* is zero. This has permitted the estimate of *DI* with an error of ± 0.5 mm.

The absolute *DIP* value is determined by minimizing the betatron oscillations of the beam, while half a turn is injected by looking at a suitable horizontal difference signal from a Pick-Up electrode. The error is ± 0.7 mrad. All other *DI* and *DIP* values different from $DIP = 0$ and $DI = 0$ can be determined from the currents in the steering dipoles placed in the injection line. The error introduced by this procedure is of the order of ± 2 mm and ± 0.2 mrad.

The efficiency finally is calculated from the signal of the slow beam transformer at $300 \pm 20\,\mu$s after the moment of injection. The injected current is calculated from the beam transformers in the injection channel and the number of injected turns. The jitter in the injected intensity and that in the incoming beam intensity, together with the imprecision of the measurement of these values using different measurement methods, have determined the error in the efficiency.

III.3.2.2 Experimental conditions

The experiments were done under the following conditions:

i) $T_{IKS} = 60\,\mu$s
ii) $n_t = 13$
iii) $\beta_l = 2$ m
iv) $I_{linac} = 17$ mA
v) T_B minimal
vi) $DS = 3$ mm.

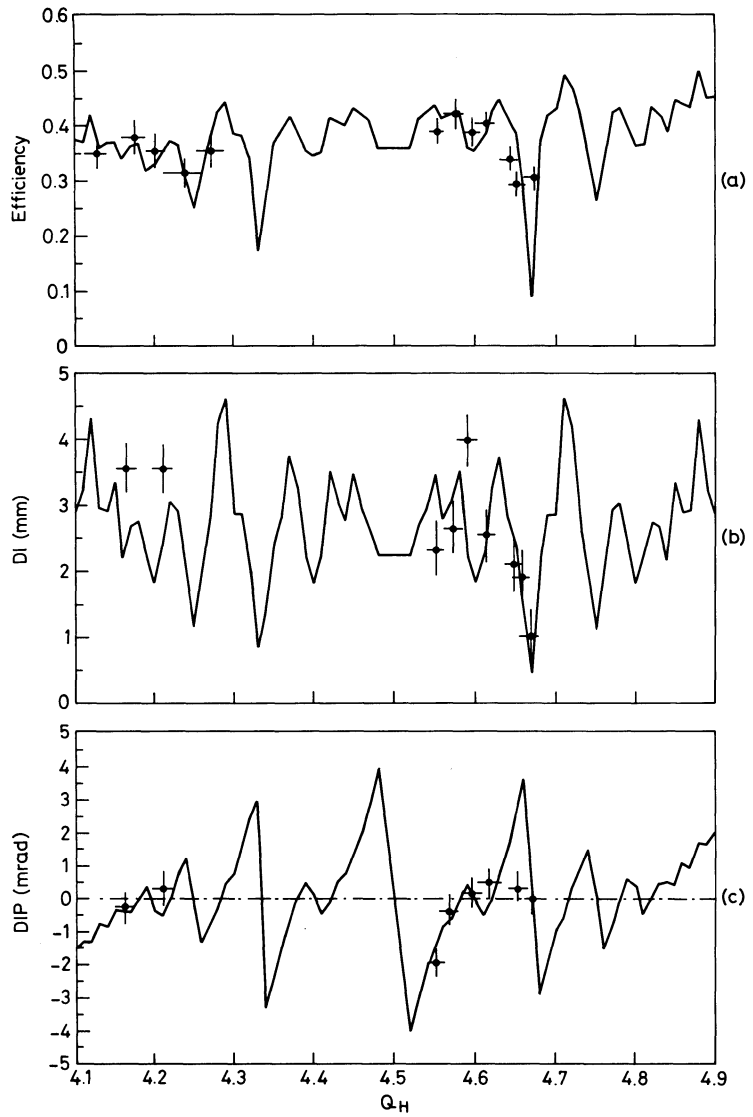

Fig. III.10 Efficiency, *DI*, and *DIP* plots versus Q_H. The solid lines represent the calculated values of the model, the dots are the measured values. $n_t = 13, DS = 3$ mm.

Below, the reasons for the choice of each parameter value will be discussed and the measurement of their values is described.

i) To obtain a good comparison of the model predictions with the experimental results around every Q_H value, each measurement should be done with an optimized T_{IKS} value such that the maximum current is injected within 130 π mm · mrad. However, this is a very long and trying procedure, which will not produce the wanted results anyway, as a horizontal emittance blow-up will occur for Q_H values around 4.67. Consequently the emittance measurements would not reflect the wanted results. Injection has thus been done with a fixed T_{IKS} value. This value is measured from an oscilloscope trace displaying the slow kicker signal.

ii) The value $n_t = 13$ is chosen, together with $T_{IKS} = 60\,\mu$s; this combination of the two parameters is known to yield beams with properties approaching the wanted characteristics. Consequently it is easier to correlate the results directly with the daily operation of the accelerator. The value of n_t is measured by displaying the signal of the distributor magnet on the oscilloscope screen. The revolution frequency of the particles in the PSB at injection is precisely known and consequently n_t is easily derived.

iii) β_l is kept fixed at a value of 2 m instead of taking the optimized value for each Q_H value to obtain accurate *DI* and *DIP* measurements. A change of β_l by means of the quadrupoles foreseen for this purpose in the injection channel will influence the alignment of the incoming beam with respect to the PSB ring, as the beam never exactly passes through the centre of the quadrupoles. Later it will be shown that a β_l value of 2 m instead of the optimized values will not significantly change the efficiency (see Fig. III.17). β_l is not measured but obtained indirectly from a program which calculates the quadrupole settings needed to create the focusing conditions wanted at the entrance of the PSB, while taking into account the space-charge forces. The form of the beam envelope on the different TV screens mounted in the injection channel then serves as a test of the program calculations[47].

iv) The incoming beam intensity is reduced from 85 mA to 17 mA by means of the insertion of the sieve into the injection line. The sieve is a graphite block with equally spaced holes, through which only 20% of the beam passes.

v) The T_B value was minimized in the following way. First the injection is roughly optimized for the above conditions. Then only half a turn is injected, the survival pattern of which is recorded on an oscilloscope displaying the Fast Beam Transformer signal. T_B can then be adjusted such that all particles occupying the first injected slice are lost on the injection septum; it is then the same as calculated for the program. The error is $\simeq 1.5$ μs, and no absolute T_B is found, as its value depends on the mean energy of the incoming particles with respect to the bending field.

vi) $DS = 3$ mm is obtained from measurements described later in this section.

III.3.2.3 Comparison of measurements with theoretical predictions

In Fig. III.10 the calculated efficiency (*Eff*), *DI*, and *DIP* plots versus Q_H are shown for the parameter values discussed in Section III.3.2.2. In the same figure the measured *Eff*, *DI*, and *DIP* values are shown for $4.55 \leq Q_H \leq 4.68$. These measurements are done in this Q_H interval to verify the predictions of the model about the partial acceptance evolution. Most important changes take place in this interval. Error bars in the interval $4.13 \leq Q_H \leq 4.27$ are larger than those of the other interval; there the measurements were done on another day and had to be corrected for the day-to-day difference of the accelerator characteristics.

Comparing the measured values with the theoretical predictions shows that the correspondence between the two is well within the expected error except for the point $Q_H = 4.67$, where the efficiency behaviour does not show the dramatic decrease. A closer investigation reveals that the injection around $Q_H = 4.67$ and a T_{IKS} value of 60 μs provokes losses due to the acceptance limitation of the PSB. Reducing the *DIP* value from the calculated one compensates for these losses. This is also illustrated in Fig. III.9, where the A_H limitation is represented by the curved line. The introduction of the acceptance limitation in the model with the aid of an additional straight cut then results in the same *DIP* and efficiency behaviour as observed in the PSB.

Why is the cut provoked by the acceptance limitation not immediately included in the model? First of all, the representation of the A_H limitation by a straight cut is not possible in most other cases, and, secondly, one is not interested by an optimization within A_H but in an optimization within E_H, while the discrepancy for the Q_H value 4.67 is of minor importance. The addition of another complication to the model was not thought necessary as only the Q_H values 4.33 and 4.67 are involved. If one wants to use the model for efficiency calculations while filling the total acceptance of the accelerator, the T_{IKS} and T_E calculations should be suppressed and be replaced by a similar procedure to calculate the influence of A_H on the optimized injection parameters. In conclusion, from these experiments it can be said that the assumptions underlying the model and its results are indeed valid for the multiturn injection process in the PSB.

III.3.3 Investigation into the *DS* and optimized n_t values

Finally a few remarks should be made regarding the values chosen for n_t and *DS*.

The intensity within a given emittance E_H of the PSB after injection is equal to the product of the total efficiency *Eff* and the total number of injected particles. As this last number is proportional to n_t, the intensity of the PSB beam after injection is proportional to $n_t \cdot Eff$.

A certain value of the PSB beam intensity can, in principle, be obtained by either injecting only a few turns at high efficiency or injecting many turns at low efficiency. It is advisable to inject the lowest possible number of turns that is compatible with maximum attainable PSB beam intensity, because in that case the radiation damage caused by lost protons is smallest.

The relation between the calculated efficiency and n_t is shown in Fig. III.11 for three values of the horizontal emittance of the PSB beam. The number of equivalent turns $n_t \cdot Eff$ is plotted against n_t for $Q_H = 4.17$. The calculation could be checked by comparing with direct measurements of the total injection efficiency for different values of n_t. These measurements were done with a low intensity beam at a Q_H value of 4.17 and this is the reason for the choice of that Q_H value in the calculations.

A discrepancy between the measured and the theoretical efficiency was obtained when a *DS* value of 1.5 mm was assumed. The measured values of $n_t \cdot Eff$ for $E_H = 130\pi$ mm · mrad shown in Fig. III.11 should be compared with the broken line, which is the theoretical curve. The discrepancy of 30% between the experimental and the theoretical values is much larger than could be expected from the accuracy of the experiments. Much better agreement is obtained when the standard value for the effective septum thickness *DS* used in the calculations is raised from 1.5 to 3 mm. The effective *DS* value of 1.5 mm was obtained from the mechanical septum thickness of 1 mm by considering only particle dynamics[45]. Mechanical imperfections of the septum and small unexpected deviations of the particle trajectories may account for another increase in the effective *DS* value of 0.5 to 1 mm. The further increase to 3 mm may be partially explained by space-charge effects (see Chapter VI).

Once the value $DS = 3$ mm is adopted, good agreement is found between the measurements and the theoretical values, shown in Fig. III.11 as solid lines for three values of E_H. From these results the best n_t value can be obtained, not only for the standard beam but also for beams of different E_H. The curve for $E_H = 130\pi$ mm · mrad indicates that $n_t = 13$ is the optimum value for injection and this number of injected turns is therefore used in normal operation.

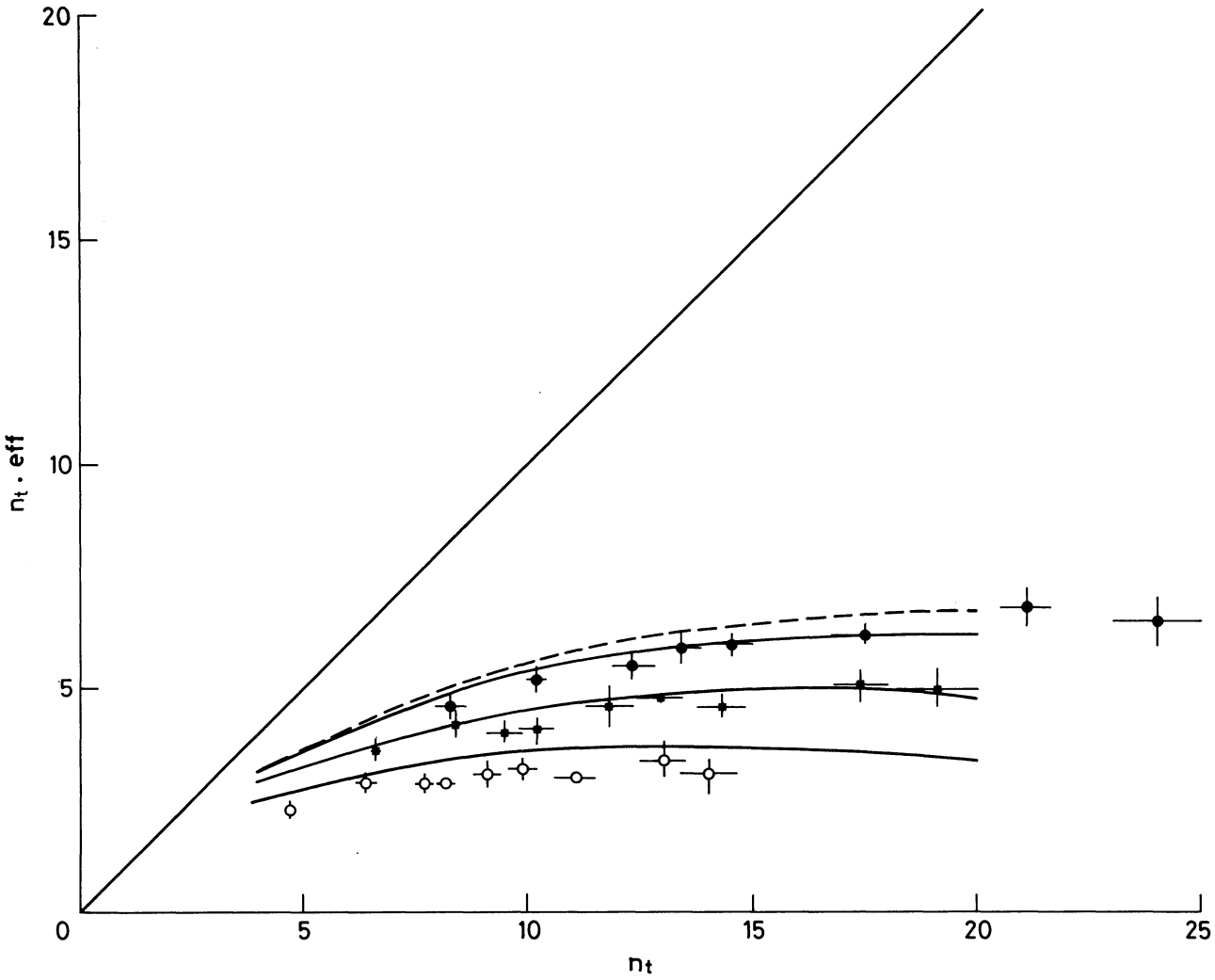

Fig. III.11 Plots of the measured number of effective turns ($n_t \cdot Eff$) versus the number of injected turns (n_t) for E_H = 100, 130, and 160 π mm · mrad. The solid lines represent the calculated plots for the same three E_H values with DS = 3 mm. The dotted line represents the same plot for $E_H = 130\pi$ mm · mrad when DS = 1.5 mm.

III.3.4 Relative merits of this model

Having verified the predictions of the model, its merits compared with those of others can be evaluated. In Refs. 43 and 44 the PSB multiturn injection efficiency is studied with the aid of a simulation program. Owing to the complexity of the optimization of all parameters, the authors assumed there that *DIP* should be zero for all Q_H values. While most of the predictions coincide with those of the model presented here, it proves that around the Q_H values 4.1 and 4.9 the predicted efficiency is 20% lower than in reality, which is not the case for the model presented in this paper, as can be verified in Fig. III.10. In the same papers the efficiencies claimed for Q_H = 4.33 and Q_H = 4.67 are not based on the n_t value they are referring to. Actually the structure of their program imposed an upper limit on their n_t value. For Q_H = 4.17 this value is 15 as found in Fig. III.11, while for Q_H = 4.33 their maximum n_t value is 6.

In Ref. 37 another approach to the multiturn injection problem was tried. Those authors thought that the β_l values could be better adjusted to the Q_H values 4.25, 4.33, 4.67, and 4.75. From the experiments and the predictions in this paper it proves that the adaptation of the incoming beam ellipse has only a secondary influence on the efficiency. As a consequence their conclusion that one should inject arount these Q_H values is wrong. This will be explained in detail below.

From the partial acceptances determined by the model, it can be seen that the value of the relation "circumference of the partial acceptance" versus "the surface of the partial acceptance" increases with decreasing optimized β_l value. As a result, the relation of the surface area occupied by the septum shadow to the surface area of the partial acceptances within E_H increases with decreasing optimized β_l value. The efficiencies around the Q_H values demanding small optimized β_l values are consequently lower, which is verified experimentally (Q_H = 4.33, 4.67, and 4.5).

In short:

a) The importance of the septum shadow increases with decreasing β_l.

b) The influence of the β_l optimization is small compared to the influence of the septum shadow.

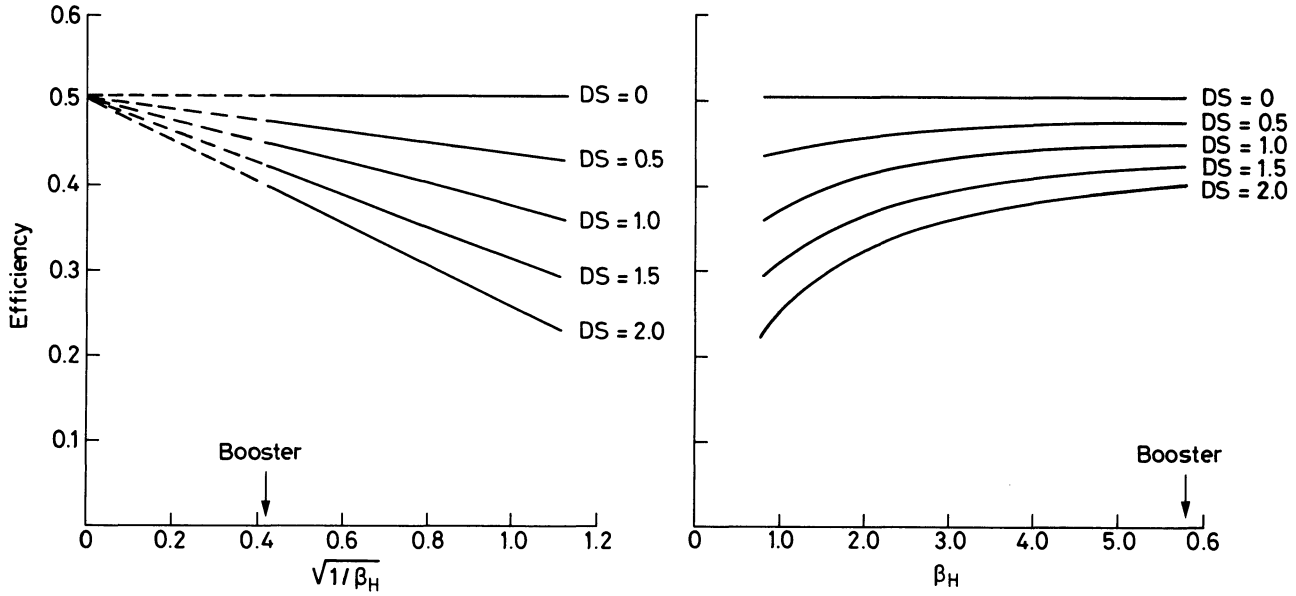

Fig. III.12 Plots of the calculated efficiency versus β_H and $\sqrt{1/\beta_H}$ for five different DS values. The arrows indicate the β_H value of the PSB.

One might now argue that if a small β_l value is detrimental for the injection efficiency this can be remedied by increasing β_s, as β_l changes linearly with β_s according to Eqs. (III.18) and (III.20). From the formulae of Sections III.2 and III.3 it is known that if the septum shadow is zero ($DS = 0$):

$$DI \sim 1/T_{IKS}, \quad \beta_l \sim \beta_s, \quad T_{IKS} \sim 1/\sqrt{\beta_s}. \tag{III.25}$$

The partial acceptance area in the case $DS = 0$ will not be affected by a β_s change there:

$$\frac{DI^2}{\beta_l} \sim 1/(\beta_s T_{IKS}^2) = \text{const.} \tag{III.26}$$

This confirms that the low efficiency around Q_H values with a relatively low optimized β_l is more influenced by the septum-shadow contribution than by the geometric properties of the partial acceptance as assumed in Ref. 37. For the multiturn injection in the PSB it is interesting to know by how much the β_s value at the injection point has to change to minimize the influence of the septum shadow. In Fig. III.12 the injection efficiency is plotted as a function of $1/\sqrt{\beta_s}$ and as a function of β_s for several DS values. The arrow indicates the β_s value of the PSB and the dotted line is an extrapolation to $\beta_s \to \infty$. Figure III.12 shows that quite a large change in β_s is needed to obtain only a small improvement in the septum-shadow contribution to the injection efficiency.

III.4 THE INFLUENCE OF SMALL FLUCTUATIONS IN THE INJECTION PARAMETERS ON THE MULTITURN INJECTION PROCESS

The characteristics of the beam entering the PSB will differ from pulse to pulse owing to all kinds of imperfections that modify the currents of the magnets in the incoming beam line and the main PSB rings. These fluctuations cause pulse-to-pulse variations in the position and profile of the injected beam, and in the energy and the position of the PSB beam. As the multiturn injection process is very sensitive to these variations the consequence will be a pulse-to-pulse variation in the intensity of the PSB beam[49].

In this section the sensitivity of the injection efficiency to small fluctuations in the injection parameters is discussed. The results can be used to specify the stability required from the various magnet power supplies. A qualitative description of the effect of these fluctuations is given in Sections III.4.1 and III.4.2, illustrated with measurements of the evolution of the intensity of a PSB beam slice during the first ten turns after injection. In Section III.4.3 the influence of fluctuations in the injection parameters is calculated, using the methods described in Section III.2. The results of the calculations are compared with direct measurements of the overall injection efficiency.

III.4.1 Injected beam parameters and their fluctuations

Owing to pulse-to-pulse changes in the currents of the quadrupoles and bending magnets in the Linac-PSB injection line, small variations will occur in the steering parameters DI and DIP and the focalization parameter β_l of the

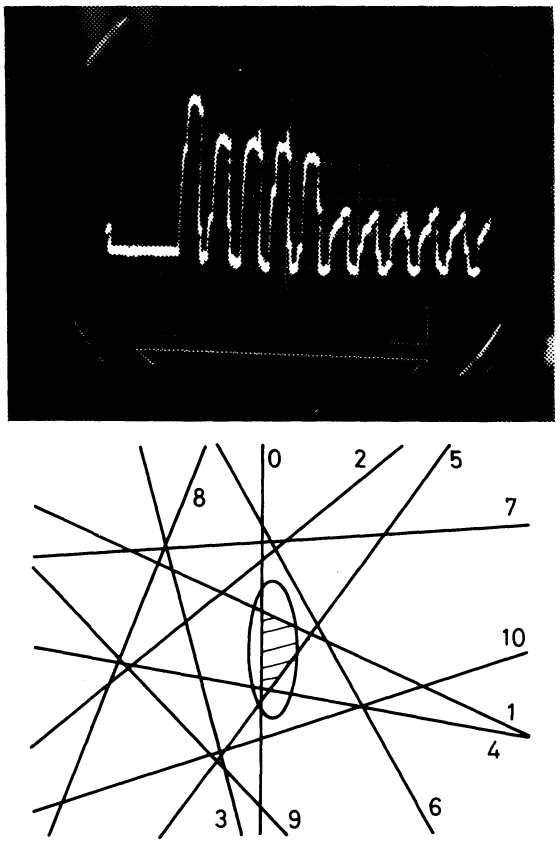

Fig. III.13 Oscilloscope trace of the slice survival pattern for a slice injected with optimized injection parameters for $Q_H = 4.17$. The drawing represents the septum cuts in the horizontal phase plane with respect to the slice centre.

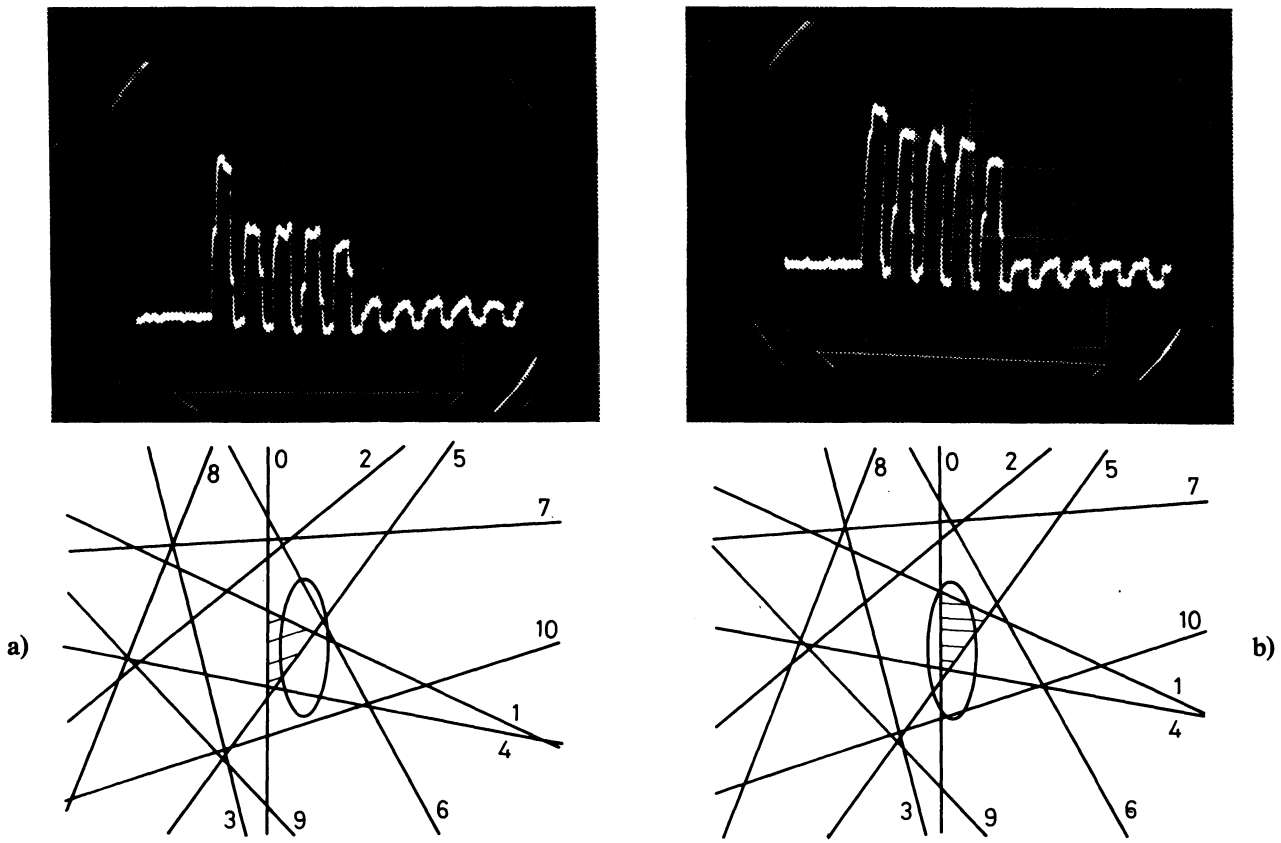

Fig. III.14 a) Oscilloscope trace of the slice survival pattern when *DI* is increased. A drawing of the slice is also shown.
b) Oscilloscope trace of the slice survival pattern when *DIP* is increased. A drawing of the slice is also shown.

injected beam. The influence of these variations on the efficiency of an injected beam slice can be qualitatively understood by considering the resultant change in the relative position of the partial acceptance and the equidensity ellipse with area ε_0 for this slice in horizontal phase space.

In the diagram in Fig. III.13 the situation in the horizontal phase plane at the injection point is shown for an undisturbed injected beam slice in the coordinate system defined in Section III.1. The diagram is analogous to Fig. III.4a in that section, while the injection time of the slice is chosen to be approximately $t \approx T_B + 3\, t_{rev}$. The slices injected around this time demonstrate best the influence of the individual cuts for the first ten revolutions of a slice. Now an easy comparison can be made with the direct beam measurements that were done on the PSB machine. For these measurements half a turn of beam was injected into the PSB and a photograph was taken of the fast beam transformer signal (see Section I.6.1), showing the intensity of the beam slice for the first ten turns in the PSB. The photograph corresponding to the diagram is shown in Fig. III.13. The effect of the septum cuts after the first and the fifth revolution can be clearly seen.

In the undisturbed situation of Fig. III.13, *DI* and *DIP* have the optimum values and $\beta_l = 2$. The effect of a change in each of these parameters will now be considered.

In Fig. III.14a the effect is shown of a change in *DI*. This variation affects in particular the percentage of beam lost in cut 0 and the cuts i for which $|\cos 2\pi Q_H i| \approx 1$.

A change in *DIP*, shown in Fig. III.14b, has the opposite effect. The percentage of beam lost by cut 0 is not affected, but big changes will occur for cuts i with $\cos 2\pi Q_H i \approx 0$, i.e. cuts that are almost horizontal in the diagram.

Magnet variations affecting the focalization of the injected beam may change both β_l and β_l'. It will be assumed here that the variation is such that β_l' remains zero and that only β_l is changed. What happens when $\beta_l' \neq 0$ can be easily deduced from the discussion below. A variation of β_l changes the number of particles lost for every cut. A diagram and corresponding beam-transformer signal for $\beta_l = 5$ is shown in Fig. III.15. This figure should be compared

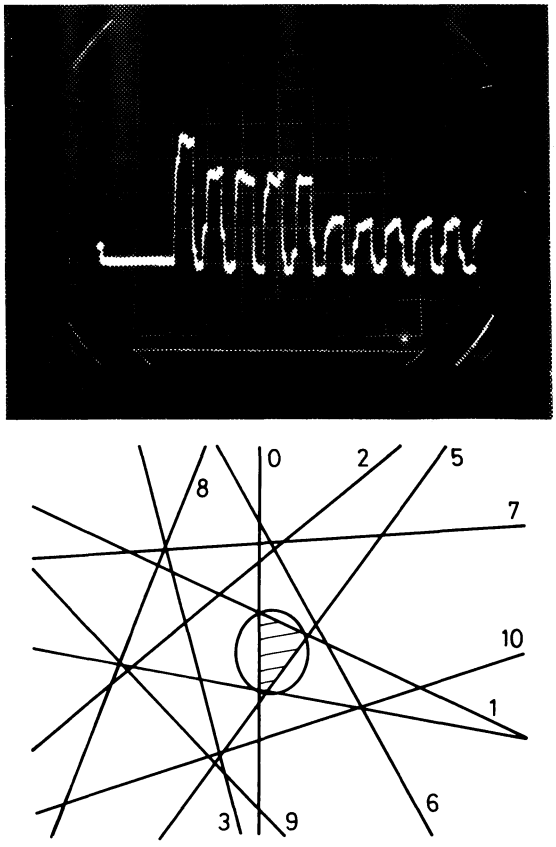

Fig. III.15 Oscilloscope trace of the slice survival pattern when β_l has been increased. A drawing of the modified slice is also shown.

with Fig. III.13, where the situation is shown for $\beta_l = 2$. When β_l increases the number of particles lost in cut 0 and in the cuts i with $|\cos 2\pi Q_H i| \approx 1$ increases, while the number of particles lost in cuts i with $|\cos 2\pi Q_H i| \approx 0$ decreases. For decreasing β_l the effect is in the opposite direction.

III.4.2 Fluctuations in the particle energy or in the magnetic field of the PSB

The closed orbit of the particles in the PSB is determined by their momentum p and by the main bending field B of the PSB. A fluctuation in either one of these quantities changes the position of the closed orbit according to the relations

$$\frac{dR}{R} = a\left(\frac{dp}{p}\right)_B = -a\left(\frac{dB}{B}\right)_p \quad , \tag{III.27}$$

where a is the the momentum compaction factor[28].

A variation in p or B, for unchanged values of all other parameters, has the effect that R and therefore the distance DSE between the undeflected closed orbit and the inner septum edge is modified (see Fig. III.2b). As DO, the maximum closed orbit deflection, is kept constant the distance DK also changes. When T_B is not readjusted Eq. (III.21) is then no longer valid, but the original injection conditions, for which Eq. (III.21) is satisfied, can be restored by changing T_B by an amount

$$\delta T_B = -\frac{T_{IKS}}{DO}\delta R \quad . \tag{III.28}$$

The diagram and the photograph in Fig. III.16 show how the injection conditions change for the injected beam slice when the injection is started 5 μs earlier than in Fig. III.13. This change in T_B is equivalent to an increase in R of 3.8 mm and this again to a decrease in B of 0.25%. A variation in B of this magnitude is seen to cause a considerable decrease in efficiency, while its magnitude will be equal to the efficiency decrease caused by an equivalent change in T_B. This manifests itself equally well in the size of the horizontal emittance measured after the end of the injection process.

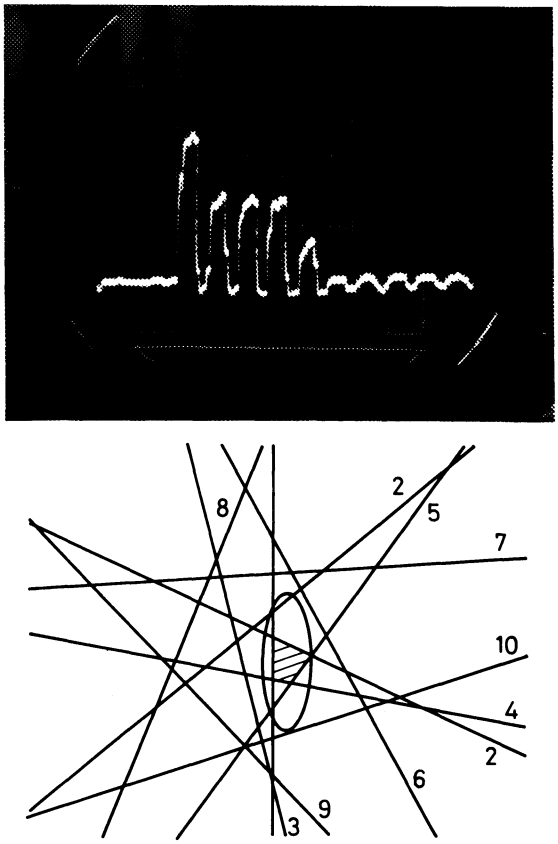

Fig. III.16 Oscilloscope trace of the slice survival pattern when the magnetic field at injection has been decreased. The drawing shows the effect on the cut pattern.

The qualitative half-turn injection behaviour when there are fluctuations in the parameters DI, DIP, β_t, or the mean energy E of the PSB beam is summarized in Table III.1, where the influence of each type of fluctuation on the number of particles removed by the septum cuts is indicated. This scheme proved to be a powerful instrument to identify the cause of pulse-to-pulse intensity variations in the PSB beam[49].

Table III.1
Influence of fluctuations in the injection parameters on the slice survival patterns

Type of fluctuation		Cut	$\lvert\cos(2\pi Q_H i)\rvert \approx 0$	$\lvert\cos(2\pi Q_H i)\rvert \approx 1$
Steering	$DIP \uparrow$	0	↑	0
	$DI \uparrow$	↑	0	↓
Focalization	$\beta_l \uparrow$	↓	↑	↓
Mean energy	$\Delta E \uparrow$	0	↓	↓

III.4.3 Influence of fluctuations in injection parameters on overall efficiency

For the specification of stability requirements for the elements in the injection line and for the injector more is needed than a qualitative knowledge of the influence of fluctuations in parameters on the injected intensity. The overall efficiency was therefore calculated for a number of values of the parameters DI, DIP, β_l, and the particle energy E. The method described in Section III.2 and Appendix IV was used and only one parameter was changed at a time, keeping the values of the other parameters constant at their standard optimized values. The results of the calculation are shown in Fig. III.17, where the overall efficiency Eff is shown as a function of each of the four parameters considered. The

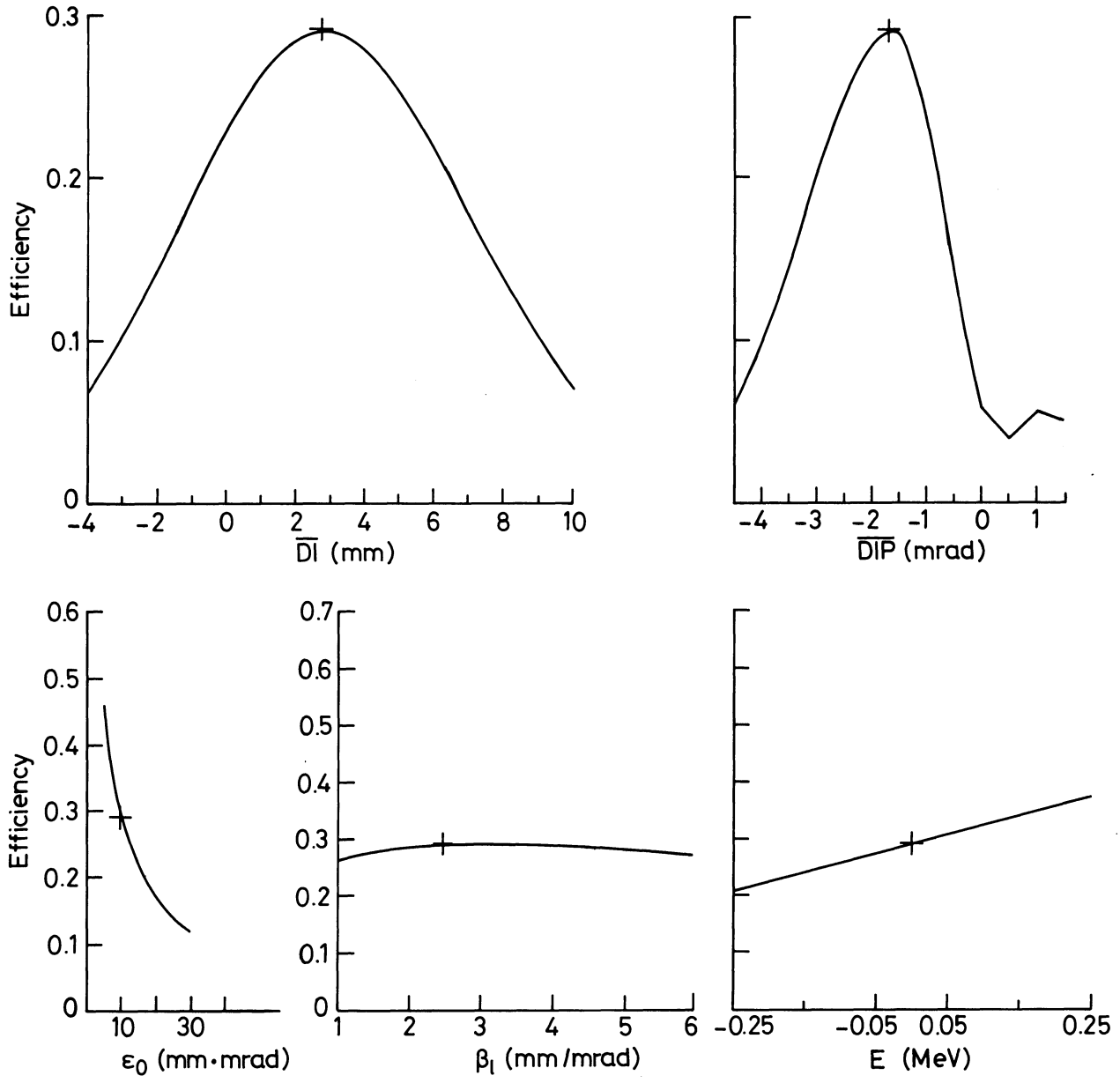

Fig. III.17 Plots of the injection efficiency versus the variations of the injection parameters.

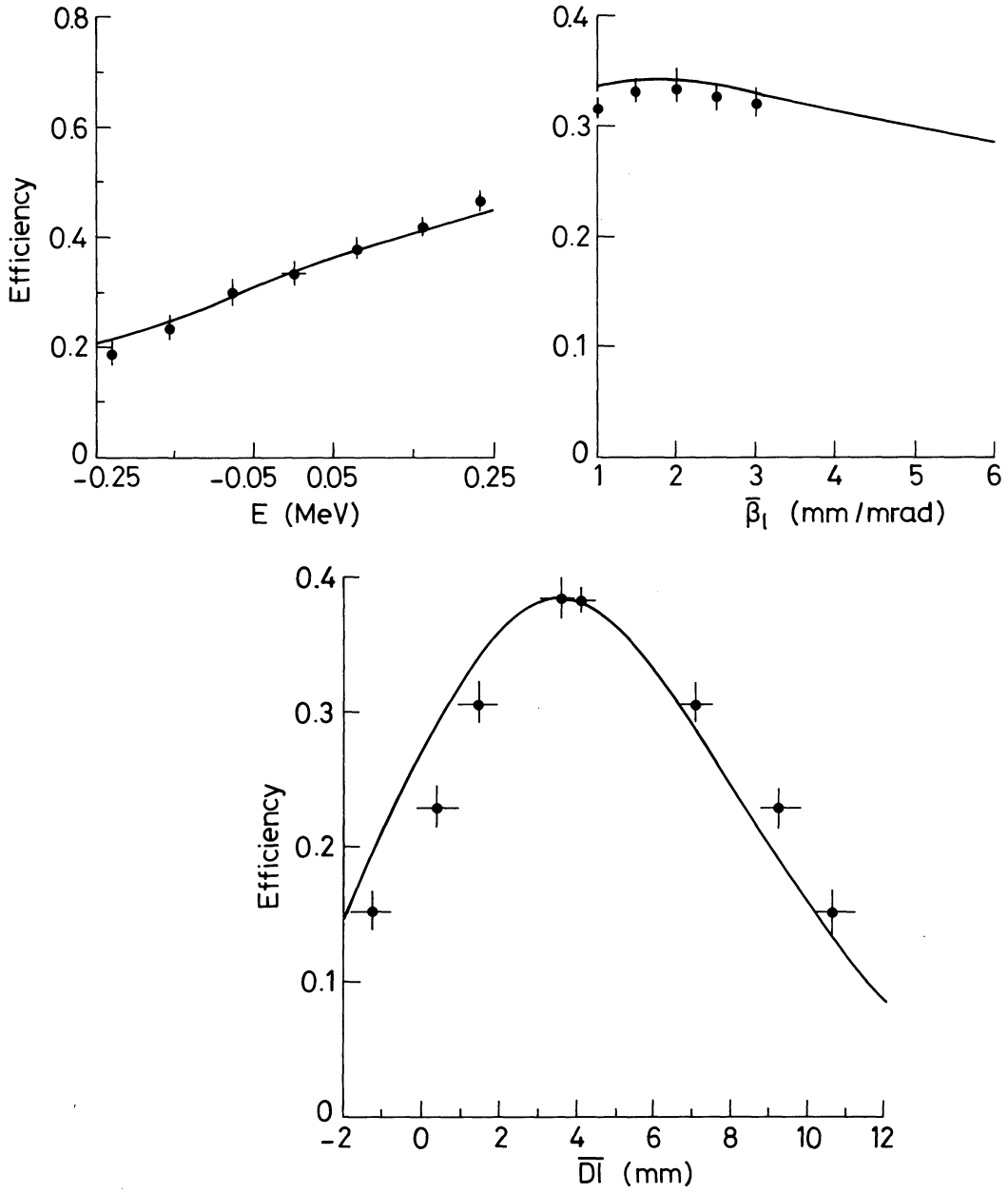

Fig. III.18 Plots of the efficiency versus the injection energy E, the injection focusing, and the injection alignment DI. Dots represent measured values, while the solid lines represent model predictions.

standard optimized values of the parameters are indicated with a cross. Also shown is the dependence of the efficiency on ε_0, the fixed parameter determining the horizontal emittance of the injected beam. As expected, the efficiency increases markedly for smaller ε_0, but ε_0 is fixed by the intrinsic properties of the injector and cannot be changed at will.

For some of the parameters the dependence of the efficiency of injection on the value of the parameter could be directly measured. The result of these measurements is shown in Fig. III.18 together with the theoretical curves calculated for the values of the injection parameters that were valid when the measurements were made. These values are given below the figures. The value for the effective septum thickness $DS = 3$ mm used in the calculation is the measured value determined from Fig. III.11.

The measurements were done with an injected intensity of 2.3×10^{12} protons per pulse. Although this is not the maximum intensity available, the injected intensity is still so large that corrections had to be made for the influence of space-charge forces. The value of DI was varied by moving the incoming beam with two horizontal dipoles placed in the injection channel. The β_l value was changed by adjusting the current in four quadrupoles in the injection line. For this measurement a Q_H value of 4.65 was chosen because the influence of a change in β_l on the injection efficiency was expected to be strongest at this Q_H value. The different values of E were obtained by changing the main magnetic field B of the PSB at injection.

The agreement between the measured and the theoretical curves for the injection efficiency is remarkedly good.

CHAPTER IV

INCREASE OF MULTITURN INJECTION EFFICIENCY BY MEANS OF SKEW QUADRUPOLES

IV.1 INTRODUCTION

In 1953 it was discovered in the Cosmotron, a weak focusing machine, that a coupling between the horizontal and the vertical betatron oscillations could improve the multiturn injection efficiency[50,51]. In the PSB, a strong focusing machine, this method was rediscovered. It made an intensity increase of 20% possible.

An injected particle has a certain chance of hitting the injection septum after i turns in the machine. If during the first few revolutions, which are important for the efficiency of the process, the horizontal betatron amplitudes can be decreased, the particle has less chance of hitting the injection septum and therefore a bigger chance of survival. This can be achieved by introducing a coupling between the horizontal and the vertical betatron oscillations of the particle, which results in a periodic amplitude exchange or beating between the vertical and the horizontal betatron amplitudes. One of the main results of the theory describing this coupling process is that the sum of the horizontal and vertical Courant-Snyder invariants for one particle is constant. The formula is $I_x + I_z = \text{const}$. This means that the vertical amplitudes increase when the horizontal ones decrease. Thus sufficient vertical acceptance should be available; otherwise the particles are lost vertically.

As already mentioned in Chapter II, the vertical acceptance of the PSB is $100\,\pi$ mm · mrad, while the vertical emittance of the incoming Linac beam is $30\,\pi$ mm · mrad. Sufficient extra space is therefore available in the PSB.

In the PSB the coupling is introduced with the aid of skew quadrupoles. These are normal quadrupoles turned through 45° around the machine axis. In each PSB ring four equally spaced skew quadrupoles were actually available, two turned 45° in one sense and two turned 45° in the opposite direction (see Fig. IV.1). They were not specifically installed for increasing the injection efficiency, but were originally foreseen for correcting possible skew quadrupole field errors. However, they were ideally placed for the purpose of coupling the horizontal and vertical betatron oscillations.

In Section IV.2 a short review will be presented of the coupling theory necessary to explain the phenomena related to the multiturn injection process.

In Section IV.3 an introduction is given to the influence of a skew quadrupole field on the behaviour of the individual slices.

In Section IV.4 the experiments[52] carried out in the PSB are discussed and the results presented, while in Section IV.5 a more extensive calculation is done to explain the results in more detail.

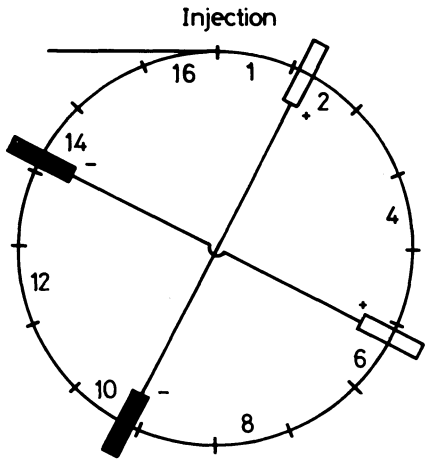

Fig. IV.1 Harmonic skew quadrupoles in the PS Booster.

IV.2 COUPLING THEORY

In the following section a short discussion will be given on the effect of a horizontal–vertical coupling term on the behaviour of the individual particles [see, for example, Chao and Month[53]]. Only skew quadrupoles are treated, as this suffices in the context of this chapter.

One starts from the following equations for betatron motion, equivalent to Eqs. (III.3) but with a coupling term added:

$$\begin{aligned} \frac{d^2x}{ds^2} + K_x(s)x &= M(s)z \\ \frac{d^2z}{ds^2} + K_z(s)z &= M(s)x \quad , \end{aligned} \tag{IV.1}$$

where $M(s)$ corresponds to the skew quadrupole fields around the circumference. The solution of Eq. (IV.1) for $M(s) = 0$ was derived in Section II.1.1. According to Eq. (II.8) the solution can be written as

$$y(s) = \sqrt{I_y}\sqrt{\hat{\beta}_y(s)}\,\cos\{\psi_y(s) + \chi_y\} \quad . \tag{IV.2}$$

The variable y indicates either the x- or the z-coordinate. I_y and χ_y are constants determined by the initial conditions of the particle. The periodic function $\hat{\beta}_y(s)$ is the betatron function for the accelerator and

$$\psi_y(s) = \int_0^s \frac{ds^*}{\hat{\beta}_y(s^*)} \quad . \tag{IV.3}$$

The solution of Eq. (IV.1) for $M(s) \neq 0$ can be found by remarking that, in the special problem considered here, the coupling terms on the right-hand side of Eq. (IV.1) are relatively small. To obtain the desired effect on the injection efficiency the period of the beating caused by the coupling should in fact be larger than 25 machine revolutions, so that the betatron frequency is about one hundred times the beating frequency. Under these circumstances the solution of Eq. (IV.1) is almost equal to Eq. (IV.2), but the constants I_y and χ_y in Eq. (IV.2) are now slowly varying. For a particle with the same starting conditions as described by Eq. (IV.2), the solution can then be written in exponential notation:

$$y(s) = \frac{a_y(s)}{2}\sqrt{\hat{\beta}_y(s)}\,\exp\{i\psi_y(s)\} + \text{c.c.}\,, \tag{IV.4}$$

where $a_y(s)$ is a slowly varying complex function with a starting value given by

$$a_y(0) = \sqrt{I_y}\,e^{i\chi_y} \quad , \tag{IV.5}$$

while $\hat{\beta}_y(s)$ and $\psi_y(s)$ are the same functions as in Eq. (IV.2). The substitution of Eq. (IV.3) into Eq. (IV.1) leads to the relations

$$\begin{aligned} \left\{\frac{d(\hat{\beta}_x a_x')}{ds} + 2i\frac{da_x}{ds}\right\} e^{i\psi_x} + \text{c.c.} &= M(s)a_z\sqrt{\hat{\beta}_x\hat{\beta}_z}\,e^{i\psi_z} + \text{c.c.} \\ \left\{\frac{d(\hat{\beta}_z a_z')}{ds} + 2i\frac{da_z}{ds}\right\} e^{i\psi_z} + \text{c.c.} &= M(s)a_x\sqrt{\hat{\beta}_x\hat{\beta}_z}\,e^{i\psi_x} + \text{c.c.} \end{aligned} \tag{IV.6}$$

As a_x and a_z are slowly varying functions of s, the first terms in Eqs. (IV.6) that contain only second-order derivatives of a_x and a_z can be neglected. The terms $\beta_x' a_x'$ and $\beta_z' a_z'$ vanish when $a_x'' = a_z'' = 0$, because in that case a_x' and a_z' are constant and the integral of β_x' and β_z' over one complete revolution yields zero. Finally, to separate the slowly varying terms from the fast oscillating terms, the first equation of (IV.6) is multiplied by $\exp(-i\psi_x)$ and the second by $\exp(-i\psi_z)$. The variable $\vartheta = s/R$ is substituted for s and the coupling terms on the right-hand side of Eqs. (IV.6) are averaged over one machine revolution. Thus the fast oscillating terms containing $2\psi_x$ and $(\psi_x + \psi_z)$ in the exponential are removed and the final result is

$$\frac{da_x}{d\vartheta} = -i\frac{R}{4\pi}a_z\int_0^{2\pi} M(\vartheta)\sqrt{\hat{\beta}_x\hat{\beta}_z}\,\exp(i\psi_z - i\psi_x)d\vartheta \tag{IV.7}$$

and a similar equation with x and z interchanged.

The right-hand terms can be written in a more useful form by introducing a number $\delta \ll 1$, defined by the relation

$$Q_H - Q_V = k + \delta \qquad k \text{ integer}. \tag{IV.8}$$

Only small $\delta \ll 1$ will be considered. By substituting Eq. (IV.8) into Eq. (IV.7) one finally obtains the equation

$$\frac{da_x}{d\vartheta} = -ia_z e^{-i\vartheta\delta} \frac{R}{4\pi} \int_0^{2\pi} M(\vartheta) \sqrt{\hat{\beta}_x \hat{\beta}_z} \exp[i(\psi_z - Q_V\vartheta - \psi_x + Q_H\vartheta)]\, e^{-ik\vartheta}\, d\vartheta \tag{IV.9}$$

and a similar equation with x and z interchanged. Integration of the right-hand side leads to the two simple equations

$$\begin{aligned} \frac{da_x}{d\vartheta} &= iQ_c a_z \exp(-i\vartheta\delta) \\ \frac{da_z}{d\vartheta} &= iQ_c a_x \exp(-i\vartheta\delta) \quad , \end{aligned} \tag{IV.10}$$

where Q_c stands for the total coupling term

$$Q_c = Q e^{iq} = -\frac{R}{4\pi} \int_0^{2\pi} d\vartheta M(\vartheta) \sqrt{\hat{\beta}_x \hat{\beta}_z}\, e^{-ik\vartheta} \exp\{i(\psi_z - Q_V\vartheta) - i(\psi_x - Q_H\vartheta)\} \quad . \tag{IV.11}$$

The relations (IV.10) can be combined to give

$$\begin{aligned} \frac{d^2a_z}{d\vartheta^2} - i\frac{da_z}{d\vartheta} + Q^2 a_z &= 0 \\ \frac{d^2a_x}{d\vartheta^2} + i\frac{da_x}{d\vartheta} + Q^2 a_x &= 0 \quad . \end{aligned} \tag{IV.12}$$

The solutions of Eq. (IV.12) are readily obtained using the initial conditions of Eq. (IV.5). The final expression for the evolution of I_x with ϑ is then

$$I_x = a_x a_x^* = I_x(0) + \frac{4Q \sin\Theta}{\delta^2 + 4Q^2} \left\{ \left[Q(I_z(0) - I_x(0)) + \delta \sqrt{I_x(0) I_z(0)} \cos\chi_q \right] \sin\Theta \right.$$
$$\left. + \sqrt{I_x(0) I_z(0)}\, \sqrt{\delta^2 + 4Q^2} \sin\chi_q \cos\Theta \right\} \quad , \tag{IV.13}$$

where Θ and χ_q are defined by the following relations:

$$\Theta = \sqrt{(\delta/2)^2 + Q^2}\,\vartheta \tag{IV.14}$$

$$\chi_q = \chi_x - \chi_z - q \quad . \tag{IV.15}$$

A similar expression is obtained for I_z. The combination of these two results leads to the important relation

$$I_x + I_z = \text{const.} \tag{IV.16}$$

Equation (IV.16) shows that the sum of the Courant-Snyder invariants is constant. This means that the motion of the particle in the horizontal as well as in the vertical phase plane is bounded, but that the maximum displacement is in general larger than for the non-coupling case. According to Eq. (IV.13) the maximum amplitude of the particles depends on δ (the distance from the coupling line) and Q (the magnitude of the harmonic of the coupling field that drives the beating).

The phase of the I_x variation is determined by the initial phase χ_x and χ_z in the two betatron phase planes, and the phase q of the k^{th} harmonic coupling term with respect to the injection point.

IV.3 PRINCIPLES OF MULTITURN INJECTION WITH A HORIZONTAL–VERTICAL COUPLING TERM PRESENT

Equations (IV.13) and (IV.16) contain the principles for increasing the efficiency of the multiturn injection by the introduction of a coupling term. An exchange between horizontal and vertical betatron oscillation amplitudes takes place. If the right conditions are fulfilled the Courant-Snyder invariant I_x decreases during the first few revoutions. The initial condition $I_x(0)$ is given by the horizontal particle amplitude at injection.

To get some feeling for the behaviour of a slice of injected beam in the horizontal phase plane, the slice can be thought of as one rigid macro-particle. Its movement in phase space is then governed by Eqs. (IV.13) to (IV.15). Assuming that the slice is ideally aligned vertically [$I_z(0) = 0$, see Section II.2.1], Eq. (IV.13) simplifies to

$$\Delta I_x = I_x - I_x(0) = -I_x(0) \frac{4Q^2}{\delta^2 + 4Q^2} \sin^2 \left\{ \sqrt{\delta^2/4 + Q^2}\, \vartheta \right\} \quad . \tag{IV.17}$$

One of the first things to remark is that ΔI_x is proportional to $I_x(0)$. So the decrease of the horizontal betatron amplitude will be enhanced with increasing $I_x(0)$. The increase in efficiency will therefore be more pronounced near the end of the injection process.

The septum cuts that are responsible for the most important losses are the cuts created when the slice returns to its initial phase χ_x. In Fig. IV.2 the situation in the phase plane at the injection point is shown for $Q_H = 4.16$. Losses occur after turn 1 and turn 6. It is clearly visible that the horizontal betatron amplitude of the slice is smaller when the skew quadrupoles are turned on, thus decreasing the number of particles that are removed by the septum.

The decrease in the horizontal emittance after a given number of turns is determined by δ and the current in the skew quadrupoles. For example, the best choice for δ should be such that the minimum I_x occurs after 6 turns. The frequency of the beating should therefore be $1/(2 \times 6 \times t_{rev}) \approx 50$ kHz.

The case $\delta = 0$ should be avoided as this corresponds to a minimum I_x value of zero. This gives too large an increase in the vertical emittance, resulting in unwanted losses on the vertical acceptance limits.

When $I_z \neq 0$ (this is the normal situation) Eq. (IV.17) no longer holds and Eq. (IV.13) should be used. The situation here is more complicated as the phase of the beating then depends on q, χ_x, and χ_z.

The lessons to be learned from Eqs. (IV.17) and (IV.13) are:

i) δ should not be zero as it leads to so large an increase in vertical emittance that particles are lost on the vertical acceptance limits.
ii) The increase in efficiency will be largest at the end of the injection process.
iii) The best parameter setting will depend on the Q_H value.
iv) The increase in efficiency will depend on the phase q of the k^{th} harmonic of the coupling field.

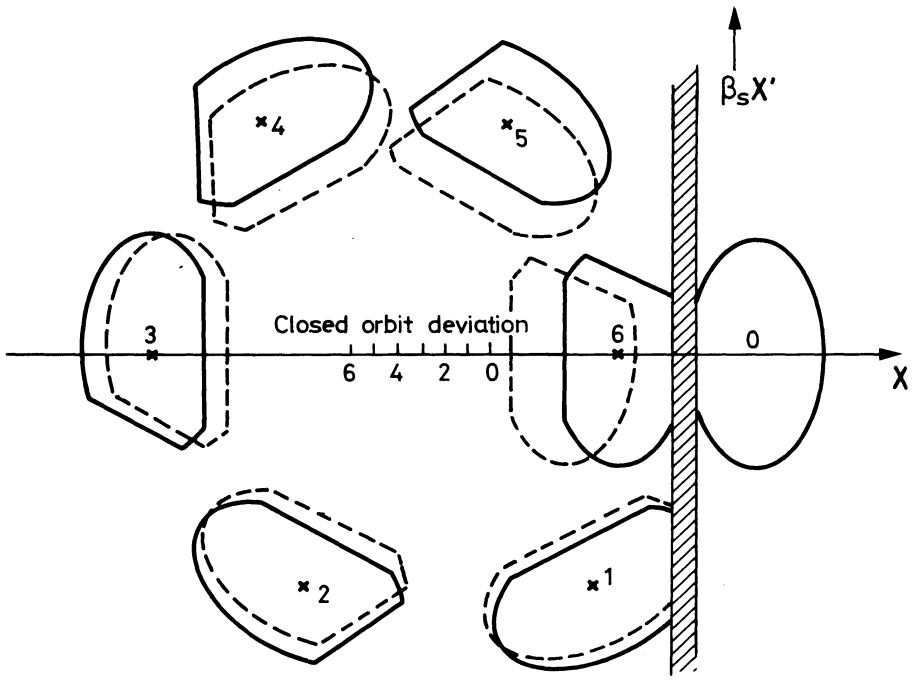

Fig. IV.2 Slice positions in horizontal phase space at the injection point. Closed line: positions with skew quadrupole off. Dotted line: positions with skew quadrupole on.

IV.4 EXPERIMENTAL RESULTS

The experiments described in this section were all done around the resonance line $Q_H - Q_V = -1$. The integrated gradient per ampere for one skew quadrupole is

$$\int_0^{l_m} \left(\frac{\partial B}{\partial x}\right) ds = 0.0006\,(\mathrm{T/A})$$

(the magnetic length $l_m = 0.287$ m). The maximum current is 30 A. With $\sqrt{\beta_x \beta_z} = 8.2$ m at the position of the lenses and all of them equally powered, the magnitude of the coupling term is $Q = 0.001\ \mathrm{A}^{-1}$ at 50 MeV.

The first question we put to ourselves was whether the skew quadrupole field indeed increases the injected and the accelerated current in the PSB during normal operation? This question could be answered in a positive sense because of an experiment, the results of which are shown in Fig. IV.3.

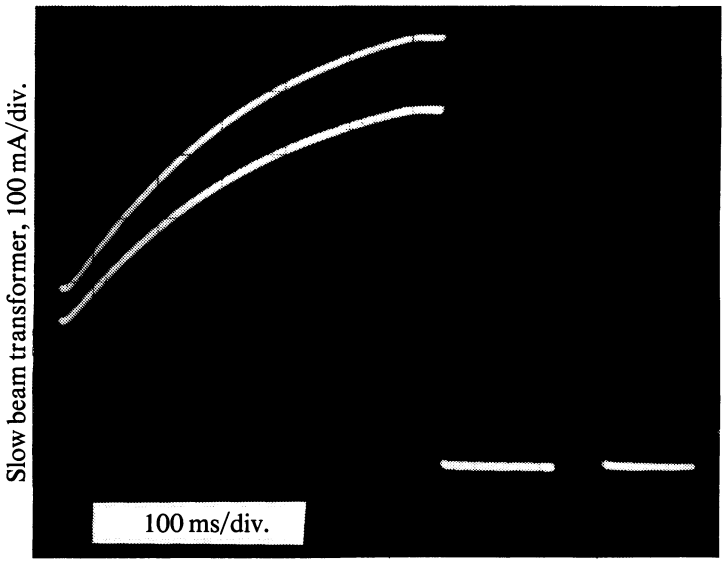

Fig. IV.3 Accelerated current in the PSB with (upper trace) and without (lower trace) skew quadrupoles powered.

Machine conditions during this experiment were: Linac current 80 mA; injection over 13 turns; $T_{IKS} = 60\ \mu$s; and all other parameters optimized as explained in Chapter III. The betatron tune was set to $Q_H = 4.23$, $Q_V = 5.31$. With the skew quadrupoles off, a total injected intensity of 3.5×10^{12} protons per pulse per ring was accelerated to 800 MeV. The RF was switched on immediately after injection, leading to a completely bunched beam 1 ms after injection. Owing to space-charge self forces, some particles will experience Q_H and Q_V values as low as 4.05 and 5.0, respectively. The vertical beam size was increased by 50%, but because of the large vertical acceptance no significant losses are observed.

Switching on the skew quadrupoles led to an intensity increase of 17%, from 3.5×10^{12} to 4.2×10^{12} accelerated particles. The vertical emittance measured at 800 MeV and containing 95% of the particles increased from 11 π to 13.5 π mm · mrad. See Fig. IV.3, where the accelerated current is displayed versus time. The beam current was measured by the slow beam transformer with and without the presence of a skew quadrupole field.

The horizontal–vertical coupling provides a welcome means to increase significantly the injected and the ejected intensity at the expense of an acceptable increase in vertical emittance. In operation, total intensities of 1.2 to 1.3×10^{13} protons per pulse were delivered thanks to the technique described in this chapter. As a consequence, the Booster design goal of 10^{13} protons per pulse could be reached in the PS, which was the intensity needed to obtain the design intensity of the SPS accelerator. This result was only obtained after a careful optimization of the parameters involved, such as the vertical injection alignment of the incoming beam in the PSB, the skew quadrupole phase, and the Q_H and Q_V values. A long series of experiments at low intensity were done to acquire a sufficient understanding of the coupling process to apply it successfully to the high-intensity case. It is also evident that the simple picture presented in Section IV.3 needed more refinement before reliable information could be obtained from it. Some of these low-intensity experiments will now be described.

The intensity of the incoming Linac beam was reduced to 16 mA by inserting a graphite sieve into the injection line. The vertical acceptance of the PSB beam was reduced to 95 π mm · mrad by the insertion of a window in the PSB vacuum chamber for BEAMSCOPE measurements. Injection was performed over 13 turns with a T_{IKS} value of 60 μs.

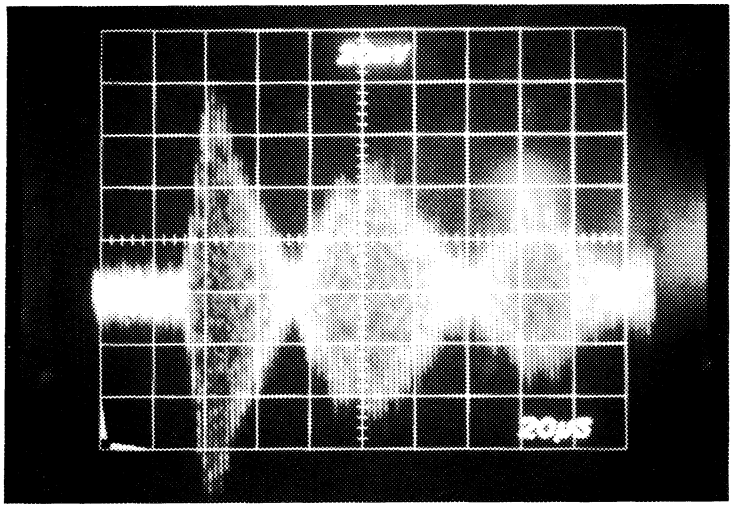

Fig. IV.4 Tuneable filter signal showing the beating frequency of the beam.

The injection steering parameters *DI* and *DIP* were optimized by observing the intensity of the injected current. The beam was vertically aligned by minimizing the vertical emittance. The Q_H value ranged from 4.17 to 4.23, while Q_V was adapted to obtain the wanted δ values. The first harmonic skew quadrupole field was generated by the arrangement shown in Fig. IV.1 and explained in Section IV.1. Several types of measurements were made:

i) Beating frequency.
ii) Injection efficiency as a function of coupling parameter Q.
iii) Interdependence of the initial phase of the injected beam in the vertical phase plane and the phase of the coupling term.
iv) Vertical emittance increase as a function of Q.
v) Vertical beam density.
vi) Sensitivity to jitter when the coupling field is present.

First of all the beating frequency was measured and compared with the values predicted by the theory of linear coupling. The difference signal of the two plates of an electrostatic Pick-Up station (see Section I.6.2) was passed through a tuneable filter to eliminate harmonics of the revolution frequency. Kicking the beam in one plane with the kicker used for Q measurements resulted in a perfect coupling pattern in both planes, from which the beating frequency can be derived (see Fig. IV.4).

In Fig. IV.5a the results of the measurement for $\delta = 0$ and $\delta = 0.05$ are shown by dots. The results of Eq. (IV.13) for the same δ values are represented by the full curves. The theoretical predictions agree well with the measurements.

The next step was to investigate how the parameters Q_c and δ influence the efficiency of the injection process around the line $Q_H - Q_V = -1$. Five δ values, $\delta = 0.01, 0.04, 0.06, 0.07$, and 0.09, were used and the injection intensity was measured for four skew quadrupole current values $I_{skew} = 0$, 10, 20, and 30 A. Even at low intensity a δ spread is present. This spread has been taken into account in the calculation of the theoretical results.

For certain parameter combinations a considerable increase in efficiency could indeed be observed in each ring. The results of these measurements are shown in Fig. IV.5b. Only those measurements are shown in Fig. IV.5b that yielded the highest intensity optimized with respect to the phase of the coupling term. The phase of the skew quadrupole field is important for the injection efficiency and the right choice of the phase is a prerequisite for the success of the method. The lines displayed in the same figures are the theoretical results from Section IV.5. The discrepancy between measured values and the theoretical curves for $0.05 \leq \delta \leq 0.07$ is still unexplained.

In Fig. IV.5b a difference between the theoretical predictions and the measurements can be seen for $\delta \leq 0.03$. A decrease in efficiency is predicted, while an increase is observed. A possible explanation is that for a large fraction of the particles with large vertical amplitudes the δ value is different from that of the particles with small vertical amplitudes. This prevents these large amplitudes from growing to their maximum value, because particles with large vertical amplitudes experience different non-linearities in the magnetic guiding fields as well as different space-charge forces.

The value of the best phase of the coupling was different from run to run and drifted slowly during the run. This phenomenon was probably due to the slow variation of the injection parameters in the vertical phase plane. In Eq. (IV.15) it can be seen that the phase of the beating indeed depends on the phase of the skew quadrupole field and on the initial phase of the particles in the horizontal and the vertical phase plane.

To confirm this relation the following experiment was done. The intensity was optimized by adjusting the phase of the skew quadrupole field. Once this phase was known, the worst case was easily found by adding π to the setting of the skew quadrupole field phase. Indeed the injected intensity was then even lower than with the skew quadrupoles switched

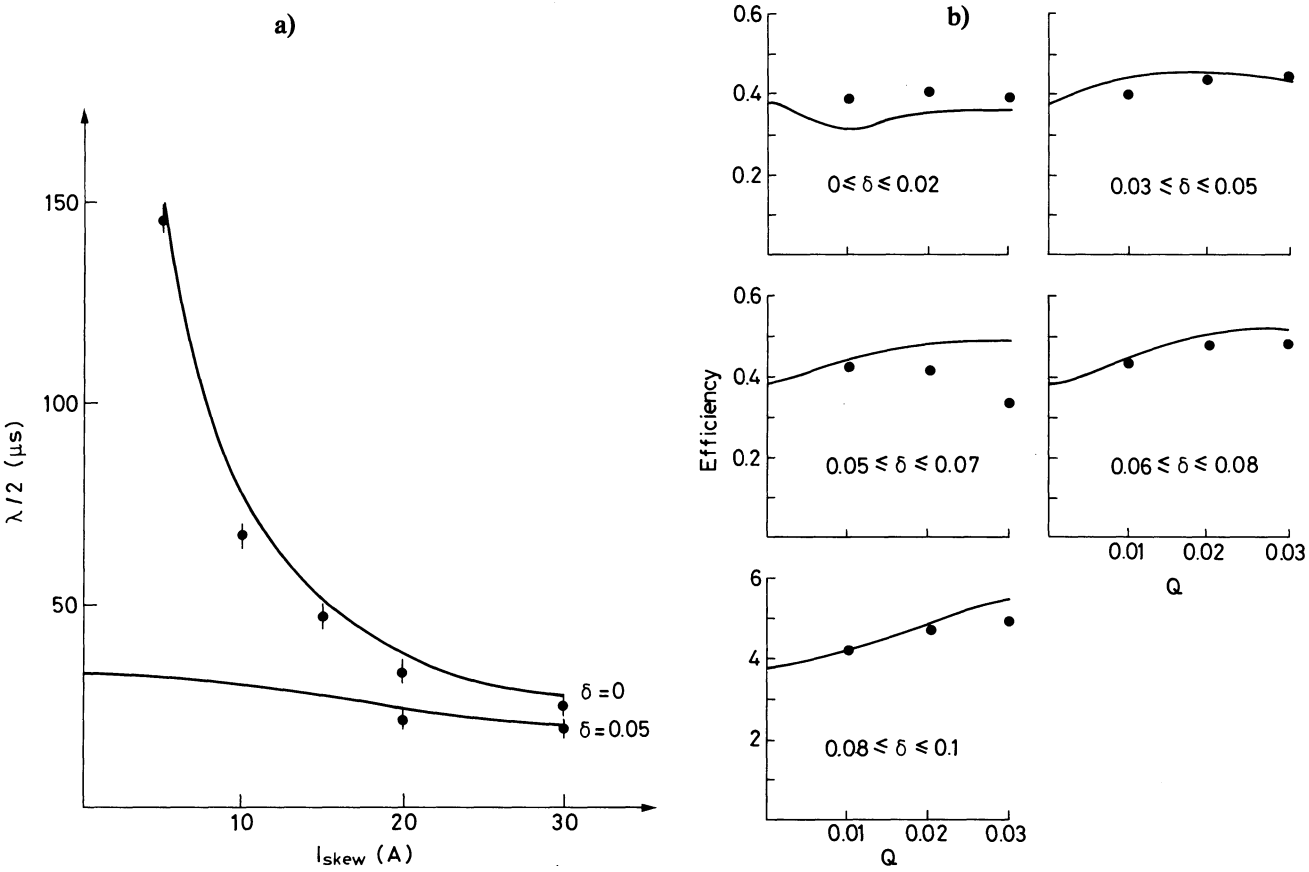

Fig. IV.5 a) Beating wavelength λ versus the skew quadrupole current I_{skew}, for two values of δ, where $\lambda = \sqrt{\delta^2/4 + Q^2}\, t_{rev}$. Dots are measured values, solid lines are results of Eq. (IV.4).
b) Multiturn injection efficiency versus Q. Dots represent measured values, solid lines are model predictions.

off. As the initial phase of the particles in the horizontal phase plane is fixed by the multiturn injection configuration, the phase in the vertical phase plane was modified by realigning the beam vertically.

It proved possible, by adjusting the initial phase of the particles in the vertical phase plane, to obtain the same intensity as before. Switching back to the original skew quadrupole setting diminished the injected intensity again to its lowest value.

The total efficiency for the four rings with full intensity (4×10^{12} protons per pulse per ring) is presented in Fig. IV.6 for various values of δ, I_{skew}, and χ_{q_0}. In this figure the efficiency for $I_{skew} = 0$ is 0.38. With high intensity, and thus larger Q spread and Q shift, it is difficult to estimate the average value of $\delta = Q_V - Q_H - 1$. Nevertheless, a plot is given showing the change in efficiency as a function of the value of δ which is obtained from the measurements of the coherent Q values via the Q kickers. The graphs show an optimum for $\delta = Q_V - Q_H - 1 = 0.08 \pm 001$.

Although the incoherent Q spread causes the particles to have different δ values, the results of the high-intensity experiments showed that the method allowed the injection of more particles in the PSB even for values of δ near to zero. The increase of the vertical emittance induced by the linear coupling was expected to be smaller than the maximum theoretical value owing to the δ spread, and this was indeed observed (no vertical losses; a measured E_V value of $70\,\pi$ mm · mrad, where $E_V \geq 80\,\pi$ mm · mrad is expected).

In order to find the best operational value for skew injection some further items had to be checked.

i) Is there a decrease in vertical density?
ii) Does this procedure increase the pulse-to-pulse fluctuations in injected intensity?
iii) Is the intensity gain preserved during acceleration?

Figure IV.7 shows that the powering of the skew quadrupoles does not cause these three beam characteristics to deteriorate significantly. The upper points show the number of injected particles. In the lower half of the figure the number of particles accelerated to 800 MeV is shown. The horizontal axis is the time; every point represents the value measured for one PSB pulse. After the measurement of the injected current but before that of the accelerated one, the target was plunged into the beam at 800 MeV, limiting E_V to $10.7\,\pi$ mm · mrad.

We saw neither an increase in the fluctuations nor a decrease in vertical density when the skew quadrupoles were switched on. The vertical density even seemed to increase. The maximum intensity of the accelerated beam was increased by 17% by using the skew quadrupoles. The number of particles within the original emittance is about the same as without linear coupling.

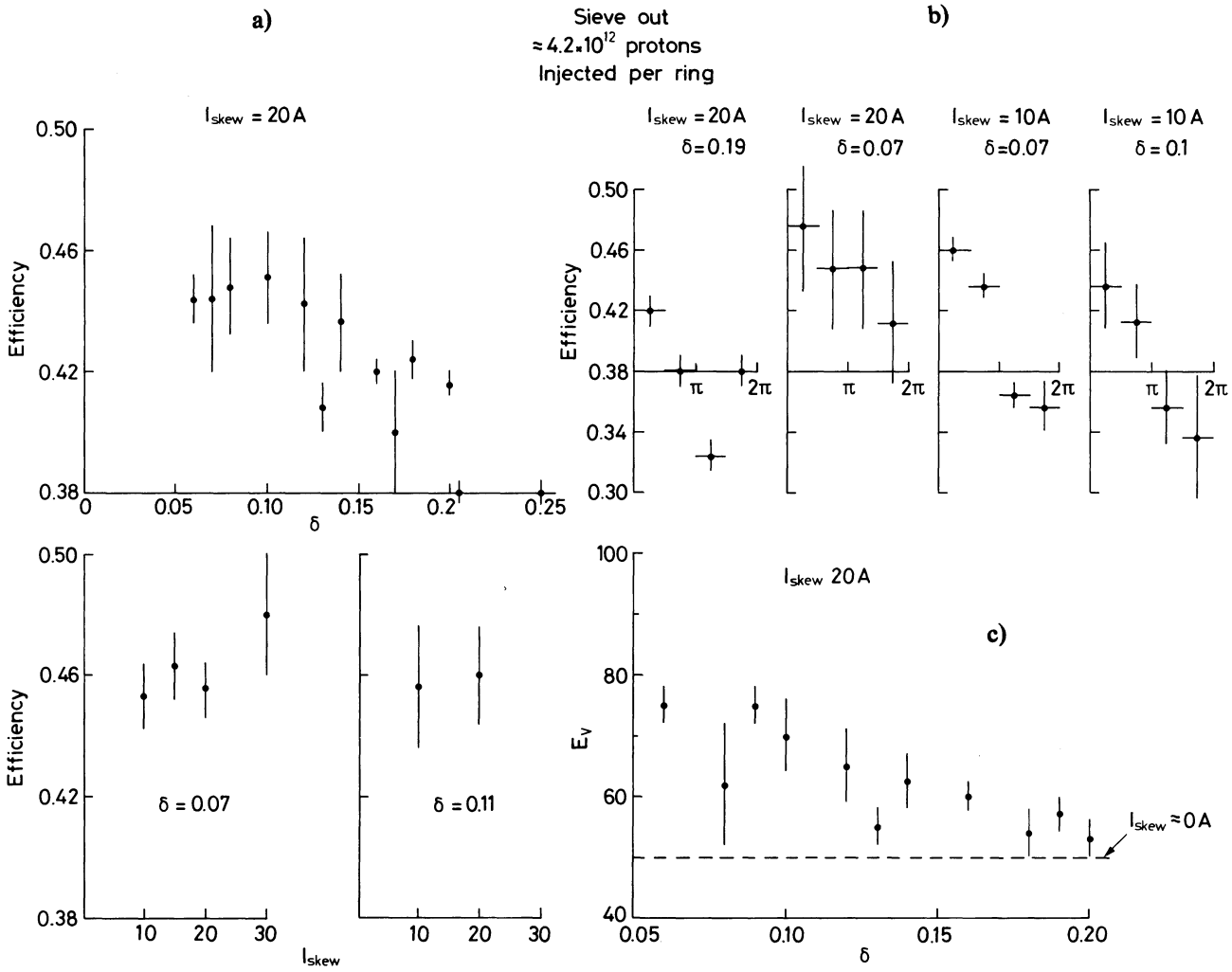

Fig. IV.6 a) Observed efficiency for high-intensity beam versus Q split δ; skew quadrupole current I_{skew} ($Eff = 0.38$ for $I_{skew} = 0$).
b) Efficiency versus the phase of the coupling term (for combinations of I_{skew} and δ).
c) Vertical emittance E_V (π mm · rad) measured as a function of δ.

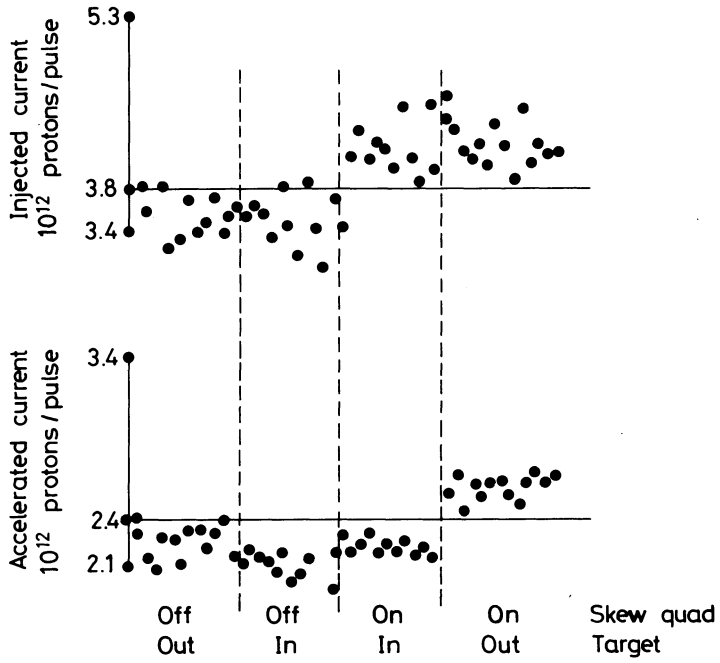

Fig. IV.7 Number of injected and accelerated particles in the PSB for four combinations of skew quadrupoles on/off and vertical targets in/out.

IV.5 THEORETICAL CONSIDERATIONS

From Chapter III it is known that the partial acceptance for each slice of incoming beam determines the efficiency of the total multiturn injection process. When linear coupling is present this is still true, but the configuration and the forms of the cuts determining the partial acceptance will change.

The change in partial acceptance due to the linear coupling can be calculated for each slice of incoming beam. Consequently, it is possible to calculate the efficiency of the whole process when linear coupling is present. The situation in this case is shown in Fig. IV.8, where a beam slice is shown in the horizontal phase plane at the injection

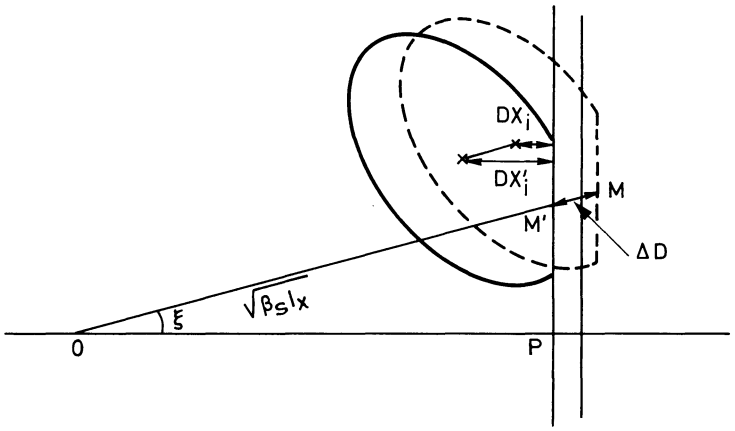

Fig. IV.8 Position of a slice of injected beam with respect to the injection septum. Full line: skew quadupoles on. Dotted line: skew quadrupoles off.

point. A cut is made by the septum after i revolutions following injection. The coordinate system is the same as the one used in Figs. III.2 and IV.2. When there is no skew quadrupole field the centre of the slice moves on a circle of radius $\sqrt{\hat{\beta}_s I_x(0)}$ around the closed-orbit position O, and $OP = D(t) - DSE$, see Fig. III.1. The distance DX_i between the centre of the slice and the septum determines the fraction of particles in the slice removed by the cut. When the linear coupling field is on, $I_x(0)$ decreases by an amount given by Eq. (IV.13).

The decrease is not the same for all particles of the slice, because within the slice the values of $I_x(0)$, χ_x, $I_z(0)$, χ_z, and even δ are in general different for each individual particle. For an exact calculation of the influence of the linear coupling on the injection efficiency of each individual beam slice, a large number of particle trajectories must therefore be traced through the injection process, starting with a given particle distribution in the horizontal and the vertical phase space of the synchrotron for each slice of injected Linac beam. However, the efficiency of the injection process with linear coupling can also be directly calculated with almost the same accuracy when a few reasonable approximations are made.

First it will be assumed that the beam is perfectly aligned vertically. The influence of a vertical misalignment of the injected beam will be discussed at the end of this section.

For a beam well aligned vertically the spread of the vertical emittance distribution is a minimum and $I_{z_0} = 10\ \pi$ mm · mrad, which corresponds to the spread of the emittance distribution of the injected Linac beam. At the beginning of the injection process when $OP = 0$, the average value of $I_x(0)$ is small. $\langle I_x(0) \rangle$ has about the same value as I_{z_0} and increases quadratically with time during injection with the displacement of the closed orbit. Equation (IV.13) shows that the decrease in I_x due to the skew coupling is roughly proportional to $I_x(0)$. As a consequence, the skew quadrupole coupling has a negligible influence on the efficiency of a slice injected at the start of the injection and the maximum influence on a slice injected near the end of the injection.

The approximations made for the calculation of the efficiency are based on the fact that changes in the efficiency are important only for slices for which $\langle I_x(0) \rangle \gg I_{z_0}$. From Fig. IV.8 it is clear that for these slices the following conditions are satisfied. The spread of $I_x(0)$ values around the cut affected by the skew quadrupole fields is relatively small. The spread of χ_x values of these particles is also small ($\approx 15°$). The influence of $I_z(0)$ values of the individual particles in the slice is then also small, because for each particle $I_z(0) \ll I_x(0)$. As illustrated by Fig. IV.8, the approximations can be summarized as follows:

i) The cuts determining the partial acceptance of each slice are assumed to move parallel to themselves when the linear coupling is switched on.

ii) The movement of one particle in the centre of the cut, averaged over all possible initial conditions in vertical phase space, determines the magnitude of the shift of the cut in the horizontal phase space.

iii) δ is the same for all particles and constant in time. This probably introduces the largest error in the calculation, because ΔI_x is very sensitive to the value of δ, which is known to vary slightly owing to space-charge self forces, the energy spread in the beams, and errors in the guiding fields.

Introducing these simplifications, the shift of the cut i into a slice near the end of the injection can be calculated in the following way. Going back to Fig. IV.8 the shift ΔDX_i in the position of the cut is given by

$$\Delta DX_i = |\Delta D \cos\xi| , \tag{IV.18}$$

where ΔD is derived from the value of ΔI_x for the mean particle in the centre of the cut i, and ξ is the angle between OP and OM.

To calculate ΔD the density distribution of the particles in the vertical phase plane is needed. This distribution is well described by a formula similar to relation (III.4) giving the distribution in the horizontal phase plane. This leads to the probability density function

$$P[I_z(0), \chi_z] = \frac{1}{2\pi I_{z_0}} \exp\left[-I_z(0)/I_{z_0}\right] . \tag{IV.19}$$

For all particles in a slice the distribution is uniform with respect to the phase χ_z.

Equation (IV.13) can be written in the form

$$\Delta I_x = w_1\{I_z(0) - I_x(0)\} + (w_2 \cos\chi_q + w_3 \sin\chi_q)\sqrt{I_x(0) I_z(0)} , \tag{IV.20}$$

with

$$w_1 = \frac{4Q^2 \sin^2\Theta}{\delta^2 + 4Q^2}, \quad w_2 = \frac{4Q\delta \sin^2\Theta}{\delta^2 + 4Q^2}, \quad w_3 = \frac{4Q \sin\Theta \cos\Theta}{\delta^2 + 4Q^2} .$$

The average $\langle \Delta I_x \rangle$ for all particles in the slice, with initial conditions $I_x(0)$ and χ_x in the horizontal phase plane but random initial conditions in the vertical phase plane, is given by

$$\langle \Delta I_x \rangle = \int\int \Delta I_x\{I_x(0), \chi_x, I_z(0), \chi_z\} P\{I_z(0), \chi_z\}\, dI_z(0) d\chi_z . \tag{IV.21}$$

When the beam is well aligned vertically so that the ellipse in the vertical phase plane at the injection point has the centre coordinates $z = 0$ and $z' = 0$, this integration eliminates the terms with $\cos\chi_q$ and $\sin\chi_q$ and the final result for $\langle \Delta I_x \rangle$ is

$$\langle \Delta I_x \rangle = -w_1\{I_x(0) - I_{z_0}\} , \tag{IV.22}$$

where I_{z_0} is the spread of $I_z(0)$ values for all particles with the initial conditions $I_x(0)$ and χ_x in the horizontal phase plane. When $I_x(0)$ and χ_x are assumed to refer to the particle in the centre of the cut i (indicated in Fig. IV.8 by the point M), the position of this particle will shift to point M' owing to the skew quadrupole coupling field. The magnitude ΔD of the shift towards the closed-orbit position is equal to

$$\begin{aligned} \Delta D &= \sqrt{\hat{\beta}_s}\left[\sqrt{I_x - \langle \Delta I_x \rangle} - \sqrt{I_x}\right] \\ \Delta D &= \sqrt{\hat{\beta}_s}\left[-\sqrt{I_x} + \sqrt{\frac{I_x - w_1 I_{z_0}}{1 - w_1}}\right] . \end{aligned} \tag{IV.23}$$

Equations (IV.13), (IV.23), and (IV.18) permit the determination of the partial acceptance configuration when a skew quadrupole field is present. The results obtained by using this model have for some characteristic cases been compared with those obtained by the more rigorous but time-consuming treatment with the simulation program. The results confirm that the errors caused by the assumptions (i) and (ii) are negligible compared to the differences found with the accelerator behaviour, which are caused by the Q_H, Q_V distribution in the beam.

In Fig. IV.9 the results of the efficiency calculations using the simplified model are shown for several δ values in plots of the coupling term Q. The upper graphs show the expected efficiency when no vertical acceptance limitation is present. In the lower graphs the vertical acceptance is restricted to a realistic value of 95 π mm · mrad. The differences between the two graphs are very dramatic for $|\delta| < 0.03$. A good working point seems to be $\delta = 0.07$ and $I_{skew} = 20$ A.

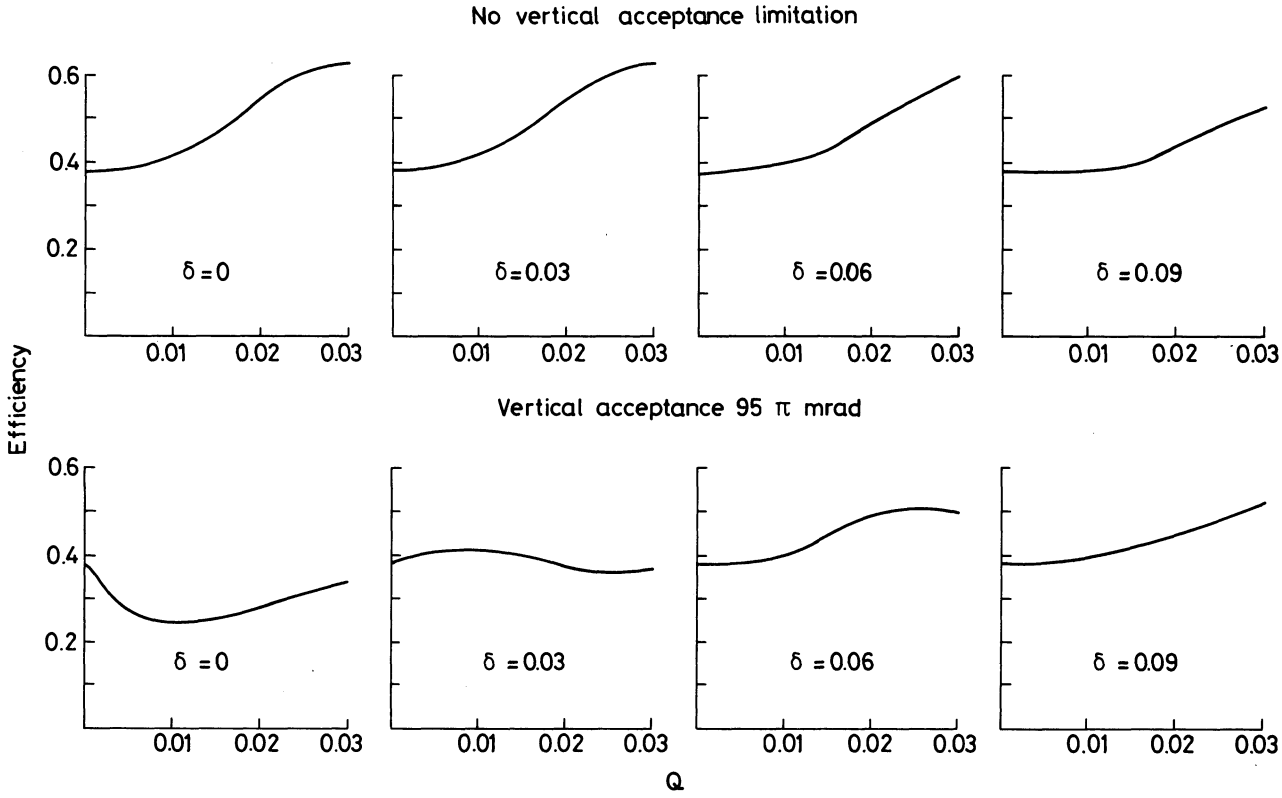

Fig. IV.9 Calculated efficiency versus the coupling term Q for four values of δ, with and without acceptance limitation.

These results are not exactly found in the PSB because as soon as a vertical misalignment is introduced the picture changes once again.

In the case of a vertical misalignment of the beam in the vertical phase plane Eq. (IV.13) has to be evaluated for a beam which is vertically injected with centre coordinates $(z_c, z_c') \neq (0,0)$. The phase of the vertical misalignment will be denoted by

$$\langle \chi_z \rangle = \text{arctg}\,\{\beta_v z_c'/z_c\} \tag{IV.24}$$

and the magnitude of the misalignment is given by

$$\Delta I_z = z_c^2/\beta_v + z_c'^2\beta_v\,. \tag{IV.25}$$

Integrating over $P\{I_z(0),\chi_z\}$ will yield a formula which contains the phase χ_z. The result can be written in the form

$$\langle \Delta I_x \rangle_M = \langle \Delta I_x \rangle + w_1 \Delta I_z + \sqrt{I_x(0)\Delta I_z(w_2 \cos\langle \chi_q \rangle + w_3 \sin\langle \chi_q \rangle)}\quad , \tag{IV.26}$$

where $\langle \chi_q \rangle$ is given by the formula analogous to Eq. (IV.15):

$$\langle \chi_q \rangle = \langle \chi_x \rangle - \langle \chi_z \rangle - q\,. \tag{IV.27}$$

The value for ΔD in the case where a vertical misalignment is present is then given by

$$\Delta D = \sqrt{\hat{\beta}_s}\left[\sqrt{I_x - \langle \Delta I_x \rangle_M} - \sqrt{I_x}\right]$$

$$\Delta D = \sqrt{\hat{\beta}_s}\left[\sqrt{\frac{I_x - w_1\left\{I_{z_0} + \Delta I_z + \sqrt{I_{z_0}\Delta I_z(w_2 \cos\chi_q + w_3 \sin\chi_q)}\right\}}{1 - w_1}} - \sqrt{I_x}\right]\,. \tag{IV.28}$$

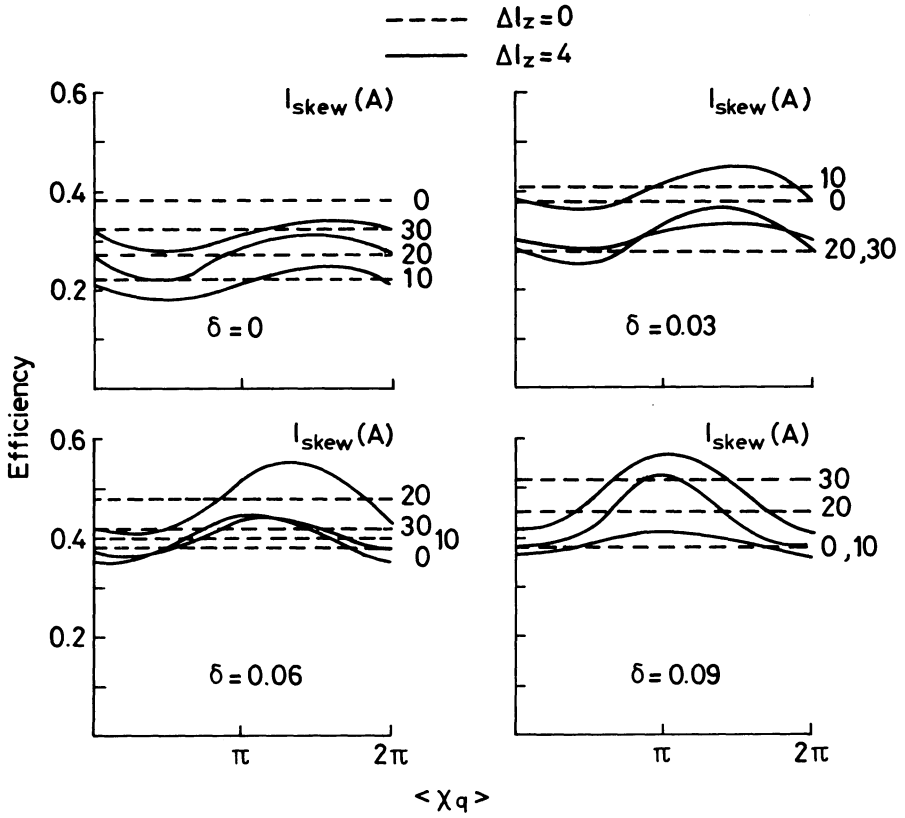

Fig. IV.10 Injection efficiency versus the phase term $\langle \chi_q \rangle$. Dotted lines are results of calculation for a well-aligned beam ($\Delta I_z = 0$). Solid lines are the results of calculation for a misaligned beam ($\Delta I_z = 4$).

In Fig. IV.10 several plots are shown for two values of ΔI_z ($\Delta I_z = 0$ for aligned beam, $\Delta I_z = 4$ for a misaligned beam) and for four δ values ($\delta = 0.0, 0.03, 0.06$, and 0.09). In each plot the efficiency is plotted versus the phase $\langle \chi_q \rangle$ defined in Eq. (IV.27) for four different skew quadrupole currents $I_{skew} = 0$, 10, 20, and 30 A.

One sees that for $\delta = 0.06$ and $\Delta I_z \approx 4$ (comparable to operational values) the vertical misalignment has an appreciable influence on the best value of the phase of the skew quadrupole field. In daily operation it is indeed important to adjust the phase of the skew quadrupole field harmonic carefully to obtain the maximum increase in the injection efficiency. When $\Delta I_z = 0$ no dependence on the phase $\langle \chi_q \rangle$ is found.

The curves of Fig. IV.5b have been derived from the curves of Fig. IV.10 with the following constraints coming from the accelerator environment:

i) The phase $\langle \chi_q \rangle$ has been optimized.

ii) A δ spread of 0.02 is present in the beam.

In this way it is possible to compare the calculated results of the model with the accelerator behaviour.

Although the theory approximates the observed beam behaviour in a global way rather faithfully, it does not explain the finer details. Probably yet other mechanisms than the ones discussed in this section interfere with the beam behaviour. A possible explanation is that the δ evolution of each particle affects the beam behaviour in a systematic way and not randomly as assumed here.

CHAPTER V

INFLUENCE OF THE SPACE-CHARGE FORCES ON THE MULTITURN INJECTION PROCESS

V.1 INTRODUCTION

In Chapter IV it was already mentioned that at high beam intensities a marked decrease in the horizontal and vertical Q values is observed, which was attributed to the influence of space-charge forces. The space charge contributes a net defocusing force that adds to the forces due to the guiding quadrupoles and makes the particles oscillate with lower Q_H and Q_V values than those observed in the zero intensity machine[2,54].

Two types of Q_H and Q_V shift can be distinguished. First the coherent Q shift, which is caused by the electric image charge induced by the beam on the wall of the vacuum chamber. This induced charge also changes the trajectory of the closed orbit. The coherent Q shift can be measured by kicking the beam with the Q kickers foreseen for this purpose.

The second type of Q shift, the incoherent Q shift, is the shift of the Q value of each individual particle under the influence of the charges of all particles. This effect decreases when the particle velocities approach the velocity of light, because the electric repulsive forces are then partially compensated by attractive magnetic forces. For the efficiency of the multiturn injection process the influence of the incoherent Q shift is by far the most important. Therefore only the incoherent Q shift will be considered in this chapter.

In Section V.2 the influence of the Q_H shift on the multiturn injection process is shown experimentally, in particular the effect of the best values of the injection parameters and the overall efficiency.

In Section V.3 the consequences of the lump-lump forces are considered. These forces are caused by the electromagnetic interaction between the subsequent turns of injected beam and modify the partial acceptance of the individual beam slices.

Finally, in Section V.4, some experiments are discussed that were performed to investigate the observation that the effective septum thickness (*DS* value) is twice as large as the expected value.

V.2 EXPERIMENTAL EVIDENCE FOR SPACE-CHARGE EFFECTS

The decrease in the Q_H value due to the space-charge effects, expected at high injected beam intensities, should cause a shift in the optimized values of the injection parameters. The existence of this effect was demonstrated qualitatively in the following injection experiment. The PSB was tuned to $Q_H = 4.68$, where the injection efficiency depends strongly on the effective Q_H value. Then, according to Fig. III.10, the measured efficiency should be 0.30 for low injected intensity, when the injection parameters have their optimized values. The machine was then injected with a high-intensity beam of 80 mA and the value of *DI*, the parameter to which the injection efficiency is most sensitive in this region, was adjusted until maximum efficiency was obtained. This efficiency was found to be 0.35, which suggests (Fig. III.10) that the high intensity caused the effective Q_H value to drop to $Q_H < 4.64$. By inserting a sieve in the injection line the injected intensity was then reduced to 16 mA. For unchanged settings of the injection parameters the efficiency was now found to be 0.22, but a maximum value of 0.28 could be obtained by adjusting *DI* 0.7 mm downwards. This is very near the value of 0.30 expected from Fig. III.10.

The above experiment confirms that the space-charge-induced Q_H shift has a measurable influence on the parameter settings for the PSB injection process. When, however, the settings of the parameters, in this particular case *DI*, are suitably readjusted at high intensities, the overall effect of space charge on the injection efficiency is negligible. This was shown in an experiment in which the injection efficiency and the optimized *DI* and *DIP* values were measured as a function of the number of injected turns n_t. The machine was tuned for $Q_H = 4.23$ and all measurements were done both at low and at high injected beam intensity. The horizontal emittance containing 95% of the injected beam was fixed at 130 π mm · mrad, the high-intensity beam was 85 mA, and the low intensity beam of 17 mA was obtained by again inserting the sieve. For each value of n_t the beam intensity was optimized at low intensity by adjusting *DI*, *DIP*, T_{IKS}, and T_B. The sieve was then removed and the injected intensity was again optimized for the high-intensity measurements by readjusting *DI* and *DIP*.

The result of this experiment is shown in Fig. V.1. The efficiency is plotted as a number of effective turns versus n_t, in the same way as was done in Fig. III.11. The efficiencies for high-intensity and low-intensity injection are equal

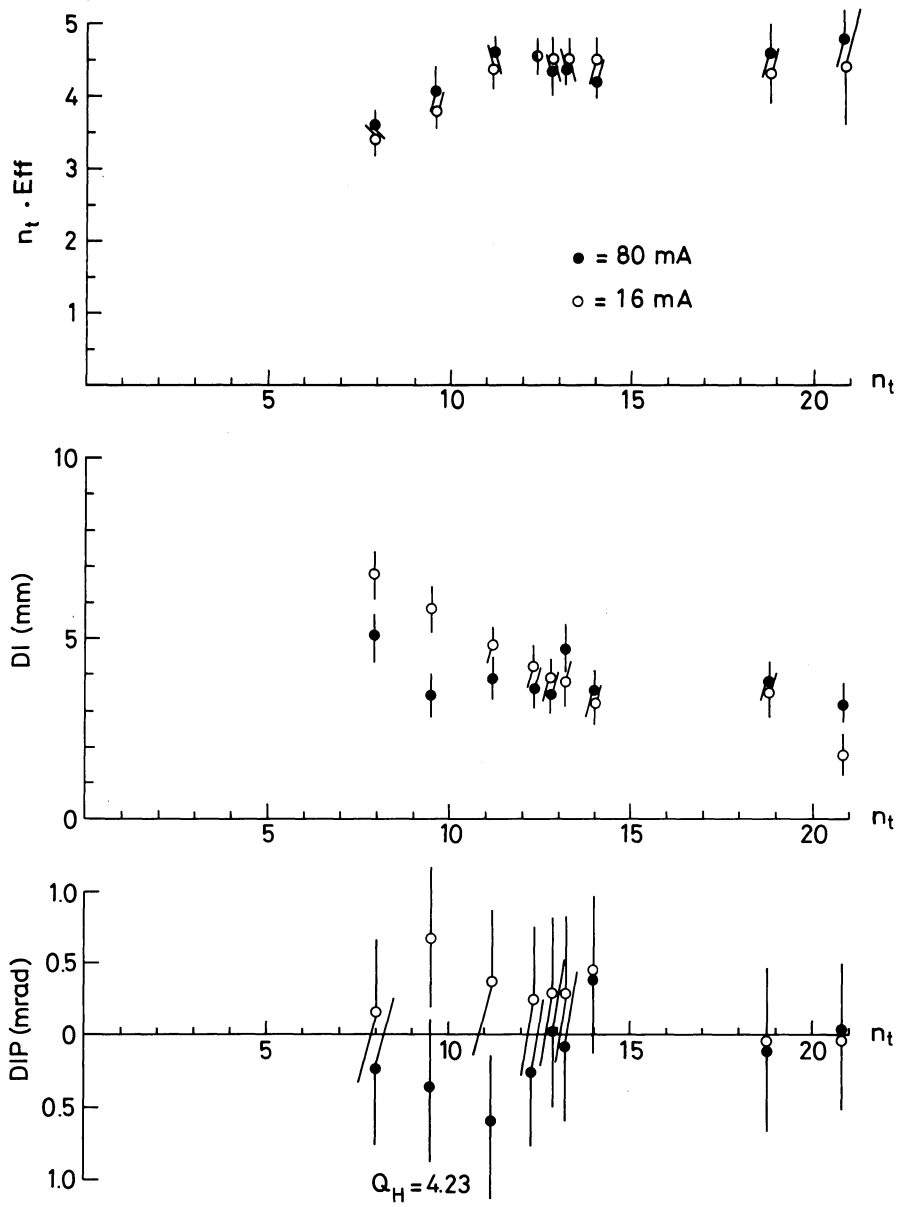

Fig. V.1 Plots of the measured number of effective turns ($n_t \cdot Eff$), and the beam alignment parameters (*DI* and *DIP*) versus the number of injected turns n_t. Open dots are low-intensity measurements. Closed dots are high-intensity measurements.

within the errors. For *DI* and *DIP* some difference is found between the high-intensity and low-intensity settings, but only for the lowest n_t values. These results confirm that the injection efficiency and the alignment depend in the expected way on the average incoherent Q_H value of the particles.

From the results of these experiments one may conclude that the influence of space-charge forces on the injection process is by no means negligible, but that, all the same, the overall injection efficiency of the PSB does not seem to depend appreciably on the intensity of the injected beam. In addition, the widening of the distribution of the incoherent Q_H values of the particles, caused by space-charge forces, decreases the sensitivity of the injection efficiency to the exact values of the injection parameters, because the actual optimized parameter settings are a compromise between the settings required for groups of particles each with a different Q_H value. Some of the consequences of the existence of this effect are:

i) Schemes to increase the intensity of the PSB that depend on Q_H tunes requiring $\delta Q_H \leq 0.08$, as proposed by some authors[41], and *DI* settings accurate to better than 0.5 mm will fail owing to the lack of well-defined partial acceptance configurations during the process.

ii) The abrupt changes in the calculated optimized parameter values and the efficiency as a function of Q_H (Figs. III.8 and III.10) will in practice be smoothed out. This is actually observed. For instance, the low efficiencies calculated for $Q_H = 4.33$ and $Q_H = 4.67$ will in practice be higher than the theoretical values, but the width of the low-efficiency region will increase.

V.3 CALCULATION OF SPACE-CHARGE EFFECTS AND THE LUMPED PARTICLE DISTRIBUTION

For a more detailed study of the influence of space-charge forces on the multiturn injection process Fig. V.2 is useful. In Fig.V.2a the situation is shown in the horizontal phase plane at the injection point at the moment of injection of the first Linac beam slice. The coordinate system is the same as the one used in Fig. IV.2. In Fig. V.2b the situation is shown at the moment that the first slice has performed one revolution in the PSB. A second slice of Linac beam has just been injected next to it, separated from it by the septum shadow. In Fig. V.2c slice one has performed two revolutions and three slices have been injected. In Fig. V.2d the final situation is shown when thirteen slices have been injected and slice one has performed 13 revolutions. Within the partial acceptances the particle density is given by Eq. (III.4), i.e. near the centre of each partial acceptance the particle density is highest, dropping off exponentially outwards. When the beam is further accelerated one expects the distribution in horizontal phase of the particles to show a lumped structure and the lumps oscillate through phase space as time goes on. The lumped structure in horizontal phase space should appear as a granular structure of the horizontal particle distribution in the vacuum chamber of the accelerator. This effect has indeed been demonstrated directly in the AGS[55]. A vertical wire that could be moved horizontally was inserted in the vacuum chamber. The charge collected on the wire was measured as a function of the horizontal position for different moments after the injection. The measured beam profiles showed the expected granular beam structure.

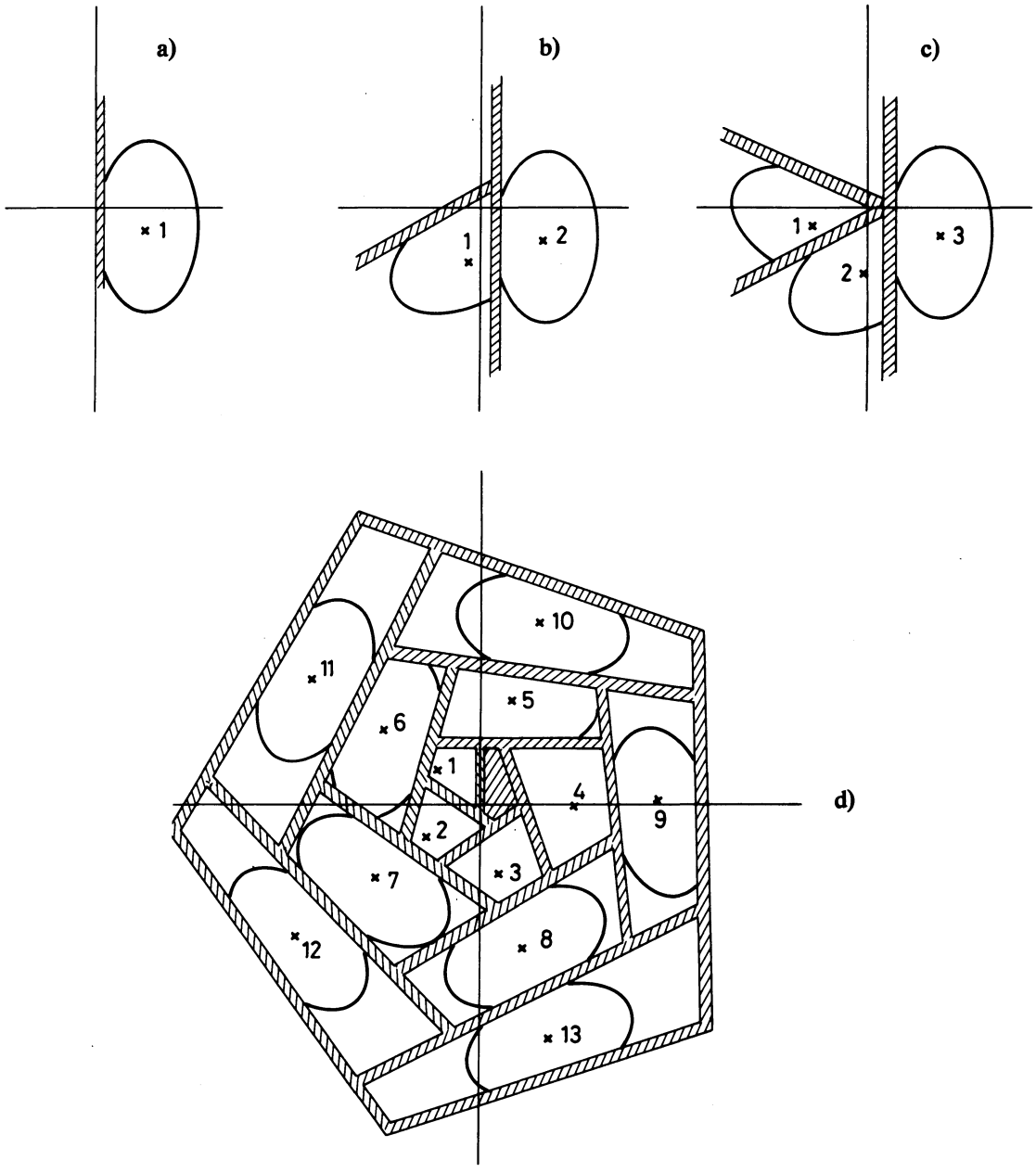

Fig. V.2 Evolution of the filling of the horizontal phase plane.

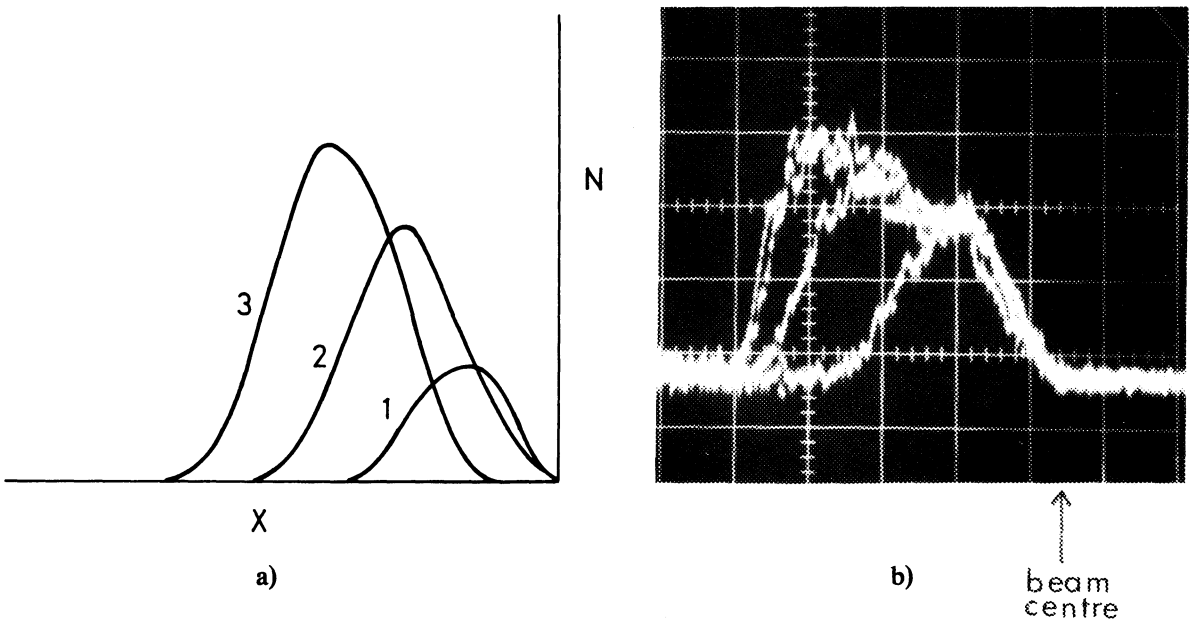

Fig. V.3 Calculated and measured horizontal amplitude distributions for different moments of the start of injection.

The measurement of the horizontal particle distribution in the accelerator after injection is a sensitive method for detecting space-charge effects. When the incoherent Q_H values of the particles spread over an appreciable range owing to space-charge effects, the lumped structure of the particle distribution in horizontal phase space will gradually fade out. This redistribution will, however, only take place along the Courant-Snyder ellipses and will therefore not affect the horizontal emittance distribution, which is more easily measured. Space-charge interactions change the horizontal emittance distribution, however, owing to a second effect. The lumped beam structure present during and just after injection will generate oscillating electromagnetic fields, which cause a coupling between the trajectories of the individual particles, resulting in a smoothing out of the horizontal emittance distribution.

Several experiments were done with the PSB to study this last effect. In the first experiment the horizontal beam profile was measured with BEAMSCOPE[25] at a number of different time intervals after injection, starting with 300 μs, and increasing to 1500 μs in 200 μs steps. The incoming beam intensity was 16 mA and the energy spread of the Linac beam was made as small as possible. With the energy spread that was finally obtained, 30 keV, the "fuzzing" of the beam due to the energy spread was only 0.4 mm. The Q_H value was 4.20, and 5.5 turns were injected with a T_{IKS} value of 40 μs to obtain a quickly moving closed orbit. By starting the injection at different moments in the closed-orbit displacement program, different parts of the horizontal particle distribution could be filled with particles. In Fig. V.3a calculated horizontal particle distributions, assuming no space-charge effects, are shown for three different injection times. Curve 1 corresponds to an injection start at the moment of maximum closed-orbit displacement. For curves 2 and 3 the start of the injection is 5 and 10 μs later, respectively. For curve 3 the central region of the horizontal phase plane is initially empty and should remain so when there are no space-charge forces.

The measured horizontal amplitude distributions for the same three cases are shown in Fig. V.3b. These particle distributions were obtained by activating BEAMSCOPE 1500 μs after injection. The curves are representative for the measurements at other moments after injection. The most striking feature is that the trace corresponding to trace 3 does not show the empty region for small amplitudes. As no particles were injected in this region, particles with larger amplitudes must have drifted towards the centre of the phase plane during the period following the injection. If this phenomenon is indeed caused by the electromagnetic interaction between the lumps of particles, it should disappear, or at least diminish, when the lump-lump structure is effaced quickly by external means that do not affect the horizontal emittance distribution directly. It is possible to do this by increasing the Q_H spread of the particles artificially with the aid of octupoles. The effect of switching on a current of 100 or 200 A in the octupole magnets is shown in Fig. V.4, measured at 500 μs after injection. For comparison also the trace for octupoles off is shown. By comparing the three traces it can be seen that progressively less particles are found in the centre of the distribution with increasing octupole current. With the simulation program it can be shown that the Q_H spread with an octupole current of 200 A is of the order of $\delta Q_H \simeq 0.04$. In that case the lumped structure of the beam has almost completely disappeared after 40 μs, corresponding to 25 revolutions.

These experiments show that a redistribution of the particles in the horizontal phase plane takes place. The fact that as many particles in the centre as in the tail of the distribution are affected proves that the redistribution is caused by internal forces. Increasing the Q_H spread diminishes the speed of the redistribution, which proves that the granular structure of the beam right after injection is the probable cause of the horizontal emittance redistribution. The

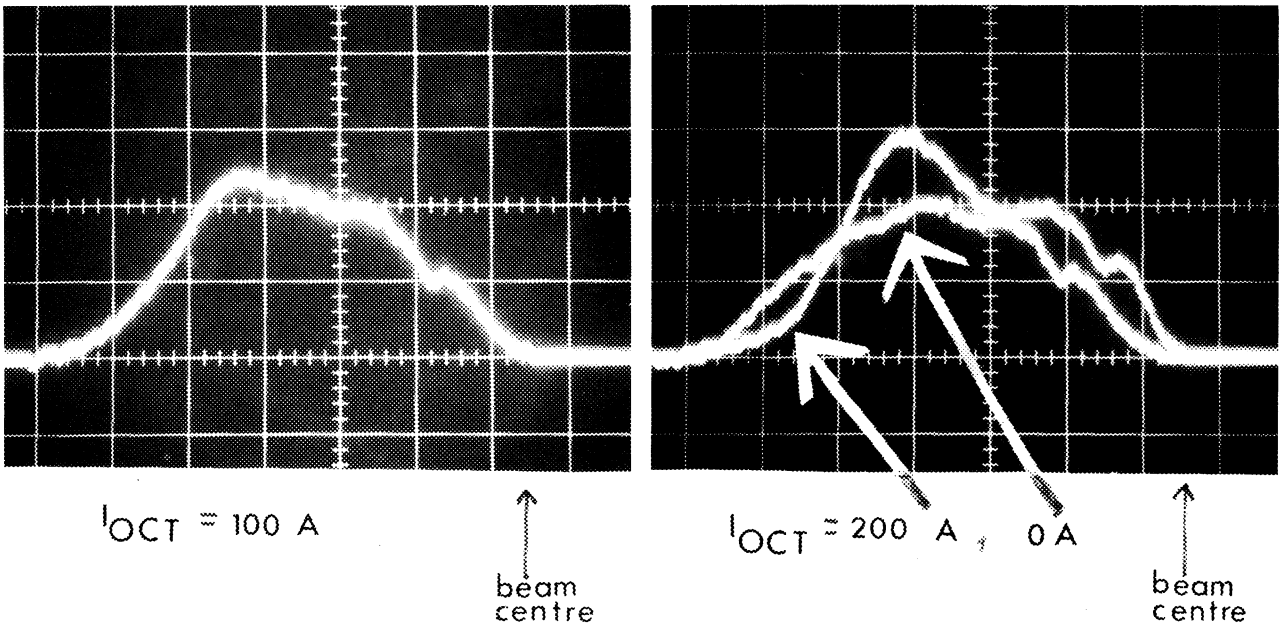

Fig. V.4 Beam particle distributions as measured with BEAMSCOPE for three different settings of the currents in the octupole magnets.

redistribution seems to be completed 300 μs after injection, since the particle distributions measured after this moment do not show any significant differences compared with the measurement at 1500 μs after injection. However the smoothing out of the granular structure with the aid of the octupoles in a time shorter than 40 μs has an appreciable influence on the final particle distribution in the horizontal phase plane. The conclusion is that the redistribution is completed in a time longer than 40 μs and shorter than 300 μs. These experiments were done with incoming beam intensities of both 85 mA and 17 mA. The shapes of the distributions were not significantly different in the two cases (only four turns injected).

In the Linac it has also been observed that a hole created in the beam at 10 MeV by placing a bar across the beam centre had almost completely disappeared after acceleration to 50 MeV[56]. This very fast redistribution was attributed to horizontal–vertical coupling caused by space-charge forces. Calculations for the Linac redistribution showed that the space-charge forces responsible for the coupling could be caused by local density fluctuations in the beam. In the PSB no definite evidence has been observed for such coupling, but the multiturn injection process certainly gives rise to local density fluctuations.

The influence of the lumped particle structure combined with space-charge forces on the single-particle behaviour can be approximately calculated by expanding the $\vec{E}$ and $\vec{B}$ fields of each lump into a Fourier series. By summation over all lumps the space-charge forces experienced by each particle can then be calculated. Keeping only the first-order terms the single-particle equation has the form

$$\frac{d^2x}{d\vartheta^2} + (Q_H^2 + K_s)x + \varepsilon \cos(Q_H\vartheta + f_0)\exp(-\chi\vartheta) = 0 \quad . \tag{V.1}$$

K_s represents a non-fluctuating space-charge term. f_0 and ε are calculated from the summation over the fields of all lumps. For each individual lump these two parameters are recalculated after one revolution in the PSB. The factor $\exp(-\chi\vartheta)$ is included as the lumps are slowly smeared out in the phase plane and finally disappear completely, leaving only K_s which is in phase with the guiding fields of the quadrupoles. Equation (V.1) has been used in the following way. For a finite number of particles the quantities K_s, ε, and f_0 are calculated. The integration of Eq. (V.1) over one revolution yields the position of the particles in the horizontal phase plane after one turn. The same procedure is repeated for several revolutions of the particles. Relatively large errors are inherent in this treatment and only rough predictions can be made for the particle motion. The results confirm nevertheless that the redistribution of the particles in the horizontal phase plane will slow down when the Q_H spread is artificially increased. A further result is that the particles are redistributed in 100 to 200 revolutions, which agrees with the measurement described above. Only for incoming beam intensities of 17 mA did Eq. (V.1) yield reliable results.

Calculations were also done in Ref. 57 to investigate the influence of the space-charge forces created by the individual particles. These authors used a simulation program for that purpose. For some of their distributions a hole was created in the centre, while for another type of distribution the particles tended to drift to the centre of the beam. In some cases the granular structure of the beam was enhanced during the first few revolutions of the beam.

The following conclusions can be drawn:

i) Because of the lumped structure of the beam, space-charge forces cause a horizontal redistribution within 300 μs.
ii) The horizontal emittance redistribution always tends to an equilibrium distribution that is rather flat in the centre. This has the consequence that no special injection kicker program is needed to achieve this type of distribution. It is, in fact, very doubtful whether any preprogrammed horizontal emittance distribution can be stable.

V.4 INVESTIGATION INTO THE CAUSE OF THE LARGE EFFECTIVE SEPTUM THICKNESS *DS*

In the beginning of Section III a theoretical effective septum thickness of 1.5 mm was assumed. Experiments, however, revealed that the actual effective septum thickness was of the order of 3 mm (see Fig. III.11). No clear reason for this discrepancy was apparent at that moment, but it was thought that space-charge forces might be responsible for this effect. One of the possibilities in this context is that the lump-lump forces affect the particle trajectories in such a way that the septum shadow is increased. The space-charge-induced oscillations of the particles around their unperturbed trajectories make each lump occupy a larger area in phase space than would be the case without fluctuating space-charge forces. Another possibility is that the increase in the Q_H spread or the redistribution in horizontal emittance is responsible for the large septum shadow.

Calculations, using Eq. (V.1) for an incoming beam intensity of 17 mA, indicate that space-charge forces indeed cause a displacement of the lumps near the septum position. The magnitude of the movement depends on the number of revolutions of the partial acceptance considered, but is never larger than 0.6 mm. This is too small to explain an increase of 1.5 mm in the septum thickness.

A series of experiments was carried out to estimate the influence of various perturbations on the multiturn injection efficiency and in particular on the septum thickness.

The graphs shown in Fig. III.11 were remeasured for a number of different octupole-induced Q_H spreads and for several values of the energy spread of the incoming Linac beam. The incoming beam intensity was 17 mA, the beam was injected into $E_H = 130\ \pi$ mm · mrad, and Q_H was set at 4.20. After measurement of each graph the maximum number of effectively injected turns was determined. The data in Fig. III.11 show that for octupoles off and a Linac energy spread of ± 150 keV the measured maximum value is $n_t \cdot Eff = 5.0 \pm 0.4$ for $n_t = 17$, to be compared with a theoretical value of $n_t \cdot Eff = 6.6$ for $n_t = 20$ assuming $DS = 1.5$ mm. The measured value of $n_t \cdot Eff$ turned out to be almost independent of the current in the octupoles and of the Linac energy spread. A maximum value of $n_t \cdot Eff = 6 \pm 1$ for $n_t = 17$ is the best that could be achieved after a general reoptimization of all the injection parameters and with a strong current in the octupoles. However, this result could not be reproduced on a day-to-day basis.

The conclusion is that the cause of the large effective septum thickness could not be established in an unambiguous way. Combining the results of the series of experiments just described with the data presented in Fig. V.1 on the influence of the intensity of the Linac beam, one may, however, safely conclude that the space-charge forces are not the main causes (≤ 0.5 mm) of the unexpectedly large effective septum thickness (~ 3 mm).

CHAPTER VI

CONCLUSIONS

The main results of the two and a half years' study presented here are summarized as follows:

i) An easy injection setting up procedure has been developed.
ii) Injection efficiencies of 45 to 47% have been reached.
iii) The consequences of the different types of beam jitters could be estimated quantitatively.
iv) The introduction of injection with dynamic injection parameters (an expensive method) proved to have little effect.
v) The observed horizontal beam redistribution immediately after injection makes it doubtful whether one can preprogram the horizontal beam distribution with the aid of the injection parameters.

Measured injection intensities are lower than the predicted ones for both low and high intensities owing to the following probable causes:

a) The effective septum shadow is larger than calculated.
b) The horizontal redistribution provokes an emittance growth.

It is demonstrated that the granular structure of the horizontal beam distribution disappears in a time between 40 and 300 μs. For low as well as for high intensities the horizontal beam distribution is modified. The powering of zero harmonic octupoles diminishes this redistribution process.

Skew quadrupoles enable the injected intensity to be increased at Q_H, Q_V values near the line $Q_H - Q_V = k$. An injected current increase of 17 to 20% is measured. The most remarkable phenomenon observed during the skew quadrupole experiments was that the high-intensity experiments yielded results which were in better agreement with the theoretical predictions than the low-intensity ones.

When the author left the PS Division, multiturn injection was no longer the bottleneck for the intensity in the PSB. Owing to the high injected currents, the space-charge-induced Q_H and Q_V shifts made the beam touch the stopbands $Q_H = 4$ and $Q_V = 5$, provoking beam blow-up in both transverse planes. At that time most studies were devoted to the search for a better working point, the compensation of the $Q_V = 5.33$ stopband, the active damping of collective instabilities, and in general the acceleration of the beam in smaller emittances.

After the comissioning of the new Linac, injection parameters had to be adapted to profit fully from the improved Linac beam characteristics:

- smaller transverse emittances
- higher beam current
- longer pulse length
- more stable beam during the pulse and also from pulse to pulse.

Consequently the optimum number of injected turns increased from 13 to 15, while the injection parameters were adjusted accordingly. The intensity curves still corresponded to the theoretical curves assuming an effective septum thickness of 3 mm. Under these conditions the injected current was sufficiently high and it was no longer necessary to switch on the skew quadrupoles for some time[58]. However, several developments in the PSB allowed the acceleration of still higher intensities and their transmission through the PS to the SPS, or to the antiproton production target: an improved working point, somewhat larger vertical emittance, and stopband compensation by additional correcting multipoles were adopted; and an additional active feedback system was installed in the PSB. Switching on the skew quadrupoles proved particularly beneficial during injection, both to increase the injected intensity, and to allow for a higher accelerated intensity by reshaping the vertical emittance distribution. Intensities of up to 2×10^{13} particles are transferred to the PS[29,30].

One could ask if a much simpler model (or no model at all) might not have yielded useful results. The answer is no. Without a model much time would have had to be spent on the accelerator itself to try out all possible parameter combinations. Obviously this is unrealistic; thus a simple model provided by a Monte Carlo simulation program[43,44] allowed a first survey of the desirable injection parameters during the running-in phase of the PSB. With ever increasing intensities, a more detailed understanding of the multiturn injection process was needed, and the development of a more basic model was launched. The principles of this model are very simple: the efficiency of the process is determined by a geometrical figure in the phase plane. The main advantage of the model is that different

constraints imposed by the outside world could be translated into other geometrical patterns. Consequently one run of the injection program based on this model was needed, where formerly several runs of the simulation program were required.

However, the model had to be tailored to include several typical PSB constraints, such as injection into a horizontal emittance smaller than the horizontal acceptance. A good compromise had to be found between the complexity of the model and its predicting power.

The modelling of the injection process, including linear coupling, was treated in a similar way. Many complications had to be introduced into the model, such as the vertical acceptance and the vertical emittance distribution. Yet the model is not complex enough to explain all phenomena observed in the PSB in sufficient detail. More research would certainly yield the wanted explanations, but is not deemed worth the effort.

The basic mechanisms of the space-charge forces on the multiturn injection process have been identified. However, the detailed behaviour of the particle distribution could only be described in a global way and many more experiments are needed to explain all details. But the influence of the space-charge forces on the injected intensity is only marginal compared to the influence of the space-charge forces during the acceleration of the particles.

In summary, one can say that the multiturn injection process is rather well understood. Only relatively small improvements can be expected. When more intensity is wanted from the process, it will be necessary to do extensive research on the form of the injection septum in conjunction with a study of the slice trajectories at the injection point. In addition, better observation equipment will be needed to look at the particle trajectories immediately after and in front of the injection septum. In this context a wire such as used in the Brookhaven AGS could yield useful results, both to obtain a better understanding about the space-charge-induced horizontal emittance redistribution, as well as to estimate precisely the effective septum thickness and to assess the merits of a very thin electrostatic septum.

Acknowledgements

An accelerator is a complex machine composed of technologically advanced equipment. A well-trained and very-skilled staff is needed to develop, maintain, and operate such a machine.

It is therefore a pleasure to acknowledge the efforts of the staff of the Booster, the Linac, and the Operations groups at CERN. They have contributed greatly to the successful execution of the experiments described in this work.

Many people have contributed on an individual basis:

- K. Schindl introduced me to the problems related to the multiturn injection process. Many experiments have been carried out together with him. The numerous discussions with him have helped in the development of the model.
- D. Harting helped me to present the results throughout this work in a consistent, understandable, and clear way. His questions and remarks have contributed to the proper understanding of the multiturn injection process.
- K.H. Reich always encouraged the work described here. Thanks to him it was possible to test the different consequences of the model, resulting in the desired improved performance of the PSB.
- F. Sacherer contributed to the description of the basic space-charge mechanisms working on the multiturn injection process.
- H. Koziol pointed out the error sources which surround each measurement. He contributed significantly to the calculation of the measurement errors.
- H. Haseroth, T.R. Sherwood and P. Têtu helped me with the understanding of the Linac beam characteristics.
- H.L. Hagedoorn, J. Gareyte, I. Gumowski and H. Schönauer commented on the experiments and the model.
- M. Bouthéon and J.P. Potier commented on the injection model.
- D. Dekkers permitted the continuation of this work after my transfer to the Operations group.

Lastly, I am very grateful to the CERN Scientific Reports Editing Section, Composition and Printing Group, and EP Drawing Office, for the excellent way in which they have realized this paper.

REFERENCES

1) CERN Annual Reports, 1955–1973.

2) L.J. Laslett, On intensity limitations imposed by transverse space-charge effects in circular particle accelerators, Proc. 1963 Summer Study on Storage Rings, Accelerators and Experimentation at Super-High Energies, Brookhaven National Laboratory, Upton, 1963, BNL 7534 (1963), p. 324.

3) Study Group for CPS Improvements, The second stage CPS improvement study, 800 MeV Booster Synchrotron, CERN MPS/Int DL/B67-19 (1967).

4) The PSB staff, The CERN PS Booster, Design expectations confronted with reality two years after start-up, Proc. 9th Int. Conf. on High Energy Accelerators, Stanford, 1974 (US Atomic Energy Commission, Washington, 1974), p. 480.

5) W. Hardt, A slow cycling injection method for intensity improvement of the CERN PS (Twin Accelerator Ring Transfer Scheme), Proc. 5th Int. Conf. on High Energy Accelerators, Frascati, 1965 (CNEN, Rome, 1966), p. 151.

6) K.H. Reich, Some reflections on the CPS-Booster, CERN MPS/Int DL/B66-5 (1966).

7) K.H. Reich, Progress report on the activity of the Booster study group, CERN MPS/Int DL/B66-6 (1966).

8) K.H. Reich, The new CPS injector (Notes for lecture to ISR users), CERN MPS/Int DL/B67-3 (1967).

9) E. Keil, Stacking in betatron phase space for the ISR, CERN ISR-TH/67-10 (1967).

10) E.D. Courant, E. Keil and A.M. Sessler, Effects of the choice of PS injector on ISR capabilities, CERN ISR-TH/67-12 (1967).

11) C. Bovet and E. Keil, ISR performances related to CPS injector schemes, CERN MPS/Int DL/B67-6 (1967).

12) K.H. Reich, Optimization of the CPS Booster taking into account ISR performance, CERN MPS/Int DL/B67-7 (1967).

13) C. Bovet, Choix de Q pour un anneau de 25 m de rayon, CERN MPS/DL/B, Note 66-5 (1966).

14) F. Giudici, Nouvel injecteur pour le CPS, Variation des paramètres de la maille, CERN MPS/Int DL/B67-5 (1967).

15) S. Battisti, Booster beam transformers, CERN MPS/SI CO/Note 70-8 (1976).

16) Proc. Meeting on Technology arising from High Energy Physics, Geneva, 1974, CERN 74-9 (1974), Vol. 1: Review Papers, Vol. 2: Technology Notes.

17) H. Koziol, Q-measurement on the PS Booster, CERN MPS/Int BR/74-14 (1974).

18) M. Rabany, The orbit measurement system of the CERN 800 MeV PS Booster, CERN MPS/Int BR/73-4 (1973).

19) G. Nassibian and M. Rabany, The optimization of the geometry of electrostatic beam position measuring electrodes, CERN SI/Int El/71-2 (1971).

20) C. Carter, The electronics for the PS Booster Q-measurement system, CERN MPS/Int BR/74-15 (1974).

21) H. Koziol, private communication.

22) K. Schindl and T.R. Sherwood, Magnetic position monitors for the new Linac and the PSB injection line, CERN MPS/BR/LIN/Note 75-12 (1975).

23) P. Têtu, Mesure d'émittance en une impulsion du faisceau de 50 MeV, CERN MPS/LIN 71-8 (1971).

24) P. Krempl, private communication.

25) H. Schönauer, BEAMSCOPE, a novel device for measuring emittances and betatron amplitude distributions, IEEE Trans. Nucl. Sci. **NS-26**, No. 3, 3294 (1979).

26) H. Koziol, Remarks on the plunging speed of measurement targets, CERN MPS/BR Note/74-18 (1974).

27) E.D. Courant and H.S. Snyder, Theory of the alternating gradient synchrotron, Ann. Phys. (USA) **3**, 1 (1958).

28) H. Bruck, Accélérateurs circulaires de particules (Bibliothèque des Sciences et Techniques nucléaires, Saclay, 1966).

29) K. Schindl, Simultaneous dynamic compensation of stopbands and multipurpose location of correction lenses in the CERN PS Booster, IEEE Trans. Nucl. Sci. **NS 26**, No. 3, 3562 (1979).

30) J.P. Delahaye, G. Gelato, L. Magnani, G. Nassibian, F. Pedersen, K.H. Reich, K. Schindl and H. Schönauer, Shaping of proton distributions for raising the space charge limit of the CERN PS Booster, Proc. 11th Int. Conf. on High Energy Accelerators, Geneva, 1980 (Birkhäuser, Basle, 1980), p. 299.

31) F. Sacherer, private communication.

32) Proposal for a 500 MeV Booster injector for the Zero Gradient Synchrotron (ZGS), Argonne National Laboratory, Accelerator Division, Argonne, Illinois (1969).

33) E. Crosbie, A. Gorka, E. Parker, C. Potts and L. Ratner, Injection and acceleration of protons in the Zero Gradient Synchrotron (ZGS) by stripping H^- ions, Proc. 6th Particle Accelerator Conf., Washington, 1975, IEEE Trans. Nucl. Sci. **NS-22**, No. 3, 1056 (1975).

34) C. Ankerbrandt, C. Curtis, C. Hojvat, R.P. Johnson, C. Owen, C. Schmidt, L. Teng and R.C. Webber, H^-charge exchange injection systems, Proc. 11th Int. Conf. on High Energy Accelerators, Geneva, 1980 (Birkhäuser, Basle, 1980), p. 260.

35) P.M. Hanney and E. Keil, How does betatron mismatching affect beam size and beam density, CERN ISR/TH/69-32 (1962).

36) P.M. Hanney and E. Keil, How do angle and position errors at injection affect beam size and density, CERN ISR/TH/69-44 (1969).

37) J. Claus, H.N. Brown, M. Month and A. van Steenbergen, Multiturn injection into the converted AGS, Proc. 5th Particle Accelerator Conf., San Francisco, California, 1973, IEEE Trans. Nucl. Sci. **NS-20**, No. 3, 342 (1973).

38) J. Claus, AGS injection with 200 MeV Linac, Brookhaven National Laboratory, BNL 15646, AADD-172 (1971).

39) P. Germain, Efficiency of stacking in betatron phase plane, CERN MPS/DL 72-12 (1972).

40) L. Nielsen, Investigation of the possibilities of multiturn injection into the Booster, CERN MPS/Int/LIN 67-8 (1967).

41) P.F. Mead, Jr., New methods for multiturn injection into synchrotrons, Proc. 5th Particle Accelerator Conf., San Francisco, California, 1973, IEEE Trans. Nucl. Sci. **20**, No. 3, 401 (1973).

42) E.D. Courant, Phase space dilution in three turn injection, Fermi National Accelerator Laboratory, NAL-FN-174 (1968).

43) C. Bovet and D. Lamotte, Numerical analysis of the PSB multiturn injection, CERN SI/Int DL/69-13 (1969).

44) C. Bovet, D. Lamotte and R. Le Bail, Macroparticle computer simulation of multiturn injection into the CERN PS Booster, Proc. 8th Int. Conf. on High Energy Accelerators, Geneva, 1971 (CERN, Geneva, 1971), p. 102.

45) C. Bovet, Beam scrapers in the PSB, CERN SI/Note DL/69-18 (1969).

46) P. Van der Stok, Multiturn injection into alternating gradient proton synchrotrons with applications to the PS Booster, CERN PS/OP/Int 76-1 (1976).

47) F.J. Sacherer and T.R. Sherwood, Effect of space charge in beam transport lines, Proc. 4th Particle Accelerator Conf., Chicago, 1971, IEEE Trans. Nucl. Sci. **NS-18**, No. 3, 1066 (1971).

48) K. Schindl and P. van der Stok, Present performance of PSB multiturn injection, CERN MPS/BR/Int/74-2 (1974).

49) G. Gelato, K. Schindl, P. van der Stok and D. Williams, Localization and cure of PS Booster multiturn injection pulse to pulse jitter, CERN MPS/BR Note/75-9 (1975).

50) M.S. Livingston and J.P. Blewett, Particle accelerators, International Series in Pure and Applied Physics (McGraw Hill, NY, 1962).

51) M.H. Blewett, G.K. Green, R.R. Kassner, W.H. Moore, L.W. Smith and H.S. Snyder, Studies of injection phenomena in the Cosmotron, Rev. Sci. Instrum. **24**, 861 (1953).

52) K. Schindl and P. van der Stok, Increase of betatron stacking efficiency via linear coupling in AG proton synchrotrons (skew injection), Application to the CERN PS Booster, CERN/PS/BR 76-19 (1976), CERN/PS/OP 76-5 (1976).

53) A.W. Chao and M. Month, Observables with linearly coupled oscillators, Brookhaven National Laboratory, CRISP 74-16 (1974).

54) L.C. Teng, Transverse space charge effects, Argonne National Laboratory, ANLAD 59 (1960).

55) K. Schindl, Data from the Brookhaven AGS, private communication.

56) P.M. Lapostolle, C.S. Taylor, P. Têtu and L. Thorndahl, Intensity-dependent effects and space-charge limit investigations on the CERN linear injector and synchrotron, CERN 68-35 (1968).

57) S. Fenster, H. Takeda and G. Bart, Multiturn injection, IEEE Trans. Nucl. Sci. **NS-28**, No. 3, 2574 (1981).

58) PS Performance Committee, Performances limites du complexe nouveau Linac-Booster-PS, 1980, CERN/PS/DL/Note 80-2 (1980).

APPENDIX I

CALCULATION OF *DI*, *DIP*, AND β_t FOR THREE-ANGLE PARTIAL ACCEPTANCE

1. CALCULATION OF *DI*(*t*) AND *DIP*(*t*)

In addition to the first cut caused by the injection septum at the arrival of the injected beam (cut 0), two other cuts j and k are considered which are chosen such that

$$\cos 2\pi Q_H j \geq \cos 2\pi Q_H k \quad . \tag{AI.1}$$

The situation is shown in Fig. AI.1, which is copied from Fig. III.6b. The cuts are drawn in the horizontal phase plane for the injection point of the PSB. The origin of the normalized coordinate is the centre of the injected slice.

The condition for injecting the core of the Linac beam into the centre of the partial acceptance during the whole injection process was described in Section III.2 and could be expressed in the form of Eq. (III.12):

$$DI(t) = \frac{DX_j}{F(jQ_H)} = \frac{DX_k}{F(kQ_H)} \quad . \tag{AI.2}$$

This means that the normalized distances from slice centre to septum edge, defined in Eq. (III.9), should be equal for the three cuts.

By substituting in Eq. (AI.2) the expression for DX_t following from Eqs. (III.13) and (III.14), two equations in $DI(t)$ and $DIP(t)$ are obtained that can be written as

$$\begin{aligned} F(jQ_H)DI(t) &= DX_j = A_j - DI(t)\cos 2\pi Q_H j - \hat{\beta}_s DIP(t)\sin 2\pi Q_H j \\ F(kQ_H)DI(t) &= DX_k = A_k - DI(t)\cos 2\pi Q_H j - \hat{\beta}_s DIP(t)\sin 2\pi Q_H k \quad , \end{aligned} \tag{AI.3}$$

where

$$A_i = 2t\frac{DO}{T_{IKS}}\sin^2(\pi Q_H i) + it_{rev}\frac{DO}{T_{IKS}} - 2DK\sin^2(\pi Q_H i) \quad . \tag{AI.4}$$

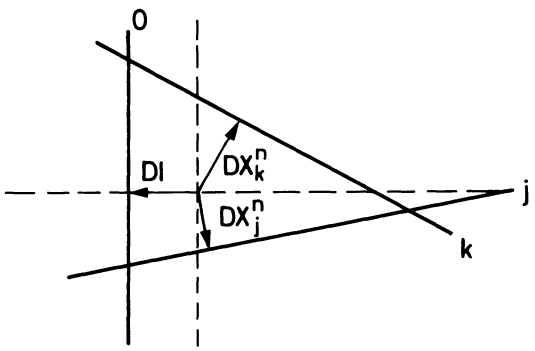

Fig. AI.1

Solving Eqs. (AI.2) for $DIP(t)$ leads to the expression

$$DIP(t) = \frac{\left\{\left[A_j/G(jQ_H)\right] - \left[A_k/G(kQ_H)\right]\right\}}{\hat{\beta}_s Z(j,k)} \tag{AI.5}$$

with

$$\begin{aligned} G(iQ_H) &= F(iQ_H) + \cos 2\pi Q_H i \\ z(j,k) &= \frac{\sin 2\pi Q_H j}{G(jQ_H)} - \frac{\sin 2\pi Q_H k}{G(kQ_H)} \end{aligned} \tag{AI.6}$$

By substitution of A_t from Eq. (AI.4) into Eq. (AI.5), $DIP(t)$ is obtained as a linear function of the injection moment t:

$$DIP(t) = \frac{A_{DIP}}{T_{IKS}} t + \frac{B_{DIP}}{T_{IKS}} + C_{DIP} \tag{AI.7}$$

with

$$\begin{aligned} A_{DIP} &= 2DO \frac{\left\{\left[\sin^2(\pi Q_H j)/G(jQ_H)\right] - \left[\sin^2(\pi Q_H k)/G(kQ_H)\right]\right\}}{\hat{\beta}_s Z(j,k)} \\ B_{DIP} &= DOt_{rev} \frac{\left\{\left[j/G(jQ_H)\right] - \left[k/G(kQ_H)\right]\right\}}{\hat{\beta}_s Z(j,k)} \\ C_{DIP} &= -DK\frac{A_{DIP}}{DO} - DS \frac{\left\{\left[1/G(jQ_H)\right] - \left[1/G(kQ_H)\right]\right\}}{\hat{\beta}_s Z(j,k)} \end{aligned} \tag{AI.8}$$

These are very useful expressions as they describe the evolution of $DIP(t)$ in terms of 3 parameters that are determined by the machine geometry. In the same way an equivalent expression for DI is obtained:

$$DI(t) = \frac{A_{DI}}{T_{IKS}} t + \frac{B_{DI}}{T_{IKS}} + C_{DI} \tag{AI.9}$$

with

$$\begin{aligned} A_{DI} &= DO \left\{\frac{\mathrm{tg}(\pi Q_H j) - \mathrm{tg}(\pi Q_H k)}{Z^*(j,k)}\right\} \\ B_{DI} &= DOt_{rev} \left\{\frac{\left[j/\sin(2\pi Q_H j)\right] - \left[k/\sin(2\pi Q_H k)\right]}{Z^*(j,k)}\right\} \\ C_{DI} &= -DK\frac{A_{DI}}{DO} - \frac{DS}{Z^*(j,k)}\left\{\frac{1}{\sin(2\pi Q_H j)} - \frac{1}{\sin(2\pi Q_H k)}\right\} \end{aligned} \tag{AI.10}$$

and where

$$Z^*(j,k) = \frac{G(jQ_H)}{\sin(2\pi Q_H j)} - \frac{G(kQ_H)}{\sin(2\pi Q_H k)} \tag{AI.11}$$

2. CALCULATION OF $\beta_l(t)$

To obtain the maximum injected current, the area of the largest equidensity ellipse of the incoming beam fitting inside the partial acceptance should be maximal. Equation (III.17) for this area leads to the expression

$$\frac{d}{d\beta_l}\left(\frac{DI^2(t)}{\beta_l}\right) = 0 \tag{AI.12}$$

for the condition where this is the case. Using Eqs. (AI.9) and (AI.10) the condition can be written as

$$\frac{d}{d\beta_l}\left(Z^*(j,k)\sqrt{\beta_l}\right) = 0 \quad . \tag{AI.13}$$

Using the fact that $\sin(2\pi Q_H j) \cdot \sin(2\pi Q_H k) < 0$, one obtains

$$\frac{d}{d\beta_l}\left[\sqrt{\frac{\hat{\beta}_s^2}{\beta_l} + \beta_l \frac{\cos^2(2\pi Q_H j)}{\sin^2(2\pi Q_H j)}} + \sqrt{\frac{\hat{\beta}_s^2}{\beta_l} + \beta_l \frac{\cos^2(2\pi Q_H k)}{\sin^2(2\pi Q_H k)}}\right.$$

$$\left. + \sqrt{\beta_l}\left\{\frac{\cos(2\pi Q_H j)}{|\sin(2\pi Q_H j)|} + \frac{\cos(2\pi Q_H k)}{|\sin(2\pi Q_H k)|}\right\}\right] = 0 \quad . \tag{AI.14}$$

After some algebra this yields

$$\frac{\cot^2(2\pi Q_H j) - \hat{\beta}_s^2/\beta_l^2}{\sqrt{\cot^2(2\pi Q_H j) + \hat{\beta}_s^2/\beta_l^2}} + \frac{\cot^2(2\pi Q_H k) - \hat{\beta}_s^2/\beta_l^2}{\sqrt{\cot^2(2\pi Q_H k) + \hat{\beta}_s^2/\beta_l^2}}$$

$$+ \frac{\cos(2\pi Q_H k)}{|\sin(2\pi Q_H k)|} + \frac{\cos(2\pi Q_H j)}{|\sin(2\pi Q_H j)|} = 0 \quad . \tag{AI.15}$$

Divide by $\cos(2\pi Q_H j)/|\sin 2\pi Q_H j)|$ and substitute

$$\begin{aligned} a &= \frac{\cos(2\pi Q_H k)}{\cos(2\pi Q_H j)} \frac{|\sin(2\pi Q_H j)|}{|\sin(2\pi Q_H k)|} \\ y^2 &= \frac{\hat{\beta}_s^2}{\beta_l^2 \cot^2(2\pi Q_H j)} \quad . \end{aligned} \tag{AI.16}$$

A simple equation in a and y is obtained, which is easily solved numerically:

$$\frac{a^2 - y^2}{\sqrt{a^2 + y^2}} + \frac{1 - y^2}{\sqrt{1 + y^2}} + a + 1 = 0 \quad . \tag{AI.17}$$

From definition (AI.1) it is known that $-1 < a \leq 1$, and $a < -1/2$ will only appear in very rare cases, because it means that two cuts are almost parallel and this situation corresponds to the four-angle case. The solution of y as a function of a is plotted in Fig. AI.2 and can be approximated by

$$y^2 = 0.82 + \frac{(a + 0.4)^2}{0.9} \quad . \tag{AI.18}$$

By substituting a and y^2 from Eqs. (AI.16), Eq. (III.18) for β_l is obtained.

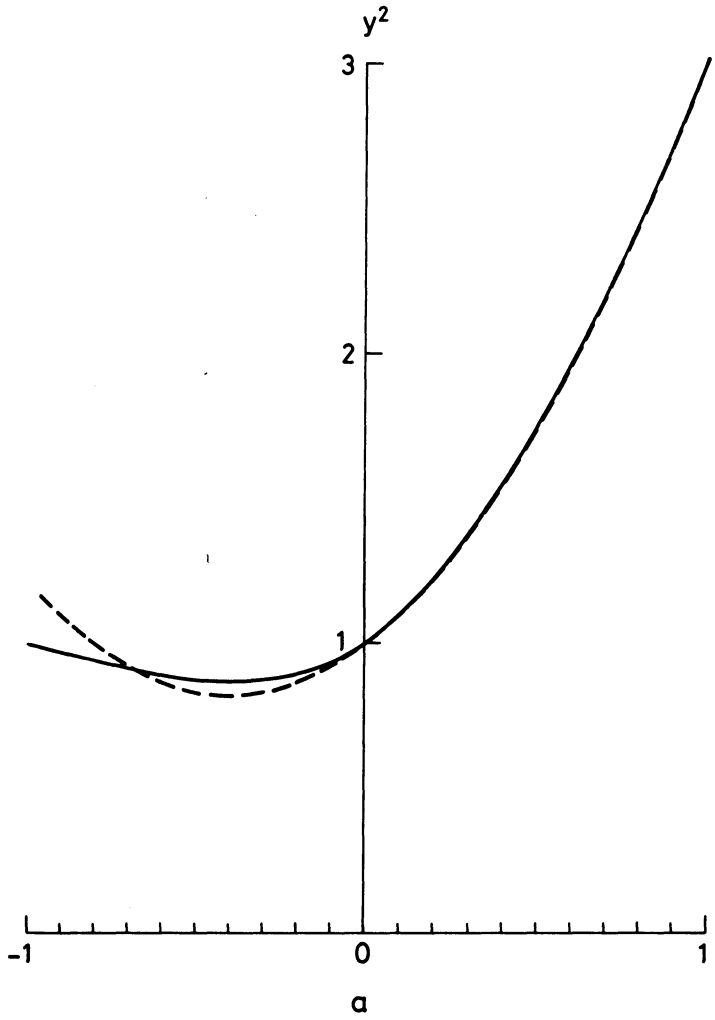

Fig. AI.2

APPENDIX II

CALCULATION OF *DI*, *DIP*, AND β_l FOR FOUR-ANGLE PARTIAL ACCEPTANCE

For the four-angle approximation the principles developed in Appendix I stay the same, but some definitions will be changed.

It is assumed that in this case $DI(t)$ is almost totally decoupled from $DIP(t)$, given that $DIP(t)$ sin $(2\pi Q_H j)$ is rather small.

The partial acceptance is given by four cuts, 0, j, k, and l, such that

$$\cos(2\pi Q_H j) > \cos(2\pi Q_H k)$$
$$\cos(2\pi Q_H j) > \cos(2\pi Q_H l) \quad . \tag{AII.1}$$

See the sketch (Fig. AII.1) where the coordinate system is defined as in Fig. III.4b. From symmetry reasons it is evident that

$$l = |k - j| \; . \tag{AII.2}$$

$DI(t)$ can then be again written in the form of Eq. (AI.9), but the coefficients have another form, namely

$$\begin{aligned} A_{DI} &= DO\{1 - \cos(2\pi Q_H j)\}/2 \\ B_{DI} &= jt_{rev} DO/2 \\ C_{DI} &= [DK\{1 - \cos(2\pi Q_H j)\} - DS]/2 \quad . \end{aligned} \tag{AII.3}$$

$DIP(t)$ can now be calculated from

$$\frac{X_l}{\sin(2\pi Q_H l)} + \frac{X_k}{-\sin(2\pi Q_H k)} = 0 \quad . \tag{AII.4}$$

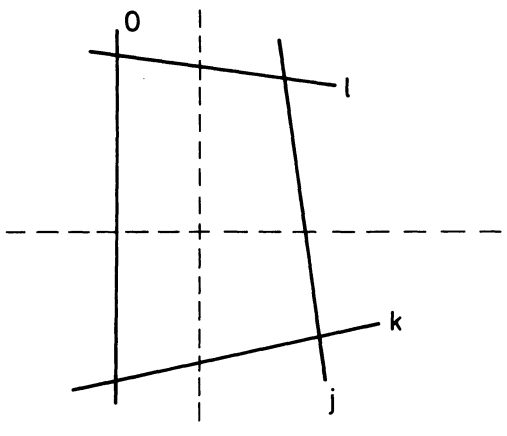

Fig. AII.1

After some rearrangement we obtain

$$DIP(t) = \frac{1}{2\hat{\beta}_s}\left[\frac{A_l}{\sin(2\pi Q_H l)} + \frac{A_k}{\sin(2\pi Q_H k)} - DI(t)\{\cot(2\pi Q_H l) + \cot(2\pi Q_H k)\}\right] \quad . \tag{AII.5}$$

This permits us to write $DIP(t)$ again in the form of Eq. (AI.7), but with the following coefficients:

$$\begin{aligned}
A_{DIP} &= \frac{1}{2\hat{\beta}_s}\left[\frac{DO\{1-\cos(2\pi Q_H l)\}}{\sin(2\pi Q_H l)} + \frac{DO\{1-\cos(2\pi Q_H k)\}}{\sin(2\pi Q_H k)}\right. \\
&\qquad \left. - A_{DI}\{\cot(2\pi Q_H l) + \cot(2\pi Q_H k)\}\right] \\
B_{DIP} &= \frac{1}{2\hat{\beta}_s}\left[\left\{\frac{l}{\sin(2\pi Q_H l)} + \frac{k}{\sin(2\pi Q_H k)}\right\} t_{rev} DO - B_{DI}\{\cot(2\pi Q_H l) + \cot(2\pi Q_H k)\}\right] \\
C_{DIP} &= \frac{1}{2\hat{\beta}_s}\left[\frac{DK\{1-\cos(2\pi Q_H l)\} - DS}{\sin(2\pi Q_H l)} + \frac{DK\{1-\cos(2\pi Q_H k)\} - DS}{\sin(2\pi Q_H k)}\right. \\
&\qquad \left. - C_{DI}\{\cot(2\pi Q_H l) + \cot(2\pi Q_H k)\}\right] \quad .
\end{aligned} \tag{AII.6}$$

The best value for $\beta_l(t)$ can be estimated in the four-angle case by remarking that to a good approximation the ratio of the axes of the ellipse inscribed in the partial acceptance is given by

$$\frac{\hat{\beta}_s}{\beta_l(t)} = \frac{\left[A_l / \left|\sin(2\pi Q_H l)\right| + A_k / \left|\sin(2\pi Q_H k)\right|\right]}{2\overline{DI}} \quad , \tag{AII.7}$$

where $\overline{DI}$ is the average value of $DI(t)$:

$$\overline{DI} = \frac{A_{DI}(T_E + T_B)}{2T_{IKS}} + \frac{B_{DI}}{T_{IKS}} + C_{DI} \quad . \tag{AII.8}$$

Then $\beta_l(t)$ can be written as

$$\beta_l(t) = \frac{\overline{DI}\hat{\beta}_s}{A_{\beta_l} t + B_{\beta_l}} \quad , \tag{AII.9}$$

with

$$\begin{aligned}
A_{\beta_l} &= \left\{\frac{1-\cos(2\pi Q_H l)}{\left|\sin(2\pi Q_H l)\right|} + \frac{1-\cos(2\pi Q_H k)}{\left|\sin(2\pi Q_H k)\right|}\right\}\frac{DO}{2T_{IKS}} \\
B_{\beta_l} &= \frac{t_{rev} DO}{2T_{IKS}}\left\{\frac{l}{\left|\sin(2\pi Q_H l)\right|} + \frac{k}{\left|\sin(2\pi Q_H k)\right|}\right\} \\
&\quad - \frac{DS}{2}\left\{\frac{1}{\left|\sin(2\pi Q_H l)\right|} + \frac{1}{\left|\sin(2\pi Q_H k)\right|}\right\} \\
&\quad + \frac{DK}{2}\left\{\frac{1-\cos(2\pi Q_H l)}{\left|\sin(2\pi Q_H l)\right|} + \frac{1-\cos(2\pi Q_H k)}{\left|\sin(2\pi Q_H k)\right|}\right\} \quad .
\end{aligned} \tag{AII.10}$$

APPENDIX III

THE CALCULATION OF T_{IKS}

When the value of $T_{IKS} = T^c_{IKS}$ obtained from Eq. (III.24) is not precise enough, a better value for T_{IKS} can be calculated by computing the number of particles inside and outside $E_H = 130\ \pi$ mm · mrad directly, using the method described in Appendix IV. The result of this calculation depends again somewhat on the T_{IKS} value itself and a fairly good starting value for T_{IKS} must therefore be available to calculate the required number of particles for each beam slice. The value T^c_{IKS} that was derived from the geometrical relation (III.24) is quite good enough for this.

Assuming that each beam slice of length δt at injection contains the same number of particles, the number of particles in the slice surviving in the PSB after injection depends only on the slice efficiency η_A. The number η_E will denote the slice efficiency counting only the particles injected inside $E_H = 130\ \pi$ mm · mrad as surviving. In the neighbourhood of the end of the injection (T_E) the efficiencies η_A and η_E will be assumed to depend linearly on time. This is allowed since the error introduced by this assumption is smaller than 0.5% of the total injected intensity and this is much smaller than the error of about 2% in the target measurements.

To find η_A and η_E as a linear function of time around T_E the efficiency must be calculated at two distinct moments. The moments T^c_E and T_M have been chosen where T^c_E is the moment shown in Fig. III.7 for which the relation (III.24) holds and T_M is defined by the relation

$$T_M = \frac{T''_E + T^c_E}{2} \quad . \tag{AIII.1}$$

Here T''_E is the time of injection of that slice for which the centre of the inscribed ellipse of the partial acceptance lies on the circle of Fig. III.7. The dependence of η_A and η_E on the time of injection of the slice is shown schematically in Fig. AIII.1. In the neighbourhood of T_E the efficiencies η_A and η_E are approximated by straight lines that are fixed by the calculated points $\eta_A(T^c_E)$, $\eta_E(T^c_E)$ and $\eta_A(T_M), \eta_E(T_M)$. These two lines intersect at the time T_I.

The total number of particles injected from the start of the injection T_B until T_I is given by

$$N(T_I) = \int_{T_B}^{T_I} \eta_A(t)dt \quad . \tag{AIII.2}$$

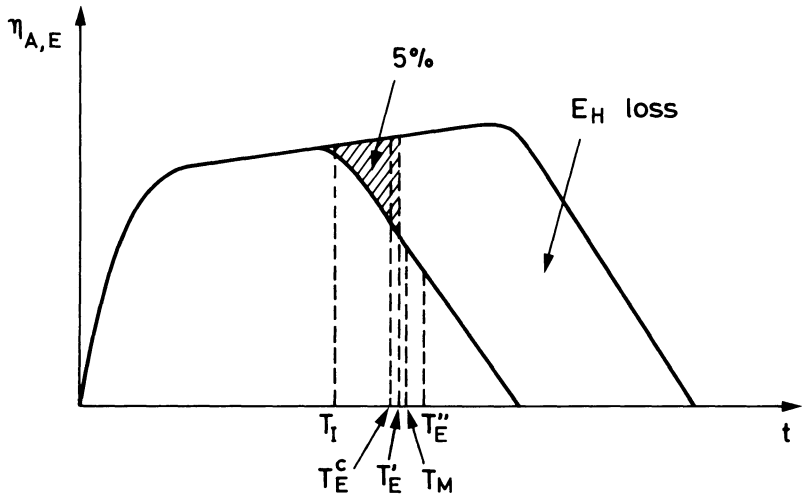

Fig. AIII.1

This number is calculated again by the standard methods described in Appendix IV. The moment of injection of the last beam slice at time T_E for which exactly 5% of the total injected beam lies outside $E_H = 130\ \pi$ mm · mrad can now be derived by considering Fig. AIII.1, since the following relation must hold:

$$0.5(T_E' - T_I)\,[\eta_A(T_E') - \eta_E(T_E')] = 0.05\,[N(T_I) + 0.5(T_E' - T_I)\,(\eta_A(T_I) + \eta_A(T_E'))] \quad , \tag{AIII.3}$$

where $\eta_A(T_E')$ and $\eta_E(T_E')$ are given by the equations

$$\begin{aligned} \eta_A(T_E') &= \eta_A(T_I) + \frac{T_E' - T_I}{T_M - T_I}\,[\eta_A(T_M) - \eta_A(T_I)] \\ \eta_E(T_E') &= \eta_A(T_I) + \frac{T_E' - T_I}{T_M - T_I}\,[\eta_E(T_M) - \eta_A(T_I)] \quad . \end{aligned} \tag{AIII.4}$$

When this substitution is made in Eq. (AIII.3), a quadratic equation is obtained for $T_E' - T_I$, from which T_E' is obtained in the following form:

$$T_E' = T_I + \frac{T_M - T_I}{2\Delta\eta}\left\{0.1\eta_A(T_I) + \sqrt{0.01\eta_A^2(T_I) + 0.4\,\frac{N(T_I)\Delta\eta}{T_M - T_I}}\right\} \quad . \tag{AIII.5}$$

with

$$\Delta\eta = 0.05\,[\eta_A(T_I) - \eta_A(T_M)] + \eta_A(T_M) - \eta_E(T_M) \quad .$$

This calculation is based on a T_{IKS} value of T^c_{IKS} and, according to Eq. (III.21), on a T_B value given by $T^c_B = (DK\,T^c_{IKS})/DO - t_{rev}$. However, $T_E' - T^c_B$ does not correspond any longer to an exact number of injected turns. In practice one desires to keep the time interval during which the beam is injected equal to $n_t \cdot t_{rev}$. From Eq. (III.1) it can be seen that $D(T_E)$ does not change when T_E and T_{IKS} are changed proportionally, and the value of $D(T_E)$ determines almost exclusively the fraction of injected beam outside $E_H = 130\ \pi$ mm · mrad at the end of the injection. For $T_E/T_{IKS} = T_E'/T^c_{IKS}$ this fraction is 5% within the accuracy of the derivation of Eq. (AIII.6). It can easily be seen that very nearly the same fraction is obtained when for T_{IKS} and T_E the following values T^f_{IKS} and T^f_E are taken:

$$\begin{aligned} T^f_{IKS} &= n_t t_{rev} T^c_{IKS}/(T_E' - T^c_B) \\ T^f_E &= T^f_B + n_t t_{rev} = \frac{DK}{DO}\,T^f_{IKS} + (n_t - 1)t_{rev} \quad , \end{aligned} \tag{AIII.6}$$

since T^f_E/T^f_{IKS} is very nearly equal to T_E'/T^c_{IKS}. The injection period is now equal to $n_t \cdot t_{rev}$.

APPENDIX IV

EFFICIENCY CALCULATION

A study of the particle density distribution on the different ellipses suggests a Gaussian distribution given by the chance $P(I_H)\,\mathrm{d}I_H$ to find a particle on an elliptical strip of width dI_H, enclosing the surface πI_H:

$$P(I_H) = \frac{\pi \exp(-I_H \pi/\varepsilon_0)}{\varepsilon_0} = \frac{\exp(-I_H/I_0)}{I_0} \quad . \tag{AIV.1}$$

The number of particles within an emittance surface ε is given by

$$\int_0^{\varepsilon/\pi} P(I_H) dI_H = 1 - \exp(-\varepsilon/\varepsilon_0) \quad . \tag{AIV.2}$$

To take into account the passage from one partial acceptance configuration to another (see Section III.1) the process has been divided in time into the two parts, I and II, and the average value of a particular parameter is calculated by an integration over both parts in time. The time dependence of a parameter x is determined by $[x^{\mathrm{I}}(t), x^{\mathrm{II}}(t)]$, while a weight function $[\eta_A^{\mathrm{I}}(t), \eta_A^{\mathrm{II}}(t)]$ is necessary. This yields

$$\bar{x} = \frac{\int_{T_B}^{T_0} x^{\mathrm{I}}(t)\eta_A^{\mathrm{I}}(t)dt + \int_{T_0}^{T_E} x^{\mathrm{II}}(t)\eta_A^{\mathrm{II}}(t)dt}{\int_{T_B}^{T_0} \eta_A^{\mathrm{I}}(t)dt + \int_{T_0}^{T_E} \eta_A^{\mathrm{II}}(t)dt} \quad . \tag{AIV.3}$$

For the three-angle approximation $\eta_A(t)$ can be approximated by

$$\eta_A(t) = 1 - \exp\left(-\frac{\pi DI^2(t)}{\varepsilon_0 \beta_l}\right) \quad . \tag{AIV.4}$$

For the four-angle case the situation is less straightforward:

$$\frac{DI(t)}{\beta_l(t)} = \frac{1}{2\hat{\beta}_s}\left\{\frac{X_l}{|\sin(2\pi Q_H l)|} + \frac{X_k}{|\sin(2\pi Q_H k)|}\right\} \quad . \tag{AIV.5}$$

After substitution of Eq. (AIV.5) into Eq. (AIV.4) one obtains

$$\eta_A(t) = 1 - \exp\left[-\frac{\pi DI(t)}{2\hat{\beta}_s \varepsilon_0}\left\{\frac{X_l}{|\sin(2\pi Q_H l)|} + \frac{X_k}{|\sin(2\pi Q_H k)|}\right\}\right] \quad . \tag{AIV.6}$$

DI, DIP, and β_l are calculated numerically, except for the DI value in the three-angle case. The above method is not quite exact but a comparison with the results shows no significant differences.

The efficiency of the injection process can be calculated for each Q_H value. The cuts j, k, and l are used, defined such that

$$\begin{aligned} &\cos(2\pi Q_H j) > \cos(2\pi Q_H l) \\ &\cos(2\pi Q_H j) > \cos(2\pi Q_H k) \\ &\sin(2\pi Q_H k) \cdot \sin(2\pi Q_H l) \leq 0 \quad . \end{aligned} \tag{AIV.7}$$

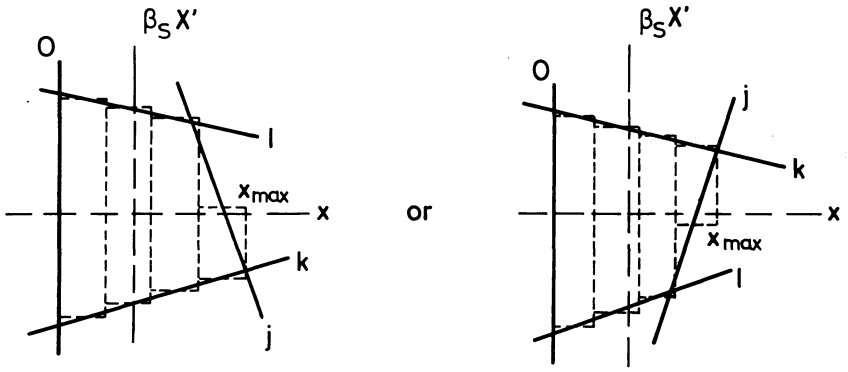

Fig. AIV.1

Then the evolution of j, k, and l with respect to one another is determined, see Fig. (AIV.1). The partial acceptance is divided into q rectangles of the same width, while the upper x_p^u and the lower x_p^l limit in the p^{th} rectangle can be calculated. The equation of cut i in the (x, x') plane is given by

$$x'(x, i) = -\cot(2\pi Q_H i)\{x - DX_i \cos(2\pi Q_H i)\} + DX_i \sin(2\pi Q_H i) \quad . \tag{AIV.8}$$

For all q rectangles the upper $x_p'^u$ and the lower $x_p'^l$ limits are found by the substitution of the x coordinate of the middle of the rectangle into the equations of the relevant two cuts. If the coordinates fall outside the admittance A_H, they are modified such that they lie on A_H. When the rectangle lies outside A_H, the efficiency of the rectangle is zero.

To calculate the number of particles in each of the q rectangles use is made of the function $f(x, x')$, defined as being analogous to Eq. (AIV.1):

$$f(x,x') = \frac{\exp\left\{-\pi(x^2 + x'^2)/\varepsilon_0 \beta_l\right\}}{\pi \varepsilon_0 \beta_l} \quad . \tag{AIV.9}$$

Then the efficiency of a slice divided into q parts is given by

$$Eff_q = \sum_{p=1}^{q} \int_{x'^l_p}^{x'^u_p} dx \int_{x^l_p}^{x^u_p} dx f(x, x') \quad . \tag{AIV.10}$$

ε_{2k} is defined to obtain a measure for the accuracy as

$$\varepsilon_{2k} = |Eff_{2k} - Eff_k| \quad . \tag{AIV.11}$$

If $\varepsilon_{2k} < \delta$, δ being preselected in the program, the total efficiency $\eta_A(t)$ of a slice is $\eta_A(t) = Eff_{2k}$. Knowing the efficiency of a slice, and knowing that the efficiency is a smooth continuous function of time, the integration over the whole process is done using Simpson's rule with the number of points equal to n_t or $n_t + 1$ depending on whether n_t is even or odd, or to any number at all depending on the desired speed and accuracy.